

2013

Studies of G Protein-Coupled Receptor Stability and Dimerization Using Novel Fluorescence and Crosslinking Approaches

Adam Knepp

Follow this and additional works at: http://digitalcommons.rockefeller.edu/student_theses_and_dissertations

 Part of the [Life Sciences Commons](#)

Recommended Citation

Knepp, Adam, "Studies of G Protein-Coupled Receptor Stability and Dimerization Using Novel Fluorescence and Crosslinking Approaches" (2013). *Student Theses and Dissertations*. Paper 230.



**STUDIES OF G PROTEIN-COUPLED RECEPTOR
STABILITY AND DIMERIZATION USING NOVEL
FLUORESCENCE AND CROSSLINKING
APPROACHES**

A Thesis Presented to the Faculty of
The Rockefeller University
in Partial Fulfillment of the Requirements for
the Degree of Doctor of Philosophy

by

Adam Knepp

June 2013

STUDIES OF G PROTEIN-COUPLED RECEPTOR STABILITY AND DIMERIZATION USING NOVEL FLUORESCENCE AND CROSSLINKING APPROACHES

Adam Knepp, Ph.D.

The Rockefeller University 2013

G protein-coupled receptors (GPCRs) comprise a large family of related seven-transmembrane-helical membrane proteins that bind to specific extracellular ligands, such as hormones or neuromodulators. The active receptor-ligand complex then engages with a heterotrimeric G protein on the cytoplasmic surface of the plasma membrane to facilitate a change in the concentration of an intracellular second messenger, such as cAMP. A number of non-canonical signaling pathways, such as β -arrestin-mediated signaling, also exist for many, if not all, GPCRs. Receptor signaling is attenuated by phosphorylation and receptor internalization. Recent advances in structural studies of GPCRs have revealed high-resolution structures of both inactive and active receptors in complex with various ligands. Endogenous ligands, drugs and the membrane environment, and even oligomerization can affect receptor signaling efficacy, but the mechanistic details underlying these allosteric effects are poorly characterized. To study allostereism of a ligand-receptor complex in a bilayer requires at least partial enrichment or isolation of the basic signaling unit. Many studies have employed biochemical

purification and reconstitution strategies, but GPCRs are inherently unstable when extracted from native membranes so conditions must be carefully selected to preserve receptor integrity. To monitor the functional state of GPCRs during purification and reconstitution, a novel homogeneous time-resolved fluorescence resonance energy transfer (FRET)-based analytical assay was developed. To enable the assay, a novel bioconjugation method was invented to prepare microgram quantities of monoclonal antibodies labeled with long-lived lanthanide fluorophores. As a proof-of-concept, the folding and stability of human C-C chemokine receptor 5 (CCR5), the primary co-receptor for HIV-1 cellular entry, was studied. The assay enabled high-throughput detection of femtomole quantities of CCR5. Thermal denaturation measurements demonstrated that small molecule antagonists substantially stabilize CCR5 and also revealed that the ligands induce distinct receptor conformations, consistent with the hypothesis that GPCRs access numerous conformations during signal transduction rather than operating as a binary active-inactive switch. In addition, high-throughput stability screens led directly to the identification of CCR5 mutants that should be sufficiently stable for crystallization and lead to a high-resolution structure of CCR5, which would significantly advance understanding of the structural basis of HIV entry. The FRET-based assay was also applied to devise and optimize a protocol to incorporate CCR5 into an artificial membrane scaffold called nanoscale apolipoprotein bound bilayers (NABBs). CCR5 was shown to retain proper folding in NABBs and proof-of-concept fluorescence correlation spectroscopy (FCS) experiments were carried out to characterize these structures. Novel FCS standard reagents were developed to facilitate these measurements. The biochemical and analytical approaches reported may be adapted to prepare stable,

functional samples of other GPCRs for structural and dynamic studies of receptor allostery. GPCRs are known to form dimers and higher-order oligomers, and despite a growing body of evidence that these complexes are functionally important, the structural basis of receptor-receptor interactions remains unknown. To address this problem, a potential dimerization interface of the prototypical GPCR, rhodopsin, was analyzed using a proteomics approach involving chemical crosslinking and liquid chromatography-mass spectrometry. The strategy was devised so that rhodopsin could be probed in the unique native environment of the rod cell disk membrane. Crosslinking results supported a model of rhodopsin dimerization involving contacts in transmembrane helix 1 and an amphipathic cytoplasmic helix at the carboxyl-terminal tail of the receptor. This novel interface is postulated to be relevant for understanding GPCR oligomerization in general.

Acknowledgements

I thank my advisor, Dr. Thomas Sakmar, for giving me the opportunity to complete my Ph.D. in his lab. I especially appreciate that he supported my work on multiple projects that I found interesting, encouraged me to develop useful technologies, and helped me forge collaborative relationships in both academia and industry. Additionally, he assembled a tremendously team-oriented group that helped make my time in the lab fruitful and enjoyable.

Many of the techniques and projects I worked on relied on the advice of my colleagues in the Sakmar Lab. I owe a special debt of gratitude to Dr. Thomas Huber, who helped me formulate ideas throughout graduate school and challenged me to be both thoughtful in my experimental design and meticulous in my execution. I thank Manija Kazmi and Dr. Pallavi Sachdev for their support and for their patience in teaching me important lab fundamentals early in my Ph.D. At various points, I worked closely with Dr. Amy Grunbeck, Dr. Saranga Naganathan, and Carlos Rico. I enjoyed these collaborations and thank them for their contributions to my projects. I also thank Dr. Shixin Ye, He Tian, Dr. Sarmistha Ray, Dr. W Vallen Graham, and Jennifer Peeler for constructive discussions and feedback. I thank all members of the Sakmar Lab, current and former, for forming a wonderfully congenial and supportive lab environment.

My work has required regular use of resource facilities at Rockefeller. I thank Dr. Fraser Glickman of the High-Throughput Screening Resource Center and Dr. Alison North and Dr. Kaye Thomas of the Bio-Imaging Resource Center for trainings and help with troubleshooting. I also thank Dr. Milica Tesic Mark and Dr. Joseph Fernandez of the Proteomics Resource Center for conducting the mass spectrometry experiments.

I have been fortunate to work with several collaborators outside of Rockefeller. Dr. Xavier Periole and Dr. Siewert-Jan Marrink conducted the molecular dynamics simulations that spurred the biochemical crosslinking project. I thank them for many helpful discussions and for their help in manuscript preparation. I thank Dr. Daniel Lamb, Dr. Ali Jazayeri, and Dr. Fiona Marshall, and others at Heptares Therapeutics for engaging in the structure collaboration with us and providing information about CCR5 constructs. I appreciate the contributions of Dr. Reem Barro and Sarya Abi-Habib in Dr. John Moore's Lab, who conducted the HIV entry experiments.

Finally, I am very grateful to have incredibly supportive friends and family. I especially thank my parents, Dennis and Vanessa Knepp, and my brother, Justin Knepp, for their constant encouragement.

Table of Contents

CHAPTER ONE: INTRODUCTION	1
1.1 G Protein-Coupled Receptors in Cell Signaling	1
1.2 GPCRs in Disease and Drug Development	4
1.3 GPCR Structural Biology	6
1.4 GPCR Allostery and Dynamics	9
1.5 Rhodopsin: A Prototypical GPCR	11
1.6 Chemokine Receptor CCR5	15
CHAPTER TWO: MATERIALS AND METHODS	17
2.1 Reagents and Buffers	17
2.1.1 Cells, Plasmids, and Chemicals	17
2.1.2 Buffers	17
2.1.3 Instruments	19
2.2 Preparation of Lipids	19
2.3 Labeling of IgG and Purification	20
2.3.1 Solid-phase labeling of IgG	20
2.3.2 Purification and characterization of labeled IgG	21
2.4 Mutagenesis and Plasmid Construction	21
2.5 Culturing of HEK-293 Cells and Heterologous Expression of CCR5	22
2.6 Solubilization and Purification of CCR5	22
2.6.1 Detergent Solubilization of CCR5	22
2.6.2 Immunopurification of CCR5	23
2.7 Quantification of CCR5 with Fluorescent Ligand Binding	23
2.8 HTRF Quantification Assays	24
2.8.1 HTRF Standard Experiment with α -DNP	24
2.8.2 HTRF Quantification of CCR5	25
2.8.3 HTRF Signal Analysis	25
2.9 Thermal Stability Measurements	26
2.9.1 Experimental Procedure	26
2.9.2 Modeling Thermal Denaturation of CCR5	27

2.10	Immunoblot Analysis	28
2.11	Cell Surface Enzyme-Linked Immunosorbent (ELISA) Assay	29
2.12	High-throughput Calcium Flux Assay	30
2.12.1	Transfection of HEK-293T Cells in a 384-Well Format	30
2.12.2	Calcium Flux Assay Measurements	30
2.13	[¹²⁵I]-RANTES Binding to Whole Cells	31
2.14	Expression and Purification of Zap1	31
2.15	Incorporation of CCR5 into NABBs and Purification	32
2.15.1	Preparing CCR5 NABBs	33
2.15.2	Purification of CCR5 NABBs	33
2.15.3	Immunoprecipitation of CCR5 NABBs with a Conformationally Sensitive Antibody	34
2.16	Flourescence Correlation Spectroscopy (FCS)	34
2.16.1	FCS Sample Preparation and Measurements	34
2.16.2	Synthesis of Oligonucleotide FCS standards	35
2.16.3	Modeling FCS Data	35
2.17	Crosslinking and Proteolysis of Rod Outer Segment (ROS) Membranes	37
2.17.1	Biochemical Crosslinking of ROS Membranes	37
2.17.2	Partial Proteolysis of ROS Membranes	38
2.18	Liquid Chromatography-Mass Spectrometry (LC-MS)	38
2.18.1	LC-MS Sample Preparation	38
2.18.2	LC-MS Measurements	39
2.18.3	LC-MS Data Analysis	39
 CHAPTER THREE: A HIGH-THROUGHPUT METHOD TO MEASURE CCR5 STABILITY AND CHARACTERIZATION OF THERMALLY STABLE MUTANTS		 41
3.1	Introduction	41
3.2	Results	46
3.2.1	Solid-phase labeling of IgG	46
3.2.2	HTRF Assay to Quantify Properly Folded GPCRs	51
3.2.3	High-throughput Measurement of CCR5 Thermal Stability	58
3.2.4	Identification and Characterization of Thermally Stable CCR5 Mutants	65
3.2.5	Probing the Allosteric between HIV Entry Inhibitor Antibodies and Small Molecule Drugs	72
3.3	Discussion	75
 CHAPTER FOUR: INCORPORATION OF CCR5 INTO MEMBRANE NANOPARTICLES AND SINGLE MOLECULE FLUORESCENCE MEASUREMENTS		 82
4.1	Introduction	82
4.2	Results	86

4.2.1 Incorporation of CCR5 into NABBs	86
4.2.2 Fluorescence Correlation Spectroscopy Measurements of Oligonucleotide Standards and CCR5 NABBs	94
4.3 Discussion	101
CHAPTER FIVE: CHEMICAL CROSSLINKING OF RHODOPSIN IN NATIVE MEMBRANES TO IDENTIFY A PRIMARY DIMERIZATION INTERFACE	103
5.1 Introduction	103
5.2 Results	106
5.2.1 Chemical Crosslinking and Partial Proteolysis Analysis	106
5.2.2 Liquid Chromatography-Mass Spectrometry Identification of Crosslinked Peptides	110
5.3 Discussion	114
CHAPTER SIX: FUTURE PERSPECTIVES	120
REFERENCES	125

List of Figures

- Figure 1-1** Schematic of GPCR signaling through G proteins
- Figure 1-2** Crystal structure of the β_2 -adrenergic receptor-Gs complex
- Figure 1-3** Schematic of the rhodopsin photocycle
- Figure 3-1** Solid-phase labeling of IgG with europium cryptate
- Figure 3-2** UV-Vis spectra of purified antibodies labeled with Alexa Fluor dyes
- Figure 3-3** Schematic of HTRF sandwich immunoassay
- Figure 3-4** HTRF standard experiment
- Figure 3-5** CCR5 HTRF assay controls
- Figure 3-6** Fluorescein-maraviroc standard curve to quantify CCR5
- Figure 3-7** Temporal stability of CCR5 in detergent solution
- Figure 3-8** Thermal stability of CCR5 in the presence of small molecule antagonists
- Figure 3-9** Time dependence of GPCR thermal denaturation
- Figure 3-10** Expression of thermally stabilized CCR5 mutants
- Figure 3-11** Ligand-induced calcium flux through wild type and stabilized CCR5
- Figure 3-12** HIV entry assays with wild type and stabilized CCR5
- Figure 3-13** Small molecule antagonists promote different receptor conformations
- Figure 3-14** Competition studies with 2D7 mAb and small molecule antagonists
- Figure 4-1** Protocol for microscale incorporation of CCR5 into NABBs
- Figure 4-2** UV-Vis spectra of NABBs
- Figure 4-3** Purification and quantification of CCR5 NABBs

- Figure 4-4** Thermal stability of CCR5 NABBs
- Figure 4-5** FCS standard curves for Alexa 488 and Alexa 647
- Figure 4-6** Oligonucleotide standards for FCS and FCCS
- Figure 4-7** FCS experiments with empty and GPCR-loaded NABBs
- Figure 5-1** Chemical crosslinking and proteolysis of rhodopsin in native rod outer segment membranes
- Figure 5-2** Chemical crosslinking of rhodopsin with a cleavable reagent
- Figure 5-3** Liquid chromatography-mass spectrometry analysis of crosslinked rhodopsin peptides
- Figure 5-4** Structural and CGMD analysis of rhodopsin dimer orientations
- Figure 5-5** Model of the rows-of-dimers organization of rhodopsin molecules

List of Tables

Table 5-1 Mass spectrometry peaks identified in analysis of crosslinked rhodopsin

List of Abbreviations

AFM	atomic force microscopy
BSA	bovine serum albumin
CGMD	coarse-grained molecular dynamics
CHS	cholesteryl hemisuccinate
DM	<i>n</i> -dodecyl β -D-maltopyranoside
DMEM	Dulbecco's modified Eagle's medium
DMSO	dimethyl sulfoxide
DNP	2,4-dinitrophenol
DOPE	1,2-dioleoyl- <i>sn</i> -glycero-3-phosphoethanolamine
DTT	dithiothreitol
EC	extracellular
EDTA	ethylenediaminetetraacetic acid
ELISA	enzyme-linked immunosorbent assay
EM	electron microscopy
EuK	europium trisbipyridine diamino cryptate
FCS	fluorescence correlation spectroscopy
FCCS	fluorescence cross-correlation spectroscopy
FPLC	fast protein liquid chromatography
FRET	fluorescence resonance energy transfer
GPCR	G protein-coupled receptor
GRK	GPCR kinase

H	helix
HRP	horseradish peroxidase
HTRF	homogeneous time-resolved fluorescence
LC-MS	liquid chromatography-mass spectrometry
LRB	Lissamine Rhodamine B
mAb	monoclonal antibody
MTS	methanethiosulfonate
NABB	nanoscale apolipoprotein bound bilayer
NEM	<i>N</i> -ethylmaleimide
ROS	rod outer segment
SA	streptavidin
SDS-PAGE	sodium dodecyl sulfate-polyacrylamide
SEC	size exclusion chromatography
SPR	surface plasmon resonance
StaR	stabilized receptor
TEM	transmission electron microscopy
TIRF	total internal reflection microscopy
TM	transmembrane
zap1	zebrafish apo A-1

Chapter One: Introduction

1.1 G Protein-Coupled Receptors in Cell Signaling

G protein-coupled receptors (GPCRs) constitute the largest superfamily of membrane proteins in the human genome, with at least 800 members (Fredriksson and Schioth, 2005). These signal transducers respond to a remarkably broad array of ligands, including photons, ions, small molecules, peptides, and small proteins. Conformational changes associated with receptor activation propagate the signal across the membrane to elicit intracellular responses. GPCRs are involved in processes as diverse as the senses of vision, smell, and taste, as well as neurotransmission, immune, and hormone responses. They thus represent a core component of vertebrate physiology. GPCRs exhibit a common topology of seven hydrophobic α -helices, an extracellular N-terminus, and an intracellular C-terminus. The International Union of Pharmacology has subdivided the GPCR superfamily into five classes, with the visual pigment rhodopsin as the prototype of class 1, the largest (also known as family A) (Foord et al., 2005). Most family A receptors have short N-termini compared with other families and interact with ligands primarily through contacts in the transmembrane (TM) and extracellular (EC) loop regions (Bockaert and Pin, 1999). Structural features common to many family A receptors include a disulfide bridge between cysteine residues in the EC1 and EC2 loops and cysteine palmitoylations at the C-terminus. A short amphipathic eighth helix has also

been observed in high-resolution crystal structures, among them the very first snapshot of rhodopsin (Palczewski et al., 2000). In addition, there are several highly conserved sequence regions, most prominently the E(D)RY, NPxxY(x)_{5,6}F, and CWxP motifs. These residues appear to be involved in key hydrogen bond networks that stabilize inactive and active conformations (Hofmann et al., 2009).

The classical, and eponymous, GPCR signaling pathway involves the activation of heterotrimeric G proteins (G α β γ). Extracellular ligand binding stabilizes a G protein-competent receptor conformation (Nygaard et al., 2009). The activated receptor catalyzes GDP \rightarrow GTP exchange in the G α subunit, which then dissociates from the receptor and G β γ subunits. G α and G β γ can proceed to interact with a number of effector proteins and second messengers depending on the subtype involved and the cellular context (Figure 1-1) (Dorsam and Gutkind, 2007). The four G α subfamilies – G α_s , G α_i , G α_q , and G α_{12} – regulate the activity of different pathways (Sprang et al., 2007). G α_s and G α_i primarily stimulate and inhibit adenylyl cyclase, respectively. G α_q binds and activates phospholipase C. G α_{12} mainly acts on guanine nucleotide exchange factors. Interestingly, many GPCRs signal through more than one type, possibly because different ligands stabilize distinct active states (Kenakin, 2003). G β γ heterodimers activate phospholipases, ion channels, and lipid kinases, among other molecules. Hydrolysis of GTP to GDP, either spontaneously or via catalysis by GTPase-activating proteins, leads to reassociation of the heterotrimer and completion of the G protein cycle. Receptor desensitization occurs through phosphorylation by GPCR kinases (GRKs) and subsequent β -arrestin binding (Krupnick and Benovic, 1998). Many GPCRs are then internalized via clathrin-mediated endocytosis, from which they may be recycled,

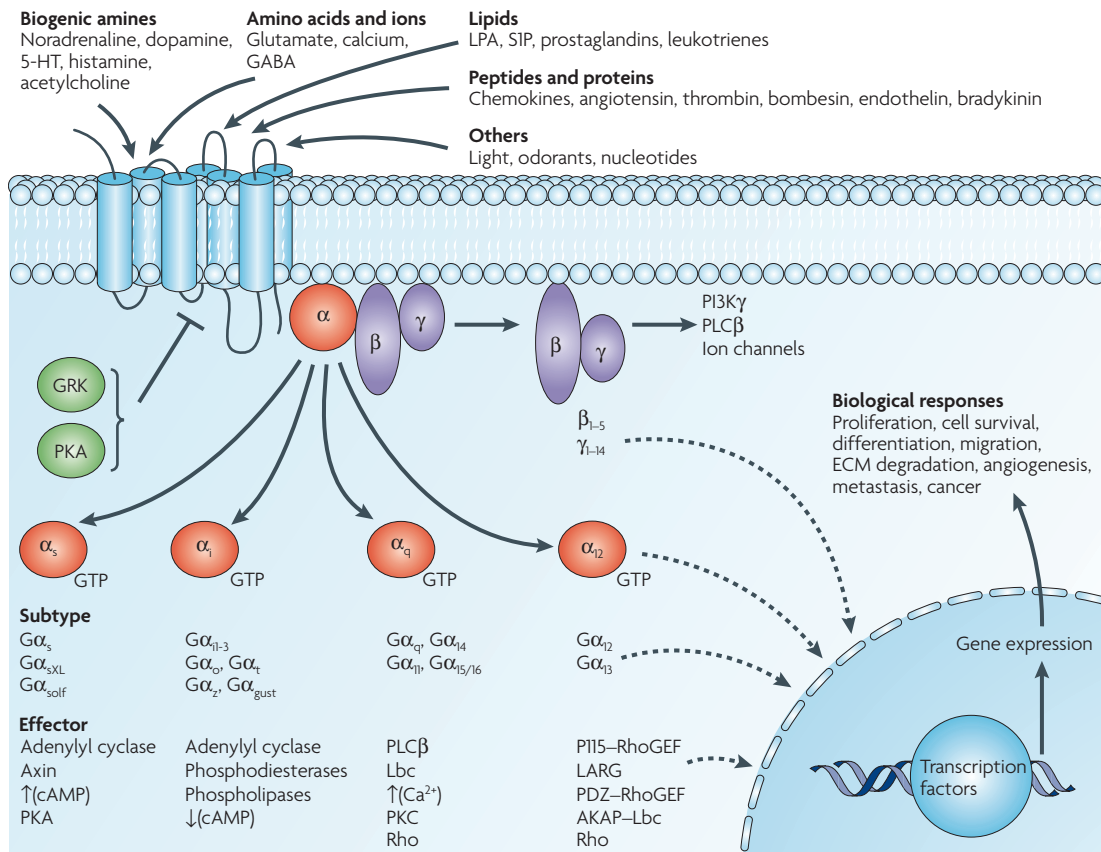


Figure 1-1. Schematic of canonical GPCR signaling through G proteins. Receptor activation in response to an extracellular stimulus leads to nucleotide exchange in a $G\alpha$ subunit. $G\alpha$ and $G\beta\gamma$ dissociate, resulting in activation and regulation of downstream signaling pathways that vary by subtype. These networks control many cellular functions and irregular activity can cause disease states. Figure taken from (Dorsam and Gutkind, 2007).

degraded, or perhaps even continue signaling through alternative pathways (Scita and Di Fiore, 2010).

GPCRs form many complexes in addition to the canonical ternary “signalosome” comprising ligand, receptor, and G protein. Following GRK-mediated seryl/threonyl phosphorylation, binding of β -arrestins can facilitate scaffolding and signaling through MAP kinase pathways (Shenoy and Lefkowitz, 2011). It is possible that some ligands stabilize a conformation that favors binding and signaling through arrestins rather than G proteins. GPCRs are also known to form dimers and higher-order oligomers, like many other membrane receptors. Though the functional implications of these complexes remain somewhat murky, heterodimerization has proven key in certain cellular trafficking and signaling contexts (Bouvier, 2001). Clearly, the structure, conformational dynamics, and composition of GPCRs and their complexes bear tremendous significance for our understanding of cell biology and physiology.

1.2 GPCRs in Disease and Drug Development

Given their expression in many cell types, functional importance, and plasma membrane localization, one would expect GPCRs to play major roles in clinical medicine. Indeed, GPCRs have been implicated in the molecular pathophysiology of a number of diseases (Insel et al., 2007). There are some examples of rare monogenic diseases involving GPCRs, perhaps most notably in rhodopsin, where certain mutations lead to retinitis pigmentosa, a leading cause of blindness (Mendes et al., 2005). GPCRs

are also the target of antibody products in autoimmune diseases such as Graves' disease, in which the thyroid-stimulating hormone receptor is chronically stimulated (Schott et al., 2005). GPCR genes also display a large number of polymorphisms; these may lead to altered receptor expression, targeting, and signaling properties that affect physiology. A famous example involves the chemokine receptor CCR5, a primary co-receptor for the HIV virus. Approximately 1% of the human Caucasian population carries a 32-base pair deletion in the EC2 loop. This CCR5 Δ 32 variant does not traffic to the cell membrane, conferring almost complete resistance to HIV-1 infection (Samson et al., 1996).

In addition to their direct involvement in disease states, GPCRs have been the most fruitful drug targets to date. An estimated 30-50% of marketed drugs act either directly or indirectly on GPCRs, including 5 of the top 15 generic drugs and 7 of the top 15 prescription drugs (Salon et al., 2011). Some especially notable examples include: β -adrenergic receptor antagonists ("beta-blockers") to treat heart disease and hypertension, dopamine receptor antagonists (schizophrenia) and agonists (Parkinson's), and antihistamines (Lagerstrom and Schioth, 2008). Despite these successes, at present only ~20 of the aforementioned >800 receptors are targets of clinically approved drugs (Overington et al., 2006). Of course, this does not imply that the rest are "undruggable." Rather, it reflects the inherent difficulties of drug development, and a tendency to use old drugs as templates for new ones. This untapped therapeutic potential demands a greater fundamental understanding of GPCR structure and allostery, as well as the development of new high-throughput screening tools and efforts to "deorphanize" receptors for which endogenous ligands remain unknown.

1.3 GPCR Structural Biology

The past few years have witnessed remarkable advances in the structural biology of GPCRs. The first crystal structure of rhodopsin was reported in 2000 (Palczewski et al., 2000), but it took until 2007 before another receptor structure, that of β_2 -adrenergic receptor, was solved (Cherezov et al., 2007; Rasmussen et al., 2007). These structures captured inactive states, with the receptor bound to the inverse agonist carazolol. Since then, a number of other GPCRs have been crystallized in antagonist- or inverse agonist-bound forms: β_1 -adrenergic receptor (Warne et al., 2008), A_{2A} adenosine receptor (Jaakola et al., 2008), M2 muscarinic receptor (Haga et al., 2012), histamine H1 receptor (Shimamura et al., 2011), chemokine receptor CXCR4 (Wu et al., 2010), dopamine D3 receptor (Chien et al., 2010), and κ - (Wu et al., 2012) and μ -opioid (Manglik et al., 2012) receptors, among others. These receptors were stabilized by ligand binding and a number of biochemical methods, including truncations, protein fusions, binding of Fab fragments, and stabilizing mutations. The overall similarity in architecture between receptors is striking; among the earliest structures, the root mean squared deviations of the transmembrane domains was less than 3 Å (Rosenbaum et al., 2009). Unsurprisingly, the intracellular regions, where GPCRs couple to comparably few binding partners, are especially similar. Subtle differences do exist – such as the presence or absence of an “ionic lock” between highly conserved residues in TM3 and TM6 and a short α -helix in the I2 loop – but overall the structures support a conserved mechanism of activation. Conversely, larger differences are apparent in the extracellular loops and ligand-binding regions. While the rhodopsin structure reveals a β -sheet in E2 that covers the 11-*cis*-

retinal chromophore, other receptors have E2 secondary structures that expose the ligand-binding cavity to solvent. This makes sense: most GPCRs reversibly bind diffusible ligands, and access to the binding pocket is necessary if energetically favorable interactions are to form. Another interesting point of variation concerns the ligand binding orientation. The β -receptor and rhodopsin ligands run roughly parallel to the bilayer plane, but the A_{2A} receptor ligand tilts closer to perpendicular resulting in substantially different contacts. This suggests that GPCRs can be activated through a variety of interactions in the extracellular loops and transmembrane regions.

Stabilizing GPCRs for crystallization in an active state has proven a trickier task, which was to be expected given the associated increased conformational flexibility. Rhodopsin has been crystallized in a G protein-interacting form (Scheerer et al., 2008) and active Meta II state (Choe et al., 2011). The β_2 receptor was stabilized in an active state by a camelid antibody fragment (nanobody) with G protein-like activity toward the receptor (Rasmussen et al., 2011a). The β_1 (Warne et al., 2011), A_{2A} adenosine (Lebon et al., 2011), and neurotensin (White et al., 2012) receptors have now also been crystallized in agonist-bound forms. These structures exhibit common differences compared to the earlier inactive structures, with a contraction of the ligand binding pocket and rotation of the cytoplasmic end of H6. The most technically impressive structure to date is the first high-resolution image of the receptor-G protein complex: β_2 -adrenergic receptor with Gs in its nucleotide-free form (Rasmussen et al., 2011b). Both nanobody binding and T4 lysozyme fusion were necessary to obtain a stable complex. The resulting structure reveals that the β and γ subunits of Gs barely make any contact with the receptor,

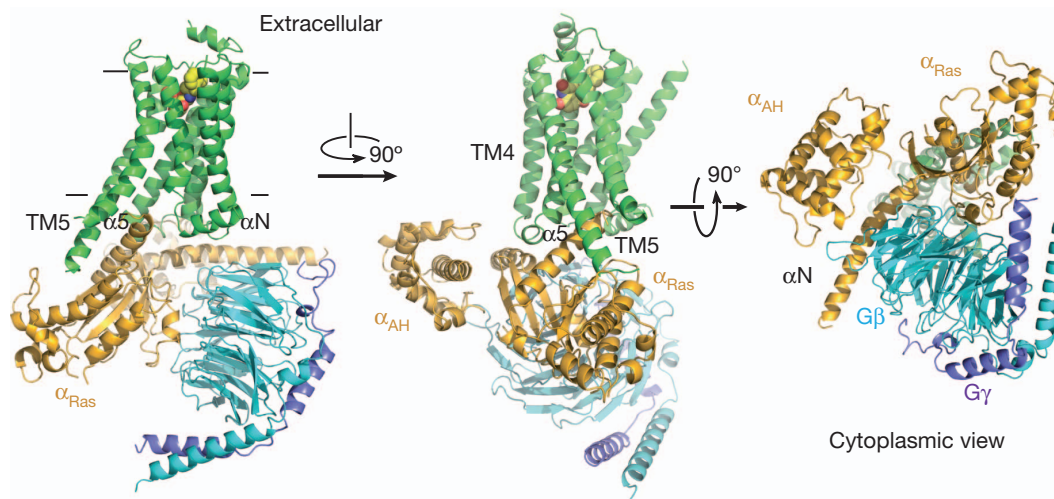


Figure 1-2. Crystal structure of the β_2 -adrenergic receptor-Gs complex. β_2 -AR (green), agonist (yellow), $G\alpha$ (orange), $G\beta$ (cyan), and $G\gamma$ (purple) are shown. The characteristic large outward movement of receptor H6 enables the $\alpha 5$ helix of $G\alpha$ to engage the receptor. The Ras-like GTPase domain and α -helical domain exhibit a very large opening to the nucleotide binding pocket in this nucleotide-free state. $G\beta$ and $G\gamma$ have few direct contacts with the receptor. Note that in these images the T4-lysozyme (receptor N-terminus) and nanobody ($G\alpha$ and $G\beta$ interface) crystallization aids have been omitted for clarity. (Figure taken from (Rasmussen et al., 2011b).)

and that the α subunit C-terminus binds in an open crevice formed by H6 motion (Figure 1-2). Though this structure marked an important milestone in the field, it is possible or perhaps likely that the considerable structural changes required to stabilize the complex resulted in a somewhat contrived system that deviates from the true physiological form. This is a common tradeoff, and achieving stability represents a core issue in GPCR structural biology. Analytical methods to assess receptor stability for crystallization and other assays are discussed in detail in Chapter 3.

Regardless of progress in structural biology, crystal structures are unlikely to reveal the basis of full versus partial agonism, or how receptor engagement facilitates G α nucleotide exchange (Schwartz and Sakmar, 2011). While additional crystal structures of different GPCRs and complexes with G proteins are needed, complementary biophysical approaches will also be necessary to grasp the signal transduction process.

1.4 GPCR Allostery and Dynamics

GPCRs may be best thought of as exquisite allosteric machines, with many accessible energetic states that are promoted by extracellular or intracellular binding partners. The classical signaling paradigm considers the receptor as a binary on-off switch, but a wealth of biochemical, biophysical, and pharmacological data has challenged this simple model (Deupi and Kobilka, 2007; Huber and Sakmar, 2011). Fluorescence lifetime spectroscopy experiments have revealed numerous receptor substates (Ghanouni et al., 2001). Some sets of agonists exhibit different potency rank

orders depending on the G protein stoichiometry, even in the same receptor system. This behavior cannot be explained by a single active state (Kenakin, 2003). There are even examples of agonists that function as partial agonists for a receptor and inverse agonists for the same receptor in a constitutively active state, again suggesting a range of conformations (Kenakin, 1997). Further, ligands can cause receptors to form oligomers, bind adaptor proteins, and internalize, among other activity (Brady and Limbird, 2002).

Clearly, GPCR signaling encompasses far more complex behaviors than a one- or even two-dimensional model might encapsulate. These qualities are not merely of academic interest, either. Given the massive role that GPCRs play in drug discovery, one can envision a therapeutic landscape in which molecules selectively promote desirable actions while avoiding others. For example, a CCR5 agonist that promotes internalization but not G protein signaling might prevent viral resistance without inflammatory side effects. How can the underlying conformational complexity be unveiled? Cell-based signaling assays are an indirect readout of activity downstream of the receptor. Despite the remarkable advances in GPCR structural biology, and the value of visualizing receptor conformations at high resolution, it seems extremely impractical to crystallize every ligand-receptor-G protein (or GRK, or arrestin, or oligomer) complex of interest. Even if one could, the structures would reveal little about their thermodynamic stability and the pathway of interconversion between states.

Purification and reconstitution of receptors in membrane bilayers, along with ligands and binding partners of interest, enables the experimenter to probe structure-function relationships in a defined system. Though *in vitro* experiments cannot replicate the full suite of roles GPCRs play in cell biology, they are well suited to determine the

sequence and kinetics of receptor binding events upon ligand stimulation. Fluorescence methods – including total internal reflection microscopy (TIRF) and fluorescence correlation spectroscopy (FCS) – are especially powerful ways to observe receptors in action. These approaches present considerable technical difficulties, however. Purified receptors are inherently very unstable, assessing sample quality is not straightforward, and labeling methods present a tradeoff between ease and sample perturbation. New tools must be developed to facilitate these kinds of experiments. The potential fruits of these efforts – observing the composition and evolution of signaling complexes over time at a single molecule level – provide ample motivation. Toward this goal, reconstitution of GPCRs into membrane nanoparticles and the development of FCS methods are discussed in Chapter 4.

1.5 Rhodopsin: A Prototypical GPCR

Rhodopsin, the visual pigment in rod photoreceptor cells, has proven to be an excellent model GPCR. Rhodopsin possesses several qualities that have made it particularly amenable to experimental study. It can be purified in large quantities from bovine retinae, is unusually stable in its dark state, and is quickly and efficiently activated upon exposure to light (Menon et al., 2001). In the dark, rhodopsin is covalently bound to its chromophore, 11-*cis*-retinal, via a Schiff base at Lys296. In this state, the chromophore acts as a potent inverse agonist; rhodopsin displays no basal activity, unlike other GPCRs. Absorption of a photon causes retinal isomerization and a propagation of

conformational changes that result in a G protein-competent state, Meta II, which catalyzes nucleotide exchange in transducin (Figure 1-3) (Hofmann et al., 2009). Transducin activates cGMP phosphodiesterase, which leads to closing of cGMP-gated ion channels in the rod cell plasma membrane and hyperpolarization of the photoreceptor cell. This remarkably sensitive light response system is capable of single photon detection and operates with extremely fast kinetics and high gain. The chromophore Schiff base hydrolyzes within minutes, leaving the apoprotein opsin. Fresh, metabolically provided 11-*cis*-retinal then binds the receptor to complete the photocycle.

Though rhodopsin is a highly specialized GPCR with unique characteristics, its overall structural features and activation pathway is generally representative of the largest family of GPCRs, which bears its name. In addition to its chromophore, rhodopsin contains a disulfide bond between the E1 and E2 loops (Cys110-Cys187), acetylation (Met1), N-linked glycosylations (Asn2 and Asn15), and C-terminal palmitoylations (Cys322 and Cys323) (Palczewski, 2006). Numerous crystal structures of rhodopsin have now been reported, including the dark state (Okada et al., 2004), Meta II state (Choe et al., 2011), and opsin bound to a G α -derived peptide (Scheerer et al., 2008). In the dark state, H3 is tethered to H6 through a hydrogen bond network that might be a common GPCR feature (Hofmann et al., 2009). In the active states, H6 is rotated outward to form a cytoplasmic crevice for G protein binding, confirming an activation model that was hypothesized in earlier cross-linking studies (Farrens et al., 1996; Sheikh et al., 1996). A more recent Fourier-transform infrared spectroscopy report showed that this helical rearrangement begins in the Meta I state, even while the G protein-binding pocket remains inaccessible (Ye et al., 2010).

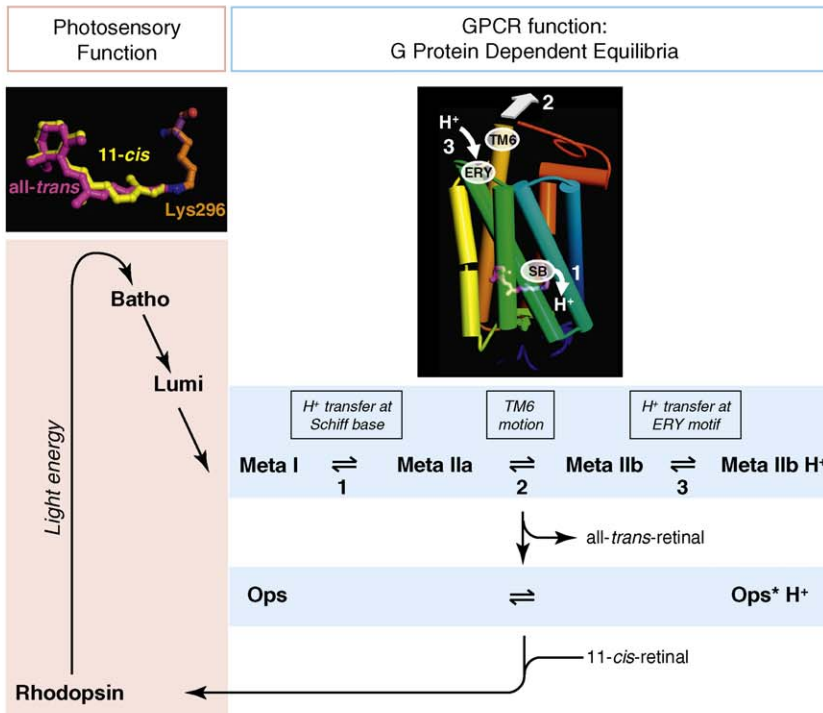


Figure 1-3. Schematic of the rhodopsin photocycle. Photoactivation causes retinal isomerization, and the receptor proceeds through a fast series of photointermediates before arriving at the active Meta II state within milliseconds. The retinylidene Schiff base hydrolyzes within minutes and all-*trans*-retinal diffuses out of the protein. Metabolically supplied 11-*cis*-retinal regenerates dark state rhodopsin. Figure taken from (Hofmann et al., 2009).

Rhodopsin has been visualized in its native membranes by atomic force microscopy (AFM) and transmission electron microscopy (TEM) (Fotiadis et al., 2003; Liang et al., 2003). These images revealed neatly arranged rows of dimers that interact to form higher-order structures. Though it is possible that this arrangement is an artifact of the experimental conditions, the isolated discs were shown to function normally. The extremely high packing density of rhodopsin (30,000-55,000/ μm^2 in the AFM images) far exceeds that of other GPCRs, but a large amount of evidence has demonstrated that other GPCRs dimerize as well (Palczewski, 2010). Despite the recent advances in GPCR structural biology, the precise structural basis of dimerization for rhodopsin and other GPCRs remains controversial. The close homology of family A receptors suggests modes of interaction may be highly similar, so the question of rhodopsin dimerization carries broad significance. Complementary biochemical, proteomics, and computational methods were applied to this problem. The results are presented and discussed in Chapter 5.

1.6 Chemokine Receptor CCR5

Unlike rhodopsin, most GPCRs reversibly bind diffusible ligands, adding another layer to the signalosome. Chemokine receptors represent one of these subfamilies. Chemokines are secreted molecules that facilitate directed cell migration in immune responses. These small proteins are thought to bind adhesion molecules called glycosaminoglycans at an inflammation site, providing a local concentration of chemoattractants for target cells expressing chemokine receptors (Springer, 1994). Roughly 50 chemokines and 20 receptors have been identified, and they are classified on the basis of cysteine residue patterning in the ligands (e.g. CC, CXC, etc.). These signaling networks exhibit significant promiscuity in biochemical binding assays: many chemokines bind multiple receptors and vice versa, though this apparent redundancy may be partially mitigated by spatiotemporal resolution *in vivo*. Nonetheless, the system is remarkably complex.

Chemokine receptors are involved in a large number of pathophysiologies, including autoimmune disorders, pulmonary disease, vascular disease, and cancer (Allen et al., 2007). In addition, as mentioned above, CCR5 (along with CXCR4) is a primary co-receptor for HIV-1 (Lusso, 2006). The native ligands of CCR5 – RANTES, MIP-1 α , and MIP-1 β – are potent inhibitors of HIV infection, likely because they promote receptor internalization. Small molecules and antibodies targeting CCR5 have also been developed to block viral entry by preventing gp120 binding to the co-receptor (Horuk, 2009). CCR5 has thus attracted much attention, and an understanding of its structure and functional properties has significant clinical relevance.

Ligand binding to chemokine receptors appears to involve multiple regions of the receptor. One model for chemokine binding to CCR5 posits that the globular body of the chemokines binds at the receptor N-terminus and extracellular loops, while the chemokine N-terminus is directed into the helical bundle (Blanpain et al., 1999). It has also been shown that tyrosine sulfation of CCR5 at multiple N-terminal sites contributes to both binding of native ligand and HIV entry. The receptor is glycosylated primarily at Ser6 (Farzan et al., 1999), and palmitoylation at C-terminal cysteine residues is important for trafficking and stability, much like in rhodopsin (Percherancier et al., 2001). While the crystal structure of CXCR4 has been reported (Wu et al., 2010), the structure of CCR5 has not yet been solved. In fact, despite its considerable importance in immunology and disease, relatively few studies with purified CCR5 have been reported to date. This receptor is thus an excellent candidate for studies aiming to understand receptor activation, functional selectivity, and allosteric modulation by native ligands and drugs.

Chapter Two: Materials and Methods

2.1 Reagents and Buffers

2.1.1 Cells, Plasmids, and Chemicals

HEK-293T cells were obtained from the American Type Culture Collection (Manassas, VA). Mammalian expression vectors and transfection reagents were obtained from Invitrogen (Carlsbad, CA). Restriction enzymes were obtained from New England Biolabs (Ipswich, MA). Chemicals were obtained from Sigma-Aldrich (St. Louis, MO) except where noted. Lipids were obtained from Avanti Polar Lipids (Alabaster, AL), except cholesterol, which was obtained from Sigma-Aldrich. Detergents were obtained from Anatrace, Inc. (Maumee, OH). Homogeneous time-resolved fluorescence (HTRF) reagents were obtained from Cisbio (Bedford, MA).

2.1.2 Buffers

Buffer N: 20 mM Tris-HCl (pH 7.0), 0.1 M $(\text{NH}_4)_2\text{SO}_4$, 10% (v/v) glycerol, 0.07% cholesteryl hemisuccinate (CHS), 0.018% 1,2-dioleoyl-*sn*-glycero-3-phosphocholine (DOPC), 0.008% 1,2-dioleoyl-*sn*-glycero-3-phospho--serine (DOPS), 0.33% *n*-dodecyl β -D-maltoside (DM), and 0.33% 3-[(3-cholamidopropyl)-dimethylammonio]-1-propanesulfonate (CHAPS)

Buffer E1: Buffer N supplemented with 400 μ M 1D5-nonapeptide corresponding to the engineered C-terminal receptor epitope C9, TETSQVAPA

Buffer S: 20 mM Tris-HCl (pH 7.0), 100 mM $(\text{NH}_4)_2\text{SO}_4$, and 10% (v/v) glycerol

Buffer C: 100 mM phosphate and 150 mM NaCl (pH 7.2)

Buffer P: 100 mM phosphate and 150 mM NaCl (pH 7.5)

Buffer E2: Buffer P supplemented with 200 mM imidazole

Buffer G: 100 mM phosphate, 150 mM NaCl, and 0.5 mg/mL BSA (pH 7.0)

Zap1 purification buffers:

Buffer HZ: 40 mM Tris (pH 8.0), 300 mM NaCl, 5 mM 2-mercaptoethanol, complete ethylenediaminetetraacetic acid (EDTA)-free protease inhibitor tablet, 2 mM PMSF

Buffer TZ: 25 mM Tris (pH 8.0), 300 mM NaCl, 20 mM imidazole, 0.5 mM TCEP, 1% (v/v) Triton X-100

Buffer CZ: 25 mM Tris (pH 8.0), 300 mM NaCl, 20 mM imidazole, 0.5 mM TCEP, 20 mM sodium cholate

Buffer AZ: 25 mM Tris (pH 8.0), 300 mM NaCl, 20 mM imidazole, 0.5 mM TCEP

Buffer BZ: 25 mM Tris (pH 8.0), 300 mM NaCl, 500 mM imidazole, 0.5 mM TCEP

Buffer GZ: 10 mM Tris (pH 8.0), 150 mM NaCl, 0.5 mM TCEP

Buffer EL: Dulbecco's PBS (pH 7.2) with 5 mg/mL BSA

Buffer CF: 1X Hank's Balanced Salt Solution (Gibco), 20 mM HEPES (pH 7.4),

2 mg/mL BSA

Buffer RB: 50 mM HEPES (pH 7.4), 1 mM CaCl₂, 5 mM MgCl₂, and 5 mg/mL

BSA

Buffer T: 10 mM Tris-HCl (pH 7.5) with 5 mM CaCl₂

2.1.3 Instruments

All UV-Vis spectra were acquired on a Perkin-Elmer Lambda 800 Ultraviolet-visible spectrophotometer. All FPLC purifications were carried out on an Äkta Explorer system (GE).

2.2 Preparation of Lipids

Lipids were dissolved in chloroform at a concentration of approximately 100 mg/mL in glass round-bottom flasks. The solvent was evaporated under a gentle stream of dry argon while the flask was rotated, forming a thin lipid film. The lipids were redissolved in dichloromethane, and the procedure was repeated. The remaining dichloromethane was removed under vacuum overnight. The lipid films were then hydrated with the appropriate detergent-containing buffers, sonicated, and frozen and thawed in liquid N₂ until they were fully solubilized.

2.3 Labeling of IgG and Purification

2.3.1 Solid-phase labeling of IgG

Ni-NTA magnetic agarose beads (QIAGEN; 200 μ L, 5% slurry) were washed with 1 mL of Buffer P. The IgG to be labeled (100 μ g, 1.3 nmol) was bound to beads via incubation for 30 min at room temperature with shaking. Half-scale reactions with 100 μ L beads and 50 μ g IgG were also performed with no additional alterations to the procedure. In all solid-phase reactions, 0.0037% (w/v) DM was added to facilitate mixing. The beads were spun down, and the tube was placed on a magnetic rack to ease removal of the supernatant fraction. The antibody was activated via addition of 2 μ L of 3.75 mM sulfo-SMCC (Pierce; 7.5 nmol, 5.6 equiv) and shaking for 60 min at room temperature. In a separate reaction, 3.68 μ L of 0.68 mM fluorophore with primary amino group (2.5 nmol), 0.67 μ L of 0.5 M sodium borate (pH 8.2), 1.32 μ L of 1 M NaF, and 0.67 μ L of 7.58 mM SPDP (Pierce; 5.0 nmol, 2 equiv) were mixed for 60 min at room temperature with shaking. The fluorophore-SPDP reaction was stopped by addition of 0.67 μ L of 7.58 mM Tris. SPDP was reduced via addition of 0.67 μ L of 8.27 mM TCEP and mixing for 15 min. The activated fluorophore was added to activated IgG and mixed overnight at 4°C. The conjugation reaction was stopped with 1 μ L of 80 mM N-acetylcysteine. The beads were washed twice with 1 mL of Buffer P. IgG was eluted with two 50 μ L volumes of Buffer E2 for 30 min each.

The solid-phase reactions were successfully carried out with 1) the following antibodies: 1D4 (National Cell Culture), 2D7 and 3A9 (BD Biosciences), and α -FLAG (Sigma-Aldrich) and 2) the following fluorophores: europium trisbipyridine diamino cryptate

(EuK) (Cisbio), Alexa 647 cadaverine, and Alexa 488 cadaverine (Invitrogen).

2.3.2 Purification and characterization of labeled IgG

When desired, combined elutions were supplemented with 0.5 mg/mL BSA and run on a Superdex 200 10/300 GL gel filtration column in Buffer G. In some cases, the purification step was skipped and the antibody was instead exchanged into Buffer P on Zeba Spin Desalting Columns (Pierce) according to the manufacturer's protocol. UV-Vis spectra were acquired using either the FPLC in-line detector or on a spectrophotometer in cuvette format.

EuK conjugates were stored at 4°C with 0.01% thiomersal. Alexa dye conjugates were stored at 4°C with 0.05% sodium azide.

2.4 Mutagenesis and Plasmid Construction

The human CCR5 gene containing the C-terminal C9 epitope TETSQVAPA was in the pcDNA3.1(+) vector (Invitrogen). Mutations were introduced using the QuikChange Lightning Site-Directed Mutagenesis Kit (Stratagene). Primers were designed to satisfy the manufacturer's guidelines.

2.5 Culturing of HEK-293 Cells and Heterologous Expression of CCR5

HEK-293T cells were grown in Dulbecco's modified Eagle's medium (DMEM) [4.5 g/L glucose and 2 mM glutamine (Gibco)] supplemented with 10% fetal bovine serum (FBS) (Atlanta Biologicals) at 37°C in a 5% CO₂ atmosphere. Cells were propagated by addition of 1 mL 0.25% Trypsin-EDTA (Gibco) per plate for 5 min, dilution in fresh media, and replating in new dishes. HEK-293T cells were transfected with human CCR5 cDNA tagged with the C9 epitope, in pcDNA3.1(+) using Lipofectamine Plus as previously described for earlier experiments with rhodopsin (Yan et al., 2003). Briefly, for one 10 cm plate at roughly 80% confluency, 0.75 mL of prewarmed DMEM was mixed with 3.5 µg of plasmid DNA. To this was added 10 µL of PLUS reagent, and the mixture was incubated for 15 min and then transferred to a separate mixture containing 0.5 mL of DMEM and 17 µL of Lipofectamine Plus. After another 15 min incubation, the volume was increased to 4 mL with DMEM and the mixture added to HEK-293T cells at 70-80% confluence. Four hours after transfection, an additional 4 mL of DMEM supplemented with 20% FBS was added. Cells expressing CCR5 were harvested 48 h after transfection in PBS buffer containing the protease inhibitors aprotinin and leupeptin.

2.6 Solubilization and Purification of CCR5

2.6.1 Detergent Solubilization of CCR5

Cell pellets from 10 cm plates were lysed in 1 mL of Buffer N (supplemented with protease inhibitors) per 5×10^6 cells. After thorough resuspension, the solution was

probe-tip sonicated with 6×1 s pulses and incubated for 2 h at 4°C. The solution was then centrifuged at 14000 rpm (20000g) using a Type 45 TI rotor for 20 min at 4°C. The supernatant fraction was collected and stored at -80°C until further use.

2.6.2 Immunopurification of CCR5

Solubilized lysate from 2×10 cm plates was thawed on ice and added to 50 μ L of packed 1D4-Sepharose resin with 2 mg/mL immobilized 1D4 mAb. The lysate/resin mixture was incubated for 16 h at 4°C. The resin was transferred to a Micro-Spin column (Pierce), centrifuged to remove the supernatant fraction, and washed twice with Buffer N. Purified CCR5 was eluted by incubating the resin with 2×50 μ L of Buffer E1 for 30 min.

2.7 Quantification of CCR5 with Fluorescent Ligand Binding

Solubilized CCR5 lysate from approximately one-fifth of a 10 cm plate was incubated with 100 nM fluorescein-labeled maraviroc analogue (FL-maraviroc; generously provided by M. Teintze, Montana State University, Bozeman, MT) and 12.5 μ L of 1D4-Sepharose resin (2 mg of 1D4 mAb/mL of packed resin) for 16 h at 4°C in the presence and absence of 1 μ M unlabeled maraviroc (Toronto Research Chemicals). The beads were washed three times with Buffer N, and samples were eluted via incubation of the beads with 1% sodium dodecyl sulfate (SDS) for 1 h at room temperature and shaking. Eluted samples were transferred to a black 96-well round-bottom polypropylene microtiter plate (Nunc/Thermo Fisher Scientific). A serial dilution of FL-maraviroc in 1%

SDS was also included for a standard curve. The plate was read on a Cytofluor II Fluorescence Multiwell Plate Reader (Perbio Science) with an excitation wavelength of 485 nm and an emission wavelength of 530 nm. A linear fit of the standard curve was used to calculate the concentration of FL-maraviroc bound to the CCR5 lysate. The difference between the values with and without excess unlabeled maraviroc was used to calculate the CCR5 concentration with a correction for nonspecific binding of FL-maraviroc.

2.8 HTRF Quantification Assays

All HTRF assays were conducted with the appropriate buffer supplemented with 50 mM NaF and 1 mg/mL BSA.

2.8.1 HTRF Standard Experiment with α -DNP

The standard experiment used commercially available reagents: 2,4-dinitrophenol (DNP)-NHS, anti-DNP-EuK, biotin-BSA (Pierce), and XL665-SA. Biotin-BSA-DNP was prepared by reacting DNP-NHS with biotin-BSA according to the manufacturer's protocol. Competition with DNP-NHS, which does not bind XL665-SA, was used to demonstrate the specificity of the observed HTRF signal. Biotin-BSA-DNP (5 nM) and XL665-streptavidin (XL665-SA, 10 nM) in PBS pH 7.0 were combined in a 1:1 ratio (v/v) and mixed for 15 min on ice (mixture 1). From the mixture in step 1, a 10-fold diluted solution in the same buffer was made (mixture 2). Anti-DNP-EuK was prepared at concentrations of 2.5 and 0.25 nM. The 2.5- and 0.25-nM anti-DNP-EuK solutions

were mixed with a serial dilution of DNP-NHS for 15 min at a 1:1 ratio (preparing series 1 and 2, respectively). Mixture 1 was combined with series 1 (25 μ L each/well) and mixture 2 with series 2 (25 μ L each/well) in a 384-well microplate. The plate was equilibrated at 4°C for at least 1 h.

2.8.2 HTRF Quantification of CCR5

Biotinylated 1D4 mAb (prepared as described (Knepp et al., 2011)) was mixed with XL665-SA for 15 min on ice at a final concentration of 128 nM. To this was added an equal volume of 8 nM EuK-labeled 2D7 mAb (2D7-EuK). For each well of the experiment, 20 μ L of this mixture was added to a black bottom 384-well microplate (Greiner). Solubilized CCR5 or CCR5 in nanoscale apolipoprotein bound bilayers (NABBs) was added to a final volume of 40 μ L. The final concentrations of labeled assay components, except where otherwise noted, were as follows: 32 nM 1D4-biotin, 32 nM XL665-SA, and 2 nM 2D7-EuK. In competition experiments, CCR5 was preincubated with competitors for 30 min on ice prior to addition to fluorescently labeled components in the 384-well plate. To obtain the maximal signal, we incubated the plate overnight at 4°C.

2.8.3 HTRF Signal Analysis

Dual-channel fluorescence was measured with excitation at 320 nm and emission collection in ten 200 μ s windows at 615 and 665 nm. An acceptable signal-to-background ratio was achieved with 5000 flashes per well. Emission counts were summed over all

windows except the first, and the F_{665}/F_{615} ratio was used as a normalized measure of sensitized emission. As an assay-to-assay control, signal enhancement ΔF was calculated:

$$\text{Eq. 1} \quad \Delta F = \left(\frac{F_{665, \text{sample}}}{F_{615, \text{sample}}} - \frac{F_{665, \text{negative}}}{F_{615, \text{negative}}} \right) \div \frac{F_{665, \text{negative}}}{F_{615, \text{negative}}}$$

where the negative control values are obtained from the mixed labeled components in the absence of receptor.

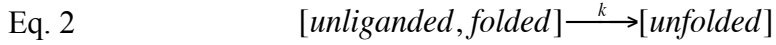
2.9 Thermal Stability Measurements

2.9.1 Experimental Procedure

Detergent-solubilized CCR5 or CCR5 NABBs were diluted to a concentration within the dynamic range of the HTRF assay, and 11 μL aliquots were added to PCR tubes. For experiments testing the stabilizing effects of the small molecule antagonists maraviroc, AD101, CMPD 167, vicriviroc, and TAK-779, the receptor was preincubated with 8 μM ligand for 1 h on ice before the next step. The CCR5-containing tubes were transferred to a Multigene Gradient Thermal Cycler (Labnet International, Inc.). The thermal cycler was set up to apply a gradient of temperatures across a row of the heating block for 30 min except where indicated, followed by cooling to 4°C. Each sample was diluted by a factor of 2 in the appropriate buffer, and 20 μL of the heat-treated material was added to each well of a 384-well microplate containing 20 μL of the fluorescently labeled HTRF components.

2.9.2 Modeling Thermal Denaturation of CCR5

Denaturation of unliganded CCR5 in detergent solution and NABBs was modeled as a simple first order process.



The HTRF signal ΔF is the sum of contributions from folded and unfolded receptor with appropriate scaling factors.

$$\text{Eq. 3} \quad \Delta F = \alpha_1 [\text{unliganded, folded}] + \alpha_2 [\text{unfolded}]$$

Because denatured receptor does not bind 2D7-EuK, α_2 was set to zero. The signal is then:

$$\text{Eq. 4} \quad \Delta F = \alpha_1 e^{-kt}, \text{ with}$$

$$\text{Eq. 5} \quad k = A e^{-E_a/RT}.$$

The curve was fit with parameters α_1 , A , and E_a ; T_M was defined as the temperature at which one-half of the receptor is unfolded. The time of incubation is designated as t .

The temperature of incubation, T , was specified in Kelvin.

Melting of CCR5-ligand complexes was modeled similarly, but as a two-step sequence with a first order reaction describing the irreversible conversion of the “loose” and “tight” binding states, and a second irreversible denaturation step from the tight state. This model assumes that no unliganded receptor exists in the system, which is likely to be true because of the high affinity of the antagonists tested.



The HTRF signal in this system is the sum of contributions from these three species.

$$\text{Eq. 7 } \Delta F = \alpha_1[\textit{liganded, loose, folded}] + \alpha_2[\textit{liganded, tight, folded}] + \alpha_3[\textit{unfolded}]$$

Again, the scaling factor for unfolded receptor, α_3 , was set to zero, making the total signal:

$$\text{Eq. 7 } \Delta F = \alpha_1 e^{-k_1 t} + \alpha_2 \left[\frac{k_1}{k_2 - k_1} (e^{-k_1 t} - e^{-k_2 t}) \right], \text{ with}$$

$$\text{Eq. 8 } k_1 = A_1 e^{-E_{a,1}/RT} \text{ and}$$

$$\text{Eq. 9 } k_2 = A_2 e^{-E_{a,2}/RT} .$$

The curve was fit in Origin with parameters, α_1 , A_1 , $E_{a,1}$, α_2 , A_2 , and $E_{a,2}$; T_M was defined as the temperature at which one-half of the receptor is unfolded. It is important to note that these models assume that the conversion from the loosely to the tightly bound state and the denaturation are irreversible processes. Moreover, we restrict our interpretation of the model to a single derived parameter, the apparent melting temperature T_M .

2.10 Immunoblot Analysis

Samples were resolved by sodium dodecyl sulfate-polyacrylamide gel electrophoresis (SDS-PAGE) (NuPage Novex 4-12% Bis-Tris Gel) and transferred onto Immobilon, a polyvinylidene difluoride (PVDF) membrane (Millipore), according to the manufacturer's protocol. Membranes were probed with primary antibodies followed by a horseradish peroxidase (HRP)-conjugated anti-mouse secondary antibody (Amersham Biosciences GE; 1:10000). Primary antibodies used were 1D4 (National Cell Culture Center, 1:5000) and α -His₆ (Sigma, 1:5000). Signals were visualized by enhanced chemiluminescence treatment (Amersham Biosciences GE) and exposed to HyBlot CL

autoradiography film (Denville Scientific, Inc.).

2.11 Cell Surface Enzyme-Linked Immunosorbent (ELISA) Assay

One day post-transfection, cells were harvested from 10 cm plates in DMEM with 10% FBS and transferred to a 96-well flat, clear bottom plate pre-coated with poly-D-lysine (100 μ L; 60000 cells/well). 48 h post-transfection, cells were washed once with DPBS containing Ca^{2+} and Mg^{2+} . Primary antibody 2D7 was diluted (1:200) in Buffer EL and added for 1.5 h with the plate on ice. The wells were then washed twice with Buffer EL. Cells were fixed with cold 100% MeOH for 5 min on ice, washed twice with DPBS, then once with Buffer EL. Secondary antibody α -mouse-HRP diluted (1:2500) in Buffer EL was added for 1 h at room temperature. The wells were washed with Buffer EL three more times before revealing. The revealing solution was prepared by diluting H_2O_2 and Amplex Red (Molecular Probes) in DPBS to final concentrations of 2 mM and 100 μ M, respectively. Each well of cells was incubated with 50 μ L solution for 15 min at room temperature. The plate was read on a Cytofluor II Fluorescence Multiwell Plate Reader (Perbio Science) with an excitation wavelength of 530 nm and an emission wavelength of 590 nm.

2.12 High-throughput Calcium Flux Assay

2.12.1 Transfection of HEK-293T Cells in a 384-Well Format

HEK-293T cells were transfected in a 384-well flat, clear bottom plate pre-coated with poly-D-lysine according to the following procedure. CCR5 (10 ng/well) and Gqi5 (20 ng/well) plasmid DNA were diluted in DMEM (5 μ L/well). Lipofectamine 2000 (0.075 μ L/well) was diluted in DMEM (5 μ L/well) and incubated for 5 min. The Lipofectamine 2000 solution was added to each DNA mixture at a 1:1 volume ratio for 20 min. Cells were harvested in DMEM and diluted to 800,000 cells/mL. The transfection mixture (10 μ L/well) and cell suspensions (10 μ L/well) were added to the plate, centrifuged for 5 min at 800 rpm, and incubated for 48 h prior to the assay.

2.12.2 Calcium Flux Assay Measurements

Calcium 4 dye (Molecular Devices) was prepared at working concentration in Buffer CF according to manufacturer's protocol, and 20 μ L was added to each well of the assay plate. The plate was centrifuged for 5 min at 800 rpm and incubated for 1 h at 37°C and 5% CO₂. The chemokine ligand, RANTES, was diluted in Buffer CF to three times the desired final concentration. Both the assay plate and ligand plate were transferred to a FlexStation II instrument pre-equilibrated at 37°C. Ligand injections were performed automatically by the instrument, and the change in fluorescence was monitored as a function of time. The percent increase of peak fluorescence after ligand addition compared to baseline was calculated for each time trace.

2.13 [¹²⁵I]-RANTES Binding to Whole Cells

HEK-293T cells expressing CCR5 were harvested 48 h post-transfection in DPBS. Cells were added to a 96-well V-bottom tissue culture plate (600,000 cells/well for low volume assays; 800,000 cells/well otherwise) depending on the concentration of RANTES to be used. At higher ligand concentrations, a lower assay volume was desirable to minimize reagent usage. The plate was centrifuged at 2000 rpm for 5 min and cells were resuspended in either 20 μ L (low volume assays) or 50 μ L Buffer RB. In control experiments, cells were preincubated with 10 μ M maraviroc for 1 h at room temperature prior to chemokine addition. [¹²⁵I]-RANTES was added to the cell suspensions at the desired final concentration and incubated for 1 h at room temperature. Wells were washed at least four times with 200 μ L 1x DPBS. After the last wash, cells were resuspended in 1x DPBS and transferred to scintillation vials. The vials were counted on a Packard Gamma Counter Model 5530.

2.14 Expression and Purification of Zap1

This procedure has been described in detail previously (Banerjee et al., 2008). The *Danio rerio* apolipoprotein A-I gene (*zap1*) in pET28a(+) vector (Stratagene) was transformed into BL21 (DE3) Rosetta 2 *E. coli* cells (Novagen). Colonies were streak purified on LB-agar plates containing kanamycin and chloramphenicol. A single colony was grown in

250 mL LB media containing 50 µg/mL kanamycin and chloramphenicol at 37°C overnight with shaking. The starter culture was diluted 1:100 in 1.6 L of sterilized Terrific Broth media at 37°C with shaking at 180 rpm. Cells were induced with 1 mM IPTG when the OD₆₀₀ reached 0.6 and harvested at an OD₆₀₀ of 1.2. The cell pellet from one flask was resuspended in 150 mL Buffer HZ. At this step, pellets can be stored at -80°C until further use. Cells were disrupted with a French press and lysed with 1% Triton X-100, DNAase I, and 5 mM MgSO₄ for 30 min on ice. Cell extracts were then spun at 16,500 rpm for 45 min at 4°C and the supernatant was filtered with a 0.45 µm syringe filter. Zap1 was initially purified on a Ni-Sepharose 6 FF column (GE) connected to the Äkta Explorer FPLC system. The column was equilibrated with Buffer TZ before loading the supernatant. The Ni column was washed with 10 column volumes (CV) of Buffer CZ and 10 CV of Buffer AZ, then zap1 was eluted with a 0-100% gradient of Buffer BZ in Buffer AZ. Protein-containing fractions from the elution gradient were pooled, concentrated using an Amicon Ultra Centrifugal Filter unit with 10 kDa MW cutoff (Millipore), and further purified on a Superdex 200 26/60 column in Buffer GZ. Fractions were collected and assayed for purity on an SDS-PAGE gel.

2.15 Incorporation of CCR5 into NABBs and Purification

Purified CCR5 in detergent solution (prepared as described in Chapter 2.6) was incorporated into nanoscale apolipoprotein bound bilayers (NABBs) by the following procedure. A number of NABBs mixtures were tested. The recipe below yielded

homogeneous preparations. This mixture is scalable provided the final concentration of zap1 is ≥ 0.5 mg/mL. The molar ratio of zap1:lipids must be held to 1:75.

2.15.1 Preparing CCR5 NABBs

Purified CCR5 was added to 3.75 nmol of zap1, 280 nmol of 1-palmitoyl-2-oleoyl-*sn*-glycero-3-phosphocholine (POPC), and 22.7 nmol of cholesterol in a total volume of 200 μ L containing 1.5% sodium cholate, 0.33% DM, 15 mM Tris-HCl (pH 7.0), 75 mM $(\text{NH}_4)_2\text{SO}_4$, and 7.5% glycerol. When desired, a POPC solution containing 0.5% Lissamine Rhodamine B-labeled 1,2-dioleoyl-*sn*-glycero-3-phosphoethanolamine (LRB-DOPE) was used to allow visualization of NABB elution. After being vortexed and incubated on ice for 30 min, the mixture was added to 1 mL of Pierce Detergent Removal Resin pre-equilibrated with at least 1 column volume of Buffer S. Elution was conducted at 4°C under gravity flow by addition of Buffer S to the column and collection of 200 μ L fractions. Fractions were analyzed for protein content by monitoring the absorbance at 280 nm.

2.15.2 Purification of CCR5 NABBs

Protein-containing fractions were pooled and applied to a Superose 6 10/300 gel filtration column. Absorbance at 280 nm (protein) and, when applicable, 570 nm Lissamine Rhodamine B (LRB-DOPE) was monitored with an in-line detector in the FPLC instrument (Akta Explorer, GE). Fractions of the peak corresponding to NABBs were combined and, if necessary, concentrated using an Amicon Ultra 30 kDa cutoff centrifugal filter device (Millipore).

2.15.3 Immunoprecipitation of CCR5 NABBs with a Conformationally Sensitive Antibody

CCR5 NABBs were mixed with Dynabeads Protein G (Invitrogen) with or without 2D7 mAb (BD Biosciences) according to the manufacturer's protocol. After overnight incubation at 4°C, the supernatant fractions were subjected to 1D4 immunoblot analysis as described in Chapter 2.10.

2.16 Fluorescence Correlation Spectroscopy (FCS)

2.16.1 FCS Sample Preparation and Measurements

FCS samples were loaded into an Ibidi μ -Dish pre-blocked with 5 mg/mL BSA. For low-volume (<10 μ L) samples, a 4 well silicone micro-insert was used and 1 mL of water was added outside the insert to prevent sample evaporation. FCS experiments were performed on a Zeiss LSM 780 inverted confocal microscope using a C-Apochromat 40x / NA 1.2 water objective. ZEN software controlled the system and was used for data analysis. The objective was focused 200 μ m into the sample using reflected laser light. Laser lines, dichroics, emission filters, and fluorescence collection windows were selected based on the fluorophores under study. The 488 nm (Alexa 488), 561 nm (Lissamine Rhodamine B), and 633 nm (Alexa 647) lines were used in the experiments presented. The GaAsP detector was used for emission wavelengths <600 nm, and the PMT detector for

wavelengths >600 nm. The confocal pinhole was set to 1.0 airy unit and automatically aligned by scanning for the highest count rate of each laser line. FCS data were typically acquired for either 10 or 30×10 s windows.

2.16.2 Synthesis of Oligonucleotide FCS standards

FCS control samples were custom synthesized by Fisher Operon. The sequences chosen were:

Forward: GCCGTCTCTGACTGCTGATGACTACTATCGTATAGTGCGG

Reverse complement:

CCGCACTATACGATAGTAGTCATCAGCAGTCAGAGACGGC

Two versions of the forward sequence were generated. The first carried Alexa 488 at the 5' end and biotin at the 3' end. The second carried biotin at the 5' end. Two versions of the reverse complement sequence were also prepared. One was labeled with Alexa 647 at the 5' end and the other with biotin at the 5' end.

2.16.3 Modeling FCS Data

The theory underlying FCS is quite complex and has been described well elsewhere, especially in Lakowicz's *Principles of Fluorescence Spectroscopy* (Lakowicz, 2006).

What follows is a brief summary of the comparatively simple models used to fit the FCS data presented.

The autocorrelation function $G(\tau)$ of fluorescence intensity time traces $I(\tau)$ is defined as:

Eq. 9
$$G(\tau) = \frac{\langle I(t)I(t+\tau) \rangle}{\langle I(t) \rangle^2}$$

where the brackets indicate a time average. Substituting $I(t) = \langle I \rangle + \delta I(t)$, $G(\tau)$ can be rewritten as:

Eq. 10
$$G(\tau) = 1 + \frac{\langle I(t)I(t+\tau) \rangle}{\langle I \rangle^2}$$

A satisfactory analytical expression for the data in this work includes contributions from triplet blinking, $G_T(\tau)$, and translational diffusion, $G_D(\tau)$:

Eq. 11
$$G(\tau) = 1 + \frac{\gamma}{\langle N \rangle} G_T(\tau) G_D(\tau)$$

with $\langle N \rangle$ the average number of particles in the focal volume. The factor γ was set to 0.35, typical for one-photon FCS.

The expression for $G_T(\tau)$ is:

Eq. 12
$$G_T(\tau) = 1 + \frac{T_t e^{-\tau/\tau_T}}{1-T_t}$$

with T_t the fraction of molecules in the triplet state and τ_t the triplet state relaxation time.

For a single species freely diffusing in three dimensions, $G_D(\tau)$ is written as:

Eq. 13
$$G_D(\tau) = \left(1 + \left(\frac{\tau}{\tau_D}\right)\right)^{-1} \left(1 + \left(\frac{\tau}{\tau_D}\right) \frac{1}{S}\right)^{-1/2}$$

where τ_D is the diffusional correlation time and S is the structural parameter defined as the ratio of the axial focal radius w_z to the lateral focal radius w_r :

Eq. 14
$$S = w_z/w_r.$$

The expression is more complicated for two diffusing species:

Eq. 15
$$G_D(\tau) = \frac{N_1 B_1^2 D_1(\tau) + N_2 B_2^2 D_2(\tau)}{(N_1 B_1 + N_2 B_2)^2}$$

where $D_i(\tau)$ and B_i are the diffusion expression and brightness of each species, respectively.

Before fitting the data, the individual time traces were examined to confirm stationarity; that is, the intensity does not deviate abnormally from the mean, nor drift to higher or lower levels over the course of the measurement. Typically, fits began at $\tau = 1.6$ or $3.0 \mu\text{s}$ to avoid detector noise effects.

In most fits the structural parameter S was fixed based on calculations from standard experiments. The effective focal volume V is simply:

$$\text{Eq. 16} \quad V = m\gamma / N_A$$

where m is the slope of a plot of calculated $\langle N \rangle$ vs. dye concentration and N_A is Avogadro's number. The lateral focal radius is determined from the observed diffusional correlation time:

$$\text{Eq. 17} \quad w_{xy} = \sqrt{4\tau_D D}$$

where D is the known diffusion coefficient.

The structural parameter S is then:

$$\text{Eq. 18} \quad S = V / \left(\pi^2 w_{xy}^3 \right)^{1/3}$$

2.17 Crosslinking and Proteolysis of Rod Outer Segment (ROS) Membranes

2.17.1 Biochemical Crosslinking of ROS Membranes

The following homobifunctional crosslinkers were used: BM(PEG)₃ (Pierce), Bis-MAL-dPEG₃ (Quanta Biodesign), and MTS-O4-MTS/MTS-O5-MTS (Toronto Research

Chemicals, Inc.). Bovine ROS membranes were prepared as described (Bigay and Chabre, 1994). The membranes were suspended at a concentration of 1.6 mg/mL in Buffer C. The crosslinking reagents were solubilized in DMSO and added to a final concentration of 200 μ M (5-fold molar excess) in the dark. The bis-maleimide reactions proceeded for 24 h at room temperature before quenching with 10 mM cysteine. The MTS reactions were allowed to proceed for 5, 15, or 60 min at room temperature before quenching with 20 mM N-ethylmaleimide. In control samples, the MTS reactions were treated with 100 mM DTT after crosslinking to cleave the disulfide linkages.

2.17.2 Partial Proteolysis of ROS Membranes

The site of the crosslink was determined, in part, by partial proteolysis with thermolysin in the dark. Crosslinked ROS membranes were resuspended in Buffer T. Thermolysin was added at a rhodopsin-to-thermolysin ratio of 50:1 by mass. The digestion proceeded for 6 h at 37°C and was stopped by adding 5 mM EDTA and placing the tubes on ice. Prior to SDS-PAGE analysis, samples were solubilized in 1% DM. Samples were resolved on NuPage Novex 4-12% Bis-Tris gels. Coomassie Blue and silver staining were carried out with standard protocols.

2.18 Liquid Chromatography-Mass Spectrometry (LC-MS)

2.18.1 LC-MS Sample Preparation

Sample preparation for LC-MS was based on a previous study (Kraft et al., 2001).

Crosslinked ROS membranes were solubilized in 1% DM and bleached. Bis-maleimide samples and the MTS negative controls were treated with 15 mM DTT for 1 h, and all samples were treated with iodoacetamide (100 mM) for 3 h. Rhodopsin was precipitated with 10% TCA and spun at 14k rpm in a tabletop centrifuge for 5 min to produce a pale yellow pellet. The pellet was washed with 95% ethanol in a bath sonicator three times to remove TCA and lipids. The pellet was then dissolved in 100% TFA containing 500 molar excess CNBr per rhodopsin methionine in the sample. Water was added to give a final concentration of 80% TFA, and the digestion proceeded overnight. Samples were dried with argon and desiccation. When ready for LC-MS analysis, the dried precipitate was resuspended in 20 μ L ddH₂O.

2.18.2 LC-MS Measurements

The samples were loaded onto a C18 5 μ m trap column (LC Packings) and run at 30 μ L/min, then on an in-house made C18 analytical column (75 μ m diameter beads) at 0.2 μ L/min. Solvent A was water + 0.1% formic acid and solvent B was acetonitrile + 0.1% formic acid, and elution proceeded from 5-40% B over 35 min. MS was performed with 5 μ L injections onto a LTQ Orbitrap XL (Thermo Scientific) with ion trap. The mass range was 400-1600 m/z.

2.18.3 LC-MS Data Analysis

LC-MS data were analyzed on Xcalibur software (Thermo). Mass spectrometry data are recorded as mass-to-charge ratios (m/z), but charges can be assigned to sets of isotope peaks based on the distance between them. All charges were automatically calculated by

the software and multiplied by the m/z values to yield absolute experimental masses. Theoretical monoisotopic masses were calculated using the online Mole Molecular Mass Calculator. Masses were calculated for the peptide of interest and the crosslinkers with several chemical modifications, isotopes, and protonation states. The experimental data were screened for these possibilities. Matches were only assigned if the peaks were within 25 ppm error of the theoretical mass and not present in negative control samples.

Chapter Three: A High-Throughput Method to Measure CCR5 Stability and Characterization of Thermally Stable Mutants*

3.1 Introduction

Decoding the complex allostery and signaling behavior of GPCRs requires advances in both structural and biophysical studies. Despite high structural homology, the utility of models from existing GPCR structures is somewhat limited (Patny et al., 2006). Subtle differences in the ligand-binding pocket between subtypes can have a large effect on specificity. High-resolution structures provide insight into the uniqueness of each receptor, perhaps enabling development of more potent and specific drugs. However, static portraits cannot tell the full story of GPCR signaling. GPCRs are conformationally flexible, and the stabilization of and exchange between states is key to their function. Dynamic studies of receptor activation and coupling between the ligand binding pocket and intracellular surface are needed to understand this finely tuned allostery. Fluorescence techniques are ideally suited for this task.

GPCRs present significant technical challenges that impede progress in both these

* Portions of this chapter have been published previously: Knepp AM, Grunbeck A, Banerjee S, Sakmar TP and Huber T (2011) Direct Measurement of Thermal Stability of Expressed CCR5 and Stabilization by Small Molecule Ligands. *Biochemistry* **50**:502-511. Knepp AM, Sakmar TP and Huber T (2013) Homogeneous time-resolved fluorescence assay to probe folded G protein-coupled receptors. *Methods in Enzymology* **522**:169-189.

threads of research. X-ray crystallography requires milligram quantities of pure, homogeneous sample, but with the exception of rhodopsin, GPCRs are expressed at low levels in native tissues (Chiu et al., 2008). This makes sense from a physiological perspective; very high expression would presumably disrupt the sensitive and interconnected signaling pathways that GPCRs regulate. Further, GPCRs are generally not modular structures. That is, constructs cannot be divided into fragments and reconstituted after purification. Recombinant expression systems for full-length GPCRs are therefore a necessity. Unfortunately, efforts to produce GPCRs in the workhorse expression system *E. Coli* typically result in misfolded protein (Lundstrom et al., 2006), perhaps because bacteria lack the proper chaperone and post-translational machinery to generate functional receptor. Expression in insect cells has fared better – a number of GPCRs have been successfully overexpressed and purified from Sf9 cells, including CCR5 (Nisius et al., 2008). In theory, mammalian cells should be the ideal expression system of choice. While these cell cultures generate samples with high levels of activity, they are difficult to scale effectively and heterogeneity of post-translational modifications can make crystallization exceedingly difficult. Generation of cell lines with more uniform glycosylation profiles, as has been achieved with rhodopsin, can circumvent this problem (Reeves et al., 2002). Still, doing so may require considerable effort.

Stabilizing GPCRs outside of their native environments poses an even greater challenge, and one that affects both structural and biophysical work. As with any membrane protein, detergents must be used in solubilization to disrupt the biological membrane and to mimic the amphipathicity of the bilayer. GPCRs are fragile structures, however, and detergents are a poor substitute for the membrane. Solubilization thus often

results in unfolding and aggregation. Careful selection of lipid/detergent mixtures can result in satisfactory preparations, but because successful conditions cannot be predicted *a priori*, identifying them is an empirical process. Protein engineering tricks have been employed to improve stability, including truncations or deletions of disordered regions, insertion of domains such as T4 lysozyme, formation of a complex with an antibody Fab fragment, ligand binding, and introduction of a combination of stabilizing mutations (Rosenbaum et al., 2009). The success of these strategies must be experimentally evaluated as well.

Because of the large number of potentially stabilizing conditions and the protein expression limitations discussed above, assays to measure sample quality should be robust, high-throughput, and require small amounts of material. Thermal stability assays are a useful way to analyze the comparative effectiveness of conditions. Typically, samples are heat-treated and some readout parameter is plotted as a function of temperature. The apparent melting temperature, T_M , represents a proxy for sample stability. While unfolding of the prototypical GPCR rhodopsin can be monitored by UV-Vis spectroscopy – loss of binding of the chromophore 11-*cis* retinal results in the disappearance of a characteristic peak – other GPCRs do not contain an intrinsic probe for proper folding. More general techniques to measure structural changes during denaturation include ligand binding, changes in cysteine reactivity, static light scattering, and surface plasmon resonance, among others (Alexandrov et al., 2008; Navratilova et al., 2005; Serrano-Vega et al., 2008; Vedadi et al., 2006). These approaches often require micrograms per assay, quantities that can quickly become prohibitive for GPCRs.

Fluorescence resonance energy transfer (FRET) is a highly sensitive method to

monitor protein-protein binding. Homogeneous time-resolved fluorescence between a europium cryptate (EuK) donor and a modified allophycocyanin (XL665) acceptor bears particular advantages. EuK has a very long fluorescence lifetime (up to 1 ms), reducing the negative effects of autofluorescence on the signal-to-background ratio. This FRET pair also has an unusually large Förster radius, permitting signal detection even if relatively long distances separate the donor and acceptor. HTRF has previously been used to monitor ligand binding to GPCRs in cell membranes, as well as in secondary messenger assays of downstream signaling (Albizu et al., 2007; Devigny et al., 2011).

The HTRF technology was applied to develop an assay suitable for rapid and sensitive screens of GPCR foldedness. The method was developed for the target receptor CCR5, but with the expectation that the overall approach should be applicable to other GPCRs and membrane proteins in general. Despite its importance in immunology and HIV-1 viral entry, no high-resolution structure of CCR5 is available. In fact, it has proven to be a particularly challenging receptor to study due to its instability. Like other non-rhodopsin GPCRs, CCR5 does not possess an internal reporter of functionality. In addition, its native ligands, chemokines, are small proteins that are difficult to express and label. Thus, rather than rely on ligand binding, we elected to use anti-receptor monoclonal antibodies as reporters of proper folding. The 2D7 antibody was developed as an anti-HIV entry blocker and binds a conformationally sensitive epitope on the second extracellular loop (Khurana et al., 2005; Lee et al., 1999). The 1D4 antibody recognizes the C-terminal nine residues of rhodopsin, an epitope that can be engineered into other GPCRs (Molday and Mackenzie, 1983).

The quantitative assay was developed with several goals in mind. The original

objective was functional reconstitution of CCR5 into membrane nanoparticles called NABBs, which were developed as a platform for studying membrane proteins in a native-like environment (Banerjee et al., 2008). Challenges during purification and subsequent evaluation of receptor quality motivated this work. The incorporation of CCR5 into NABBs, demonstration of receptor integrity, and applications are discussed in detail in Chapter 4.

Two additional applications emerged once the full utility of the HTRF technique became apparent. One was identification of mutations that thermally stabilized CCR5. This project was undertaken in collaboration with Heptares Therapeutics with the end goal being the first crystal structure of CCR5. Mutagenesis carries notable advantages over other approaches to stabilize GPCRs. Unlike fusion constructs or complexes with bulky Fab fragments, a combination of point mutations does not necessarily result in large structural perturbations. In particular, the intracellular region involved in binding heterotrimeric G proteins need not be significantly altered. In addition, mutations can be identified that stabilize a single preferred receptor conformation (Robertson et al., 2011), with ligand-binding and cell based assays used to evaluate receptor states. Thermally stabilized mutants, called StaRs, have been identified for several GPCRs and led to crystal structures of the β_1 -adrenergic receptor and adenosine A_{2A} receptor (Dore et al., 2011; Warne et al., 2008). Several stable CCR5 constructs were identified; data from the functional assays I used to characterize them are presented in this chapter.

A third application involved the determination of the allosteric relationship between anti-HIV entry antibodies and small molecule drugs. In experiments measuring the stabilizing effect of small molecule binding, the molecules appeared to induce unique

receptor conformations. This had been suggested in earlier studies involving native chemokine binding (Watson et al., 2005). Better understanding of this behavior has implications for HIV therapy with respect to both synergism of antiviral activity and perhaps in avoiding viral resistance to a particular receptor conformation (Ji et al., 2007).

3.2 Results

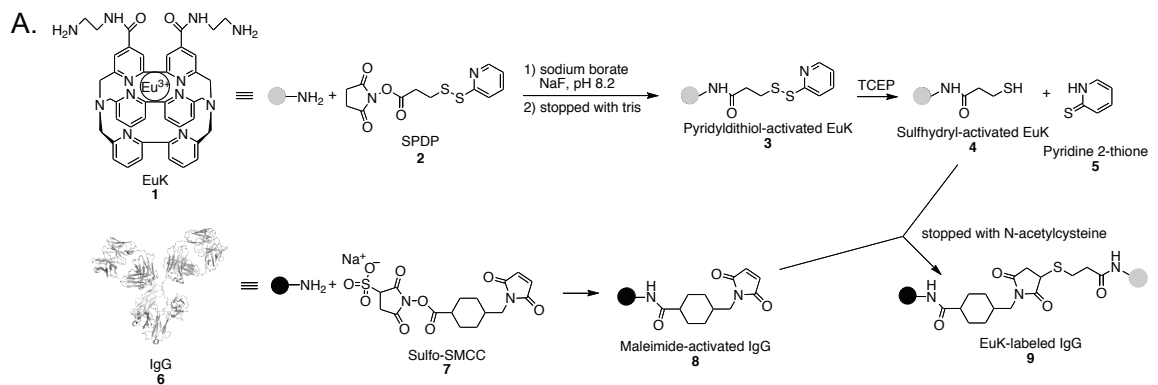
3.2.1 Solid-phase labeling of IgG

We first developed a scalable procedure for labeling small amounts of IgG with EuK. IgG molecules bind magnetic Ni-NTA beads through a conserved histidine-rich region of the Fc stem. For the CCR5 HTRF assay, we labeled 2D7 mAb with EuK. 2D7 and EuK were activated separately before combining for the final conjugation: 2D7 with sulfo-SMCC and EuK with SPDP. This strategy was chosen because we found that reducing SPDP to produce the free thiol resulted in significant breaking of IgG disulfide linkages. When EuK is activated with SPDP, TCEP treatment is carried out in the absence of IgG and antibody integrity is preserved. The overall reaction scheme is shown in Figure 3-1A.

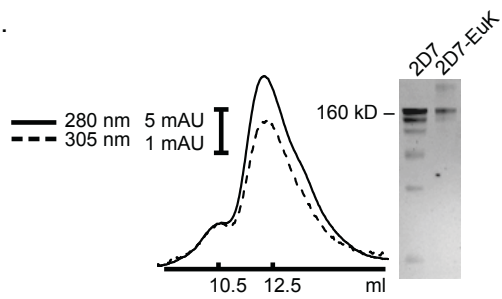
The labeled IgG was first analyzed by nonreducing SDS-PAGE (Figure 3-1B). The gel shows that the chosen labeling strategy results in minimal fragmentation. In fact, the labeled product appears not to contain some lower molecular weight species that were present in the original sample. The product was supplemented with 0.5 mg/mL BSA and

Figure 3-1. (A) Scheme depicting strategy to synthesize EuK-labeled 2D7 mAb (**9**). EuK (**1**) is activated by addition of a sulfhydryl by reaction with SPDP (**2**) and reduction by TCEP (top). Separately, 2D7 mAb (**6**) is immobilized on Ni-NTA resin and reacted with sulfo-SMCC (**7**) to generate a maleimide derivative (**8**). A crystal structure of IgG (PDB ID: 1IGY) is shown as a model. The two activated reagents are combined and labeled 2D7 is eluted from the resin with imidazole. (B) Left: Size-exclusion chromatography with monitoring of absorbance at 280 nm (solid; protein) and 305 nm (dashed; EuK) to determine yield and labeling ratio. Right: Coomassie blue-stained non-reducing SDS polyacrylamide gel electrophoresis showing a single band of the intact 2D7-EuK after labeling. Note the impurities of the initial 2D7 sample have been largely removed by the procedure. (C) Fluorescence of purified, EuK-labeled antibodies. SEC fractions (400 μ L) were collected from 8-19 mL elution and EuK emission was measured at 615 nm. They also revealed some sample heterogeneity. The main peak is monomeric 2D7-EuK, and the earlier and later peaks are presumed to be dimeric and fragmented IgG, respectively.

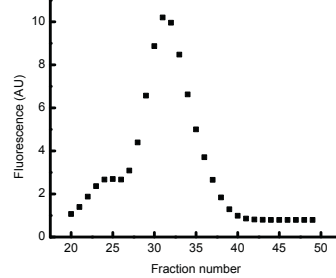
Figure 3-1



B.



C.



loaded onto a Superdex 200 10/300 GL gel filtration column equilibrated with Buffer G. We found that using BSA as a carrier protein significantly improved recovery of the microgram sample quantities. This column resolves samples in this molecular weight range well. Absorbance was monitored at 280 and 305 nm for protein and EuK (Figure 3-1B). Using known molar extinction coefficients, an approximate labeling ratio of 1.3 EuK/IgG was calculated (Lopez-Crapez et al., 2008).

To further confirm the presence of EuK, size exclusion chromatography (SEC) fractions were collected and loaded into a microplate, and fluorescence was measured. The peak profile corresponds very well to UV absorbance off of the column (Figure 3-1C). The fluorescence points were fit to three Gaussian peaks to determine the fractions most likely to contain monomer. We estimated that 30 μg of labeled 2D7 monomer (~90% of the total protein content) were ultimately pooled.

Having successfully established the solid-phase labeling strategy for this particular antibody and probe, we sought to generate other useful reagents by the same method. The 1D4 and α -FLAG antibodies, as well as a second α -CCR5 mAb, 3A9, were conjugated to EuK with similar results. In addition, 1D4 and 2D7 were labeled with Alexa Fluor 488 and 647 dyes carrying a reactive cadaverine moiety. Comparable yields and labeling ratios were achieved for these conjugations. UV-Vis spectra of eluted products are shown in Figure 3-2. These reagents could be useful in a wide range of assays, including fluorescence-activated cell sorting (FACS), immunofluorescence, FCS, and TIRF imaging.

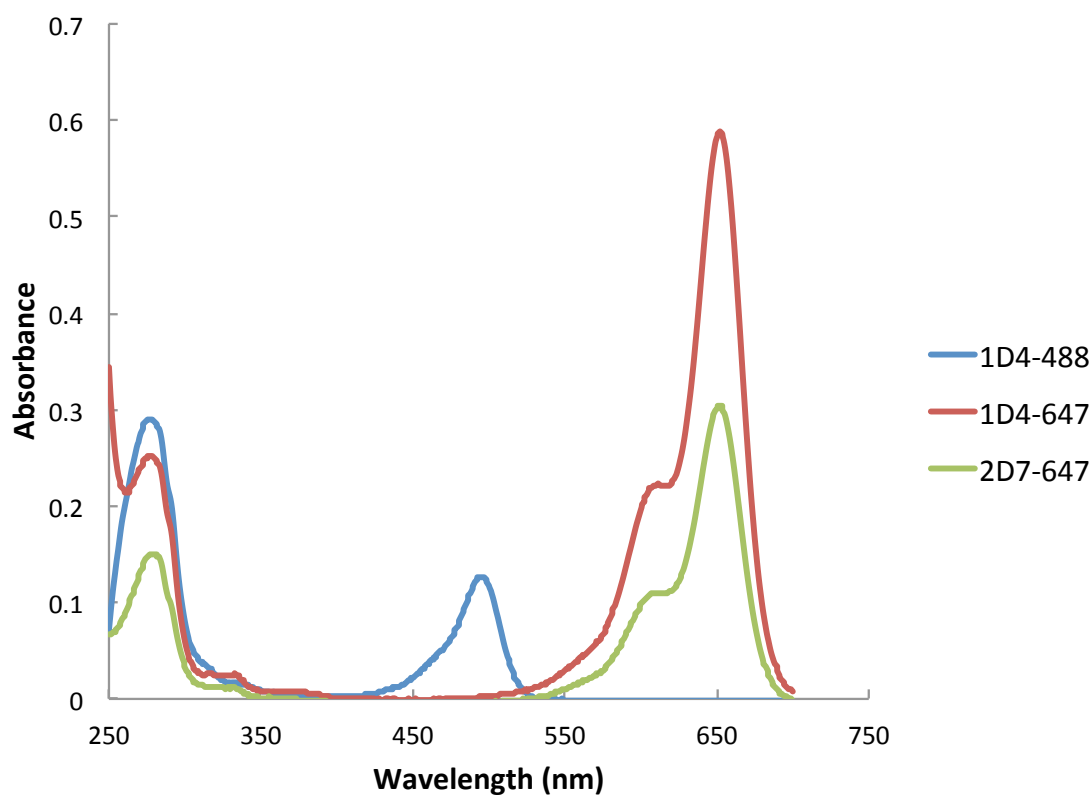


Figure 3-2. UV-Vis spectra of purified antibodies labeled with Alexa Fluor dyes using the solid-phase method. 1D4-Alexa 488 (blue), 1D4-Alexa 647 (red), and 2D7-Alexa 647 (green) are shown. Using the peak absorbances and known molar extinction coefficients, the labeling ratios were determined to be 1.3, 2.1, and 1.8 fluorophores/antibody for 1D4-488, 1D4-647, and 2D7-647, respectively. These values are in line with results obtained with europium cryptate labeling, indicating the generality of the procedure.

3.2.2 HTRF Assay to Quantify Properly Folded GPCRs

Signal detection was first optimized in a system similar to the immunosandwich in Figure 3-3. The standard experiment used anti-DNP-EuK, DNP-NHS, biotin-BSA, and XL665-SA. Biotin-BSA-DNP was prepared by reacting DNP-NHS with biotin-BSA. This reagent binds the EuK-labeled antibody and links to XL665 through a biotin-streptavidin interaction, bringing the donor and acceptor into proximity. We reasoned that initial signal detection would be easier in this scheme because biotin-BSA-DNP is smaller than the analogous CCR5-1D4 complex shown in Figure 3-3. Competition with DNP-NHS, which does not bind XL665-SA, was used to demonstrate the specificity of the observed HTRF signal. The signal enhancement ΔF was calculated using the wells with a saturating concentration of DNP-NHS as a negative control. Figure 3-4 shows the results of the standard experiment. A maximum ΔF of approximately 5 is observed in the experiment with higher concentrations of EuK and XL665. The competition curves demonstrate the specificity of the HTRF signal, and its robustness suggests that the fluorescence acquisition parameters are suitable. After establishing these conditions, the more complex immunosandwich with expressed CCR5 was characterized.

The donor/acceptor fluorescence, time-dependence, dynamic range, and specificity of the CCR5 assay were all measured using the acquisition settings outlined in Chapter 2.8.3. These quality control checks were necessary to ensure that the fluorescence signal accurately reflects the quantity of folded target receptor. As controls, the fluorescence at 615 and 665 nm was measured in the presence and absence of 1D4-biotin, XL665-SA, 2D7-EuK, and CCR5 (Figure 3-5A). The bars show that 1D4-biotin and XL665-SA in the absence of the EuK donor results in minimal counts at 615 nm and

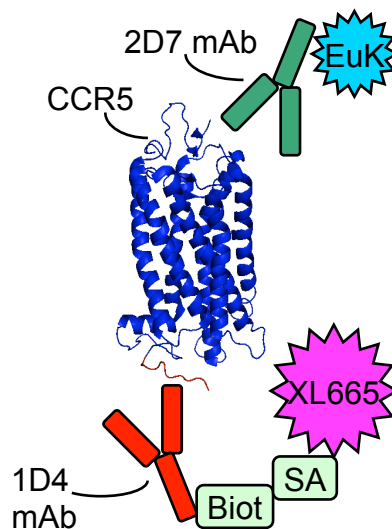


Figure 3-3. HTRF sandwich immunoassay schematic. A hypothetical model of CCR5 based on the crystal structure of rhodopsin (PDB ID: 1U19) is shown. 2D7-EuK recognizes a conformation-sensitive split epitope on the extracellular side of CCR5. Biotinylated 1D4 (1D4-biot) binds an engineered nine-residue C-terminal epitope and is linked to streptavidin-conjugated XL665. FRET is observed between EuK and XL665 when 2D7 binds properly folded CCR5. The Förster radius for this donor-acceptor pair is approximately 95 Å.

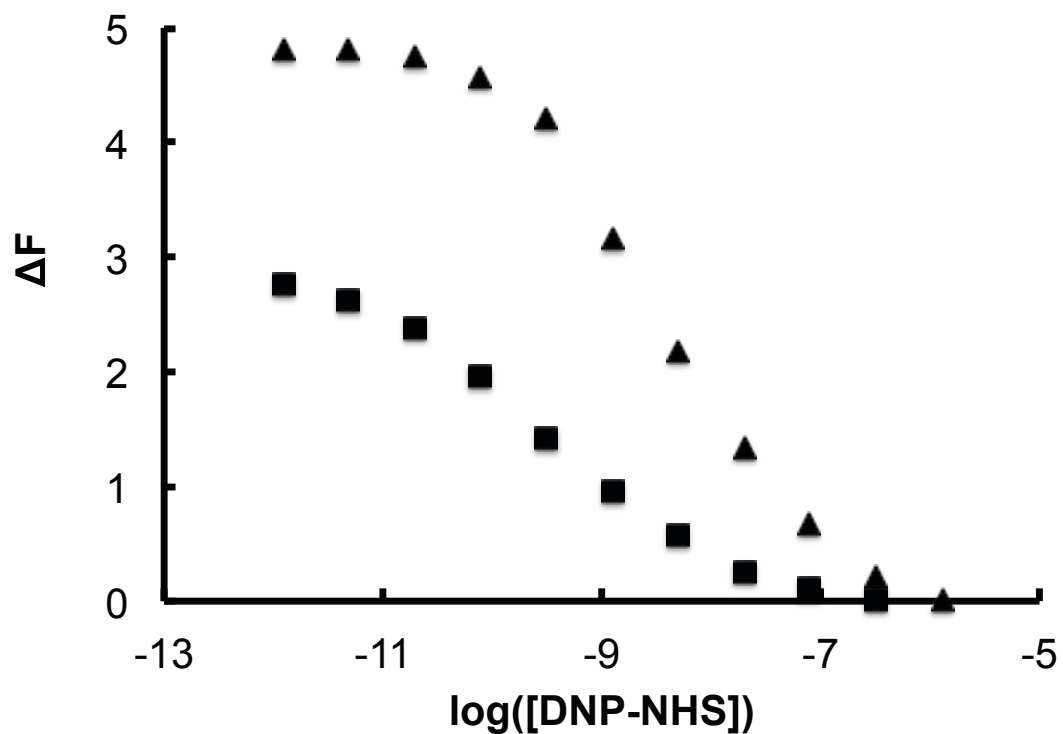


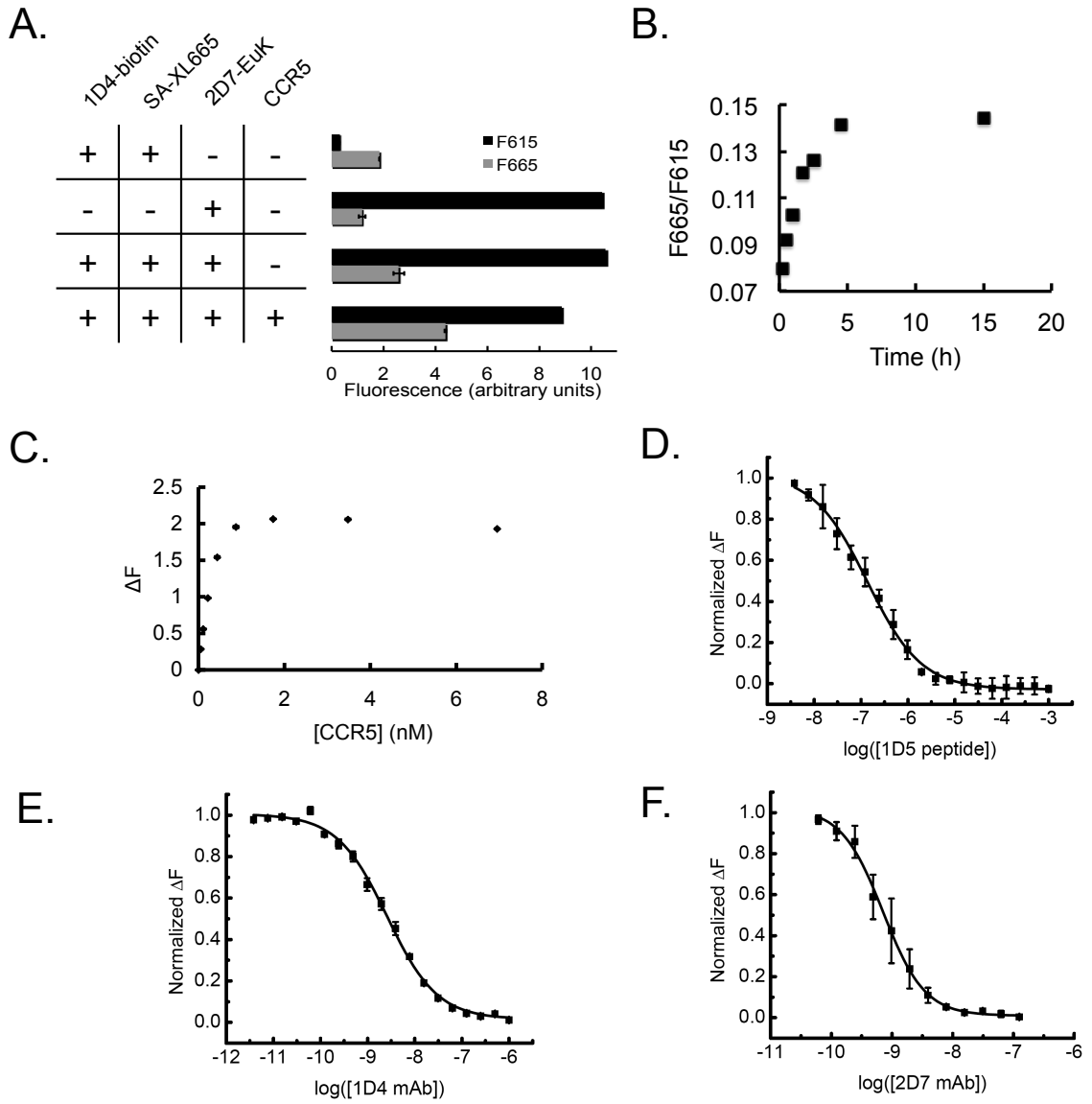
Figure 3-4. HTRF standard experiment with donor anti-DNP-EuK and acceptor XL665-SA. The fluorophores are brought in proximity by biotin-BSA-DNP. Two different concentrations of donor and acceptor were used: 0.625 nM anti-DNP-EuK/2.5 nM XL665-SA/1.25 nM biotin-BSA-DNP (triangles) and 0.0625 nM anti-DNP-EuK/0.25 nM XL665-SA/0.125 nM biotin-BSA-DNP (squares). The curves depict the competition of biotin-BSA-DNP with DNP-NHS, which does not link to XL665-SA.

Figure 3-5. (A) Assay controls with fluorescence counts at 615 nm (black) and 665 nm (gray) after excitation at 320 nm. CCR5-specific signal is seen as a signal increase at 665 nm and decrease at 615 nm. (B) Time course of HTRF signal with detergent-solubilized CCR5. After loading samples into a 384-well microplate, fluorescence was measured at the indicated time points. The plate was stored at 4°C between readings. (C) A serial dilution of CCR5 shows the dynamic range of the assay. The signal saturates at ~200% enhancement over background. ΔF is defined as:

$$\Delta F = \left(\frac{F_{665, sample}}{F_{615, sample}} - \frac{F_{665, negative}}{F_{615, negative}} \right) \div \frac{F_{665, negative}}{F_{615, negative}}$$

(D-F) Competition experiments with the 1D5 nonapeptide (D), 1D4 mAb (E), and 2D7 mAb (F) demonstrate signal specificity.

Figure 3-5



some emission at 665 nm. 2D7-EuK without acceptor gives a strong signal at 615 nm and some bleed-through at 665 nm. When these three components are combined in the absence of CCR5, the 615 nm signal is close to that of 2D7-EuK alone, and the 665 nm is only slightly greater than of the acceptor alone. This suggests that minimal FRET occurs without the receptor to bring the donor and acceptor near each other. In the presence of CCR5, sensitized emission is observed, with a decrease in 615 nm fluorescence and increase at 665 nm. This results in an increased F_{665}/F_{615} ratio. The time course of the CCR5-dependent signal was measured (Figure 3-5B). The signal increases significantly during the first few hours of incubation at 4°C as the system equilibrates, and is then stable overnight. For maximum signal-to-background and assay reproducibility, plates were incubated for 12–16 h before fluorescence measurement.

For quantification applications, the dynamic range of the signal must be determined (Figure 3-5C). This was done by incubating labeled components with a serial dilution of detergent-solubilized CCR5. A linear range precedes signal saturation near $\Delta F = 2$. The signal was calibrated to an absolute concentration by incubating receptor immobilized on 1D4-Sepharose beads with a high-affinity fluorescent antagonist FL-maraviroc. The amount of CCR5 in cell lysate was estimated to be 13.9 ± 0.2 nM by comparing the fluorescent signal in the elution to a FL-maraviroc standard curve (Figure 3-6). This concentration represents a lower bound, though we assume that all folded receptor can bind the high-affinity ligand. With this value, we estimated that 0.02–1.0 nM CCR5 can be effectively quantified in the HTRF assay, which corresponds to 0.8–40 fmol in a volume of 40 μ L. The assay is therefore remarkably sensitive. In subsequent experiments, receptor concentrations near the middle of the dynamic range were used to

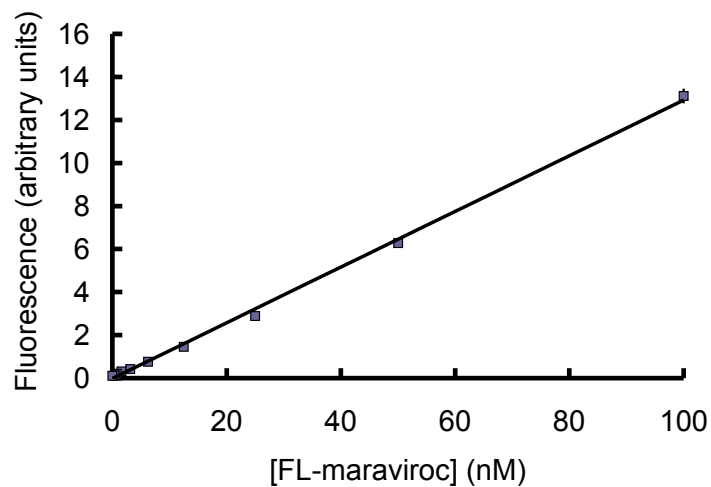


Figure 3-6. FL-maraviroc standard curve used to bring the HTRF signal to an absolute scale. A serial dilution of FL-maraviroc was used to generate the curve. CCR5 was immobilized on 1D4 mAb-Sepharose beads and incubated with a saturating concentration of FL-maraviroc. The concentration of CCR5 was back-calculated from the standard curve.

minimize measurement errors.

The specificity of the HTRF signal was determined in competition experiments with a serial dilution of TETSQVAPA nonapeptide (“1D5”), 1D4, and 2D7 (Figure 3-5D-F). Signal enhancement ΔF was normalized to the end points of 0% and 100% inhibition. The data were fit to sigmoidal curves, and the IC_{50} values for 1D5, 1D4, and 2D7 were 130, 2.7, and 0.79 nM, respectively. Having demonstrated the sensitivity and specificity of the signal, we next focused on applying the technology to measure receptor stability.

3.2.3 High-throughput Measurement of CCR5 Thermal Stability

CCR5 stability over time was first measured in buffer containing only 1% DM and in the more complex lipid-detergent mixture Buffer N. Results are shown in Figure 3-7. Aliquots were stored at 4°C for the time indicated prior to measurement. Time points shorter than the time necessary to equilibrate CCR5 with the labeled antibodies are not accessible, but the longer-term trends are observable. Whereas CCR5 in DM alone denatures over the course of several days, CCR5 in Buffer N is remarkably stable. This shows additional buffer components may be necessary to achieve optimal GPCR stability, motivating high-throughput screening techniques such as the one described.

Thermal stability is a crucial indicator of receptor tractability outside of its native membrane environment. We adapted the HTRF assay to measure CCR5 thermal stability under a variety of conditions. In short, a range of temperatures was applied to CCR5 aliquots for 30 min, and then the samples were cooled to 4°C and added to the microplate containing the labeled 1D4 and 2D7 FRET pair. Plotting the ratio of the fluorescence

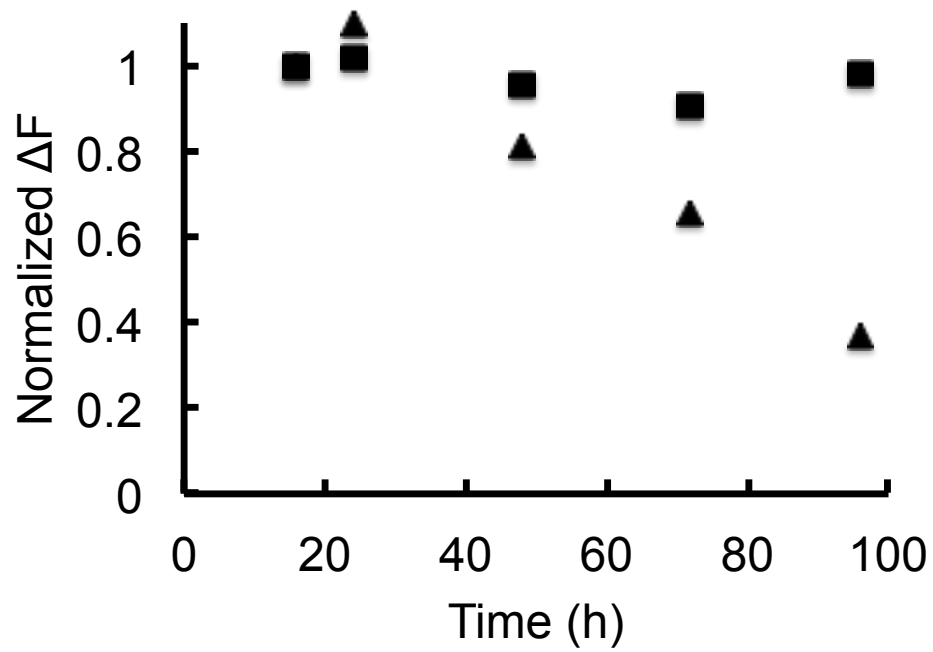


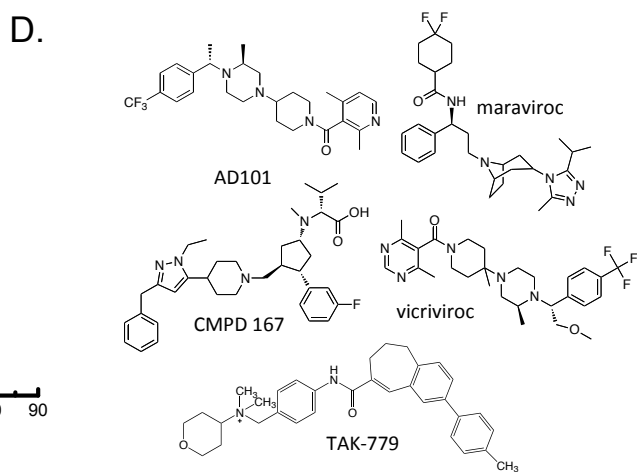
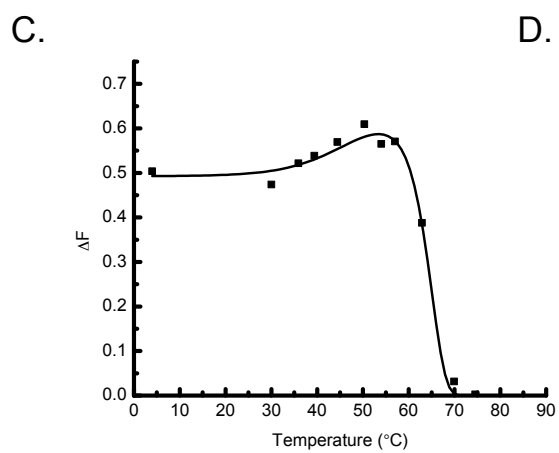
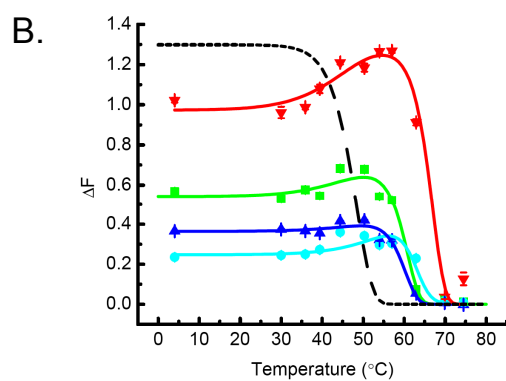
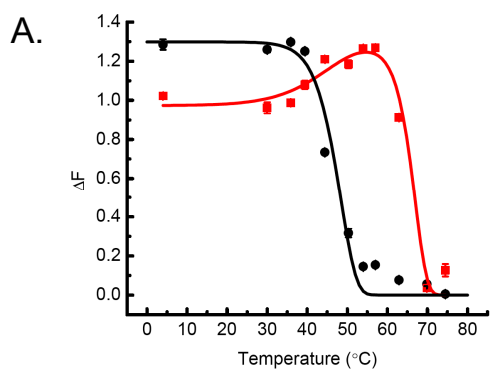
Figure 3-7. Temporal stability of CCR5 solubilized in 1% DM (triangles) and a buffer containing a complex mixture of lipids and detergents, as well as 10% (v/v) glycerol (squares). Aliquots were thawed and stored at 4°C for the indicated time prior to measurement.

signal as a function of temperature generates thermal denaturation or melting curves (Figure 3-8). Receptor denaturation, aggregation, and subsequent loss of 2D7-EuK binding presumably cause this loss of signal.

The thermal stability of CCR5 was measured in the presence and absence of high-affinity small molecule receptor ligands. CCR5 solubilized in buffer N has a T_M of $47.1 \pm 0.6^\circ\text{C}$ (Figure 3-8A, black). Preincubation of CCR5 with $8 \mu\text{M}$ maraviroc, AD101, CMPD 167, vicriviroc, or TAK-779 before the application of heat conferred a significant increase in thermal stability (Figure 3-8A-C). Maraviroc stabilizes CCR5 to the greatest extent, shifting the T_M to $66.0 \pm 0.3^\circ\text{C}$ (Figure 3-8A, red). The T_M values for AD101, CMPD 167, vicriviroc, and TAK-779 are 59.9 ± 1.0 , 62.7 ± 2.3 , 59.5 ± 1.4 , and $64.1 \pm 1.2^\circ\text{C}$, respectively (Figure 3-8B-C). Another interesting effect of these ligands is the reduction of the level of 2D7-EuK binding. Preincubation with all ligands results in a decrease in the magnitude of the HTRF signal, but to varying degrees. This indicates that antagonist binding reduces the accessibility of the 2D7 epitope on the EC2 loop, consistent with earlier work (Tsamis et al., 2003). This phenomenon is explored in further detail in Chapter 3.2.5. In addition, each of these melting curves displays an increase in the signal near 50°C before complete loss due to denaturation. This profile suggests that at least two distinct binding states might be involved in the antagonist-CCR5 interaction, with the “slower” being more amenable to 2D7 binding. These ligand-CCR5 denaturation curves were modeled as a sequence of two irreversible first-order processes. It is interesting that the conversion of the two inhibitor-bound conformations occurs around the temperature at which the empty receptor is denatured. The molecular structures of the antagonists tested are shown in (Figure 3-8D).

Figure 3-8. The HTRF assay was applied to make high-throughput thermal stability measurements with femtomole quantities of CCR5. A range of temperatures was applied to detergent-solubilized CCR5 or CCR5 NABBs before adding to labeled HTRF components in a 384-well plate. (A) Melting curves of unliganded CCR5 (black) and CCR5 preincubated with the small molecule antagonist maraviroc (red). Maraviroc shifts the T_M of detergent-solubilized CCR5 from 47.1°C to 66.0°C (rightward-pointing arrow) and appears to display a two-step binding profile. The first ligand-receptor state reduces the accessibility of the 2D7 epitope on the EC2 loop compared with unliganded receptor (downward-pointing arrow). The second ligand-receptor state results in a higher HTRF signal (upward-pointing arrow). (B) Thermal denaturation of CCR5-ligand complexes. CCR5 was preincubated with maraviroc (red), AD101 (green), vicriviroc (blue), and CMPD 167 (cyan). All of these antagonists appear to promote two distinct FRET levels in this immunoassay. The calculated T_M for maraviroc, AD101, vicriviroc, and CMPD 167 is 66.0°C, 59.9°C, 59.5°C, and 62.7°C, respectively. The unliganded receptor, which melts at a lower temperature, is shown as a black dashed line for reference. (C) Thermal denaturation of CCR5 preincubated with TAK-779. The calculated T_M is 64.1°C. Note that this curve is only presented separately because a preparation of solubilized CCR5 at a different concentration was used. (D) Molecular structures of the CCR5 antagonists tested.

Figure 3-8



It is important to note that these experiments probe the kinetics of receptor denaturation rather than the equilibrium distribution. The denaturation was modeled as an irreversible first-order process, and the data were fit using nonlinear regression analysis. The melting temperature (T_M) is defined as the point at which 50% (calculated) of the receptor is unfolded (see Materials and Methods for a description of models and curve fits). Error estimates for the T_M values were determined by bootstrap analysis, in which random subsets of the empirical data were fit to the model and the standard error was calculated from the distribution of calculated melting temperatures. This yielded error estimates of $\sim 1-3^\circ\text{C}$.

Because the process is kinetically controlled, the apparent T_M is dependent on the time of heat treatment. The choice of a 30 min incubation time was somewhat arbitrary, and we hypothesized that heat-treating the samples for longer would result in a shift to a lower apparent T_M . To demonstrate this effect, a set of simulated melting curves based on the activation energy of opsin denaturation were generated (Figure 3-9A) (Hubbard, 1958). These curves show a progressive shift to lower T_M values as the incubation time increases from 2 to 128 min. These theoretical curves correspond nicely with the results from an experiment in which the heat treatment time was increased to 120 min (Figure 3-9B). In fact, the actual T_M extracted from this experiment was within 0.5°C of the simulated curve based on the opsin activation energy.

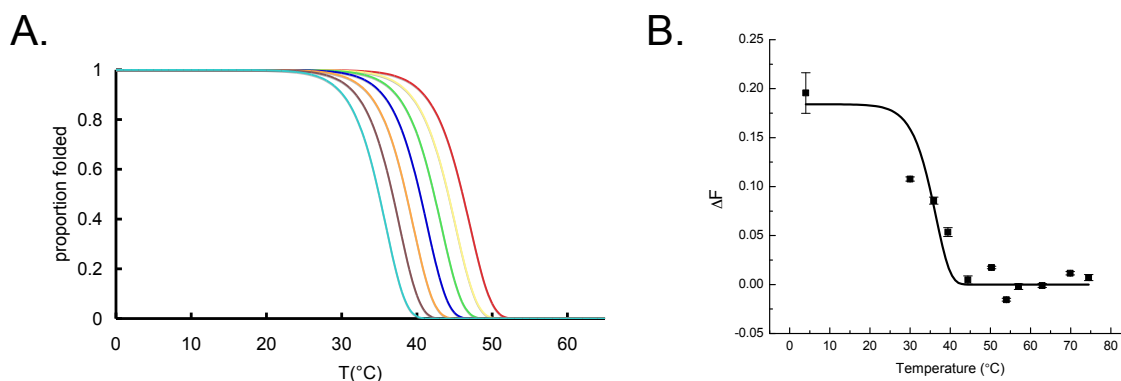


Figure 3-9. (A) Simulated melting curves of the GPCR opsin using a previously reported value of E_a for denaturation (Hubbard, 1958). Denaturation is modeled as an irreversible, and thus kinetically-controlled, first-order process. Each curve represents heat treatment for a specified length of time: 2 min (red), 4 min (yellow), 8 min (green), 16 min (blue), 32 min (orange), 64 min (brown), and 128 min (cyan). The apparent T_M depends on incubation time, with longer heat treatment causing a shift to lower T_M . For this reason, it is important to interpret the T_M values in this report as relative measures of receptor stability rather than as concrete thermodynamic parameters. (B) CCR5 melting curve with 120 min heat treatment rather than 30 min as shown in Figure 3-8. The T_M shifts to 35.3°C, remarkably close to the predicted value obtained from the simulated curves. This suggests the kinetic models used to fit the data are appropriate.

3.2.4 Identification and Characterization of Thermally Stable CCR5 Mutants

The sensitivity and throughput of the HTRF assay lent itself to rapid screens for mutations that stabilized CCR5 for crystallographic study. In collaboration with Heptares Therapeutics, a variation of the HTRF formulation depicted in Figure 3-3 was developed. The principle remained the same, but α -Myc-Terbium, 2D7-biotin, and streptavidin-d2 were used in place of 2D7-EuK, 1D4-biotin, and XL665-SA. Terbium, another long-lived lanthanide fluorophore, and d2 are an alternative HTRF donor-acceptor FRET pair with similar excitation and emission maxima. The d2 acceptor is only 1 kDa compared to the 105 kDa XL665, so it likely causes less steric hindrance. This assay produced nearly identical CCR5 denaturation profiles as those presented in Chapter 3.2.3. Further, experiments using binding of a custom radiolabeled CCR5 antagonist as a readout yielded similar curves, except at a slightly lower T_M . It could be that lower energies are required to disrupt the ligand-binding pocket than the extracellular antibody epitope. Analytical size-exclusion chromatography runs supported the notion that receptor melting corresponds to a shift from largely monomeric or dimeric species to aggregates.

A number of mutations were systematically screened using a methodology that has facilitated crystallization of both the β_1 -adrenergic receptor and adenosine A_{2A} receptor (Dore et al., 2011; Warne et al., 2008). Mutants that exhibited improved thermal stability compared to wild type in both the HTRF and radioligand binding assays were identified as hits, or StaRs (stabilized receptors), and subjected to further rounds of mutagenesis. Several generations of mutants were produced each using the prior version as a template. Data with four of these generations, termed CCR5_N α 2.1, CCR5_N β 5.2, CCR5_N γ 9.2, and CCR5_N δ 10.2 are presented here. The final combination of mutants,

CCR5_N810.2, increased CCR5 T_M by $\sim 20^\circ\text{C}$ over wild type in 1% DM; the presence of Ca^{2+} and Mg^{2+} cations improved stability still further. This exceptionally stable construct could be purified even in harsher detergents such as octyl-glucoside (OG).

In parallel with crystallization efforts of our collaborators, I sought to characterize the properties of these StaR mutants. Specifically, expression, ligand binding, ligand-induced calcium mobilization, and HIV-1 viral entry data were collected. In line with observations from Heptares, the StaRs expressed at higher levels than wild type CCR5 in whole cell lysates. In fact, only the mutations of CCR5_α2.1 were necessary to significantly improve expression in lysates, as probed by western blot (Figure 3-10A). In addition, the StaRs expressed at least as well in whole-cell ELISAs probing receptors localized to the plasma membrane (Figure 3-10B). This shows that high expression levels are not merely misfolded receptor.

Despite proper trafficking to the cell surface, the StaRs did not induce intracellular calcium mobilization upon stimulation with the chemokine RANTES (Figure 3-11A). This was true even at very high (100 nM) chemokine concentrations. The observation that the StaRs did not mediate calcium flux led to the hypothesis that they were locked into an inactive conformation that permits 2D7 mAb and small molecule binding but precludes binding of the native chemokine ligand. To test this, cells expressing wild type CCR5 and two generations of stabilized mutants were analyzed for their ability to bind [^{125}I]-RANTES. In experiments with a serial dilution of the radiolabeled chemokine and in the presence and absence of the antagonist maraviroc, no specific binding of the ligand was detected (Figure 3-11B-C). This contrasted with wild type CCR5, which exhibited robust ligand binding even at sub-nanomolar concentrations.

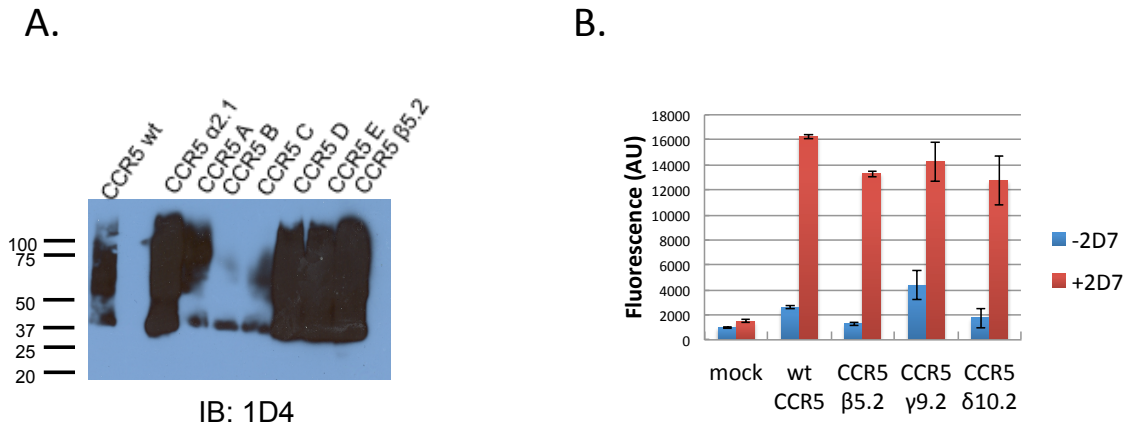
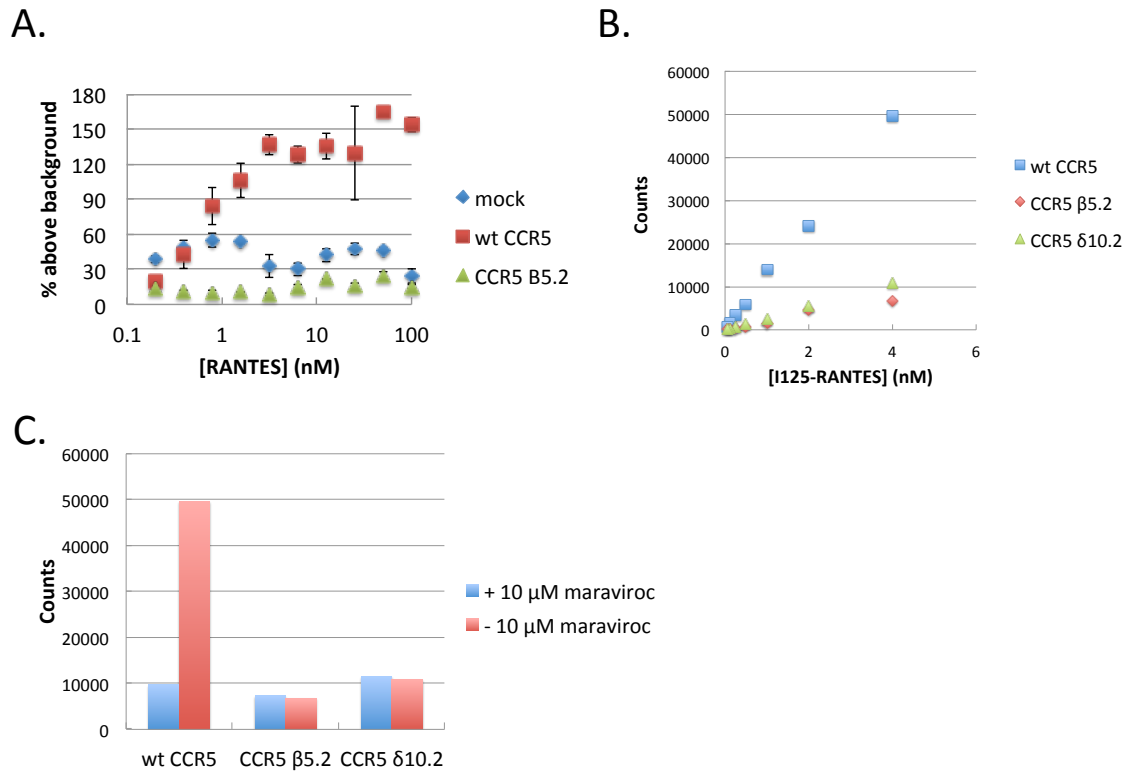


Figure 3-10. Expression data for thermally stabilized CCR5 mutants. (A) Western blots of whole cell lysates with 1D4 primary antibody show that constructs containing the CCR5 $\alpha 2.1$ mutations are sufficient for expression at higher levels than wild type receptor (including CCR5 D-E). Single point mutants at sites that were included in the CCR5 $\beta 5.2$ construct did not express as well (CCR5 A-C). (B) Whole-cell ELISA of HEK-293T cells with 2D7 primary antibody and α -mouse secondary antibody. The thermally stabilized mutants show plasma membrane expression comparable to wild type CCR5.

Figure 3-11. (A) Dose-response curve of RANTES-induced intracellular calcium flux. Cells were transfected with the chimeric G protein subunit Gqi5 and wild type CCR5 (red), CCR5 β 5.2 (green), or a mock transfection (blue). Cells expressing wild type CCR5 exhibit calcium mobilization as measured by changes in Calcium 4 dye fluorescence. The CCR5 β 5.2 mutant, despite strong cell surface expression, cannot mediate signaling through this pathway. (B) Cells expressing wild type CCR5 (blue), CCR5 β 5.2 (red), or CCR5 δ 10.2 (green) were incubated with a dilution series of [125 I]-RANTES. The wild type CCR5 cells showed much higher radioactive counts than the thermally stabilized CCR5 cells. (C) Preincubation of cells with a saturating concentration of maraviroc prior to addition of 4 nM RANTES show that the thermally stabilized mutants do not specifically bind the chemokine ligand. This suggests that the counts for these mutants observed at higher concentrations in (B) are due to nonspecific sticking to cells.

Figure 3-11



Finally, the StaRs were tested for their capacity to be used by HIV-1 for entry into mammalian cells. These assays were conducted by collaborators in John Moore's Lab. An HIV-1 pseudovirus-luciferase reporter construct was expressed in HEK-293T cells. U87 cells expressing CD4 and the CCR5 mutants were infected with the pseudovirus and luciferase activity was measured 72h post-infection. Two HIV strains resistant to drug treatments were tested alongside sensitive virus (Kuhmann et al., 2004; Marozsan et al., 2005). Remarkably, despite the mutants' inability to bind chemokine, all of the StaRs were used as HIV co-receptors (Figure 3-12). The luminescence signals indicating viral entry were roughly proportionate to receptor expression levels as measured by FACS.

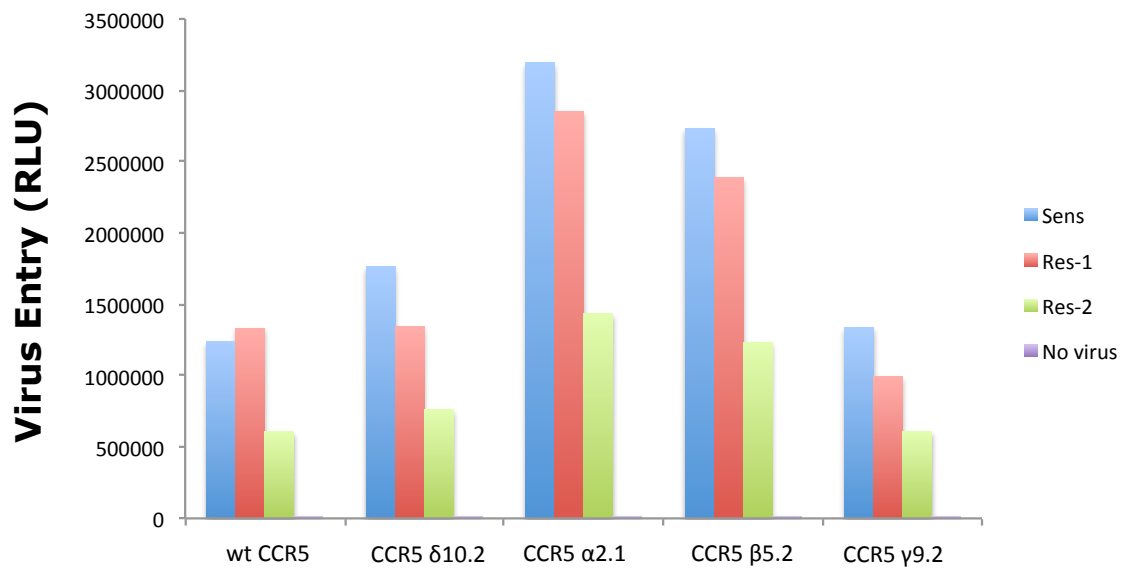


Figure 3-12. HIV entry assays using HIV-1 pseudovirus-luciferase reporter constructs. Cells expressing CD4 and each of the CCR5 mutants were infected with sensitive virus (blue), virus resistant to AD101 (red), virus resistant to SCH-D (green), and no virus (purple). All of the mutants tested are effectively used as co-receptors by all of the viruses tested.

3.2.5 Probing the Allostery between HIV Entry Inhibitor Antibodies and Small Molecule Drugs

As shown in Chapter 3.2.3, preincubation of CCR5 with small molecule anti-HIV entry drugs caused different FRET signals. This effect is demonstrated more clearly in Figure 3-13. Preincubation with 10 μ M of all inhibitors tested resulted in a lower signal compared to a negative control without inhibitor. The order from highest to lowest signal was the following: TAK-779, maraviroc, AD101, vicriviroc, and CMPD 167. The differences in FRET signals suggest that each small molecule stabilizes a slightly different conformation of the receptor. This result supports the idea that GPCRs are highly sensitive allosteric machines with many energetically accessible states.

The allosteric relationship between the small molecules and 2D7 was examined in more detail with competition experiments. First, a serial dilution of CCR5 was measured with concentrations of 2D7-EuK below 2 nM. This showed that acceptable signal-to-background could be achieved with lower donor fluorophore concentrations (data not shown). CCR5 in lysate was then preincubated with a serial dilution of each small molecule and then mixed with HTRF components. Representative results for TAK-779 are shown in Figure 3-14A. As expected, the HTRF signal increases at higher concentrations of 2D7-EuK; high concentrations of TAK-779 result in a decrease. Similar experiments were conducted with vicriviroc, AD101, CMPD167, and maraviroc. A plot of the IC_{50} values for these competition curves against the concentration of 2D7-EuK shows relatively little concentration dependence (Figure 3-14B).

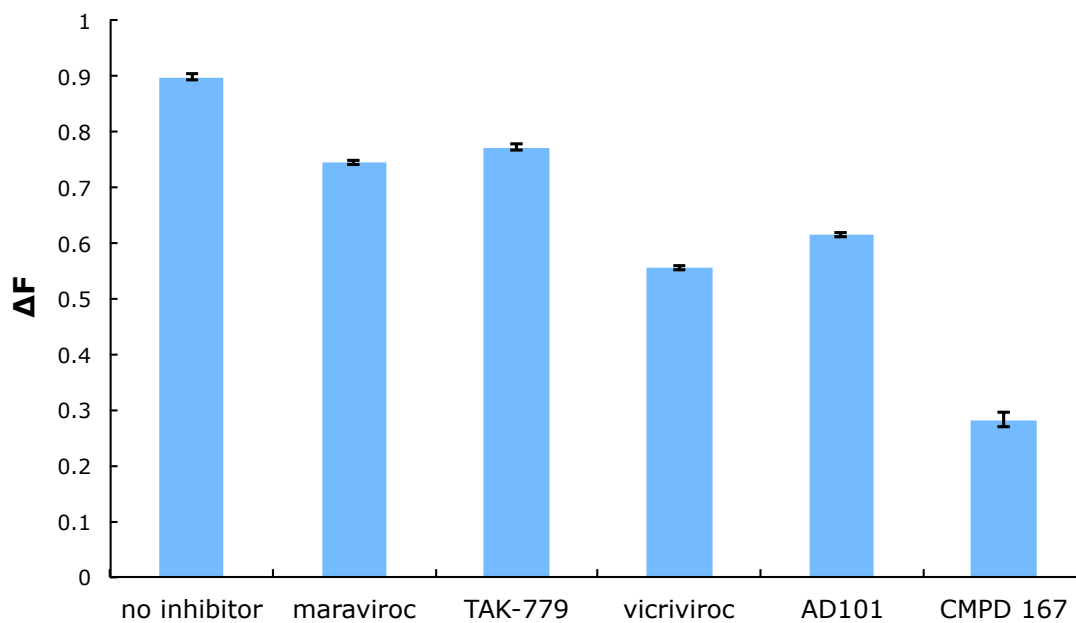


Figure 3-13. HTRF measurements of CCR5 in the presence and absence of small molecule antagonists. The total amount of CCR5 in each experiment was the same, so differences in signal indicate that the receptor probably adopts different conformations upon binding to each.

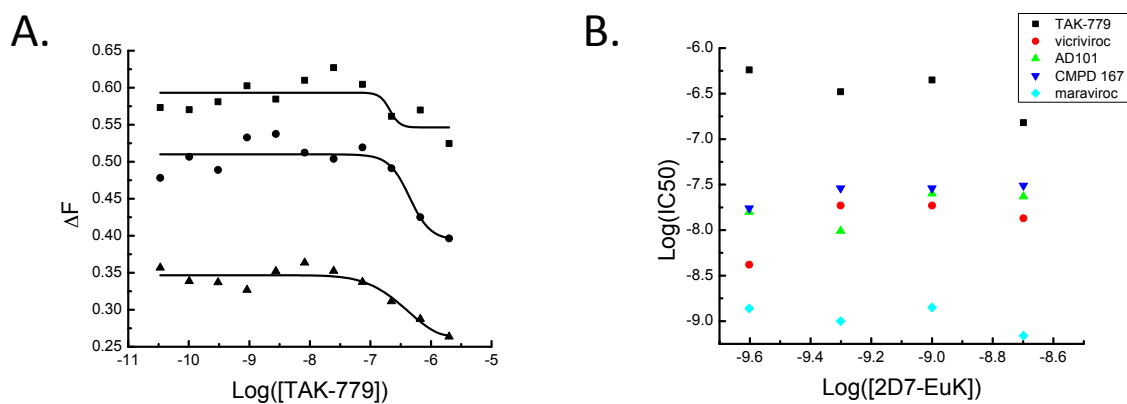


Figure 3-14. (A) Competition curves between TAK-779 and 2D7-EuK. CCR5 was preincubated with the indicated concentration of TAK-779, and then the fluorescently labeled assay components were added with 0.5 (triangles), 1.0 (circles) or 2.0 nM (squares) 2D7-EuK. (B) Log-log plot of competition curve IC_{50} values against the concentration of 2D7-EuK for each of the antagonists tested. The flatness of each curve indicates a relationship of noncompetitive antagonism. The small molecule binds at an allosteric site and permits binding of 2D7.

3.3 Discussion

CCR5 is an important family A GPCR because of its role as a primary HIV-1 co-receptor (Allen et al., 2007; Lusso, 2006). Its natural ligands, including MIP-1 α , MIP-1 β , and RANTES, are potent inhibitors of HIV infection, and a number of small molecule antagonists that block HIV entry have been reported (Kuhmann and Hartley, 2008) (Horuk, 2009). Detailed molecular studies of purified CCR5 are important for understanding its biological function, role in HIV entry, and mode of binding to pharmacological agents. Its high lability in solution makes it a particularly challenging target, even by GPCR standards. Some progress has been made, as detergent conditions that maintain proper CCR5 folding for several hours have been identified (Navratilova et al., 2006; Navratilova et al., 2005). These reports use binding of the well-characterized conformationally sensitive 2D7 mAb as a reporter for receptor folding and integrity (Farzan et al., 1999; Mirzabekov et al., 1999; Wu et al., 1997).

The challenge of generating quality GPCR samples amplifies when receptors cannot be easily expressed at high levels, as is the case with CCR5. We estimate that 1 μ g of CCR5 can be obtained from one 10 cm plate of transfected HEK-293T cells, so an extremely sensitive quantitative assay is desirable. Ideally, this assay should also be capable of high-throughput screening so that a large number of potentially stabilizing conditions can be evaluated in parallel. We decided on a strategy of HTRF, with fluorescently labeled antibodies forming an immunosandwich on distinct epitopes of CCR5. HTRF occurs when a EuK fluorescent donor is brought into the proximity of a modified allophycocyanin (XL665) acceptor (Bazin et al., 2001; Mathis, 1995). The dual-

wavelength detection of donor (615 nm) and acceptor (665 nm) fluorescence after EuK excitation at 320 nm results in a specific signal with excellent well-to-well reproducibility and internal correction for inner filter effects. Figure 3-3 depicts the CCR5 formulation. The key reporter is EuK-labeled 2D7 mAb, which binds to the split epitope QKEGL-TL on the EC2 loop of the receptor (Khurana et al., 2005; Lee et al., 1999). This FRET pair has a Förster radius of approximately 95 Å, making signal detection feasible even though the fluorophores are probably separated by at minimum the distance between the intracellular and extracellular faces of the receptor.

To maximize HTRF assay sensitivity, we labeled 2D7 directly rather than rely on a secondary antibody. Typically, conjugations require fairly large amounts of antibody and/or fluorophore (Cummings et al., 1999; Kane et al., 2000). We therefore developed a scalable solid-phase procedure for labeling small amounts of IgG with EuK. Solid-phase chemistry bypasses two technical drawbacks associated with labeling reactions in solution. First, the conjugated product is easily separated from excess reagents and side products without chromatographic or other means. This saves several additional purification steps and likely increases yield. Immobilization of the IgG permits simple and thorough washing steps, particularly with magnetic beads. Second, the tethering to beads results in significant concentration of IgG compared to commercial solutions. This reduction in reaction volume increases the efficiency of the conjugation and eliminates the necessity of a large molar excess of the label. Both of these advantages are particularly noteworthy when the antibodies and/or labels are expensive, which is often the case. To demonstrate the general utility of this method, we labeled other antibodies with amino-derivatized fluorophores. These conjugations yielded similar results.

After optimizing HTRF signal detection in a simplified system, we applied the assay to detect folded CCR5. We estimate that ~1 fmol of correctly folded CCR5 in a single 384-microtiter plate well can be detected, far greater sensitivity than alternative techniques. The assay is more informative than immunoblots, as it reports on the quality of the receptor as well as the quantity. Unlike surface plasmon resonance (SPR), conditions can be screened without the need for a common binding buffer and the time-consuming microchip regeneration step. If automated, the HTRF approach combines high-throughput capability and sensitivity at a level exceeding even the best available SPR equipment, which is also more expensive (Rich et al., 2009).

We were able to make high-throughput measurements of CCR5 stability with small amounts of material. These experiments are crucial for determining conditions for structural studies. While DM is considered an excellent detergent for GPCR solubilization, the data in Figure 3-7 suggest that more complex detergent/lipids mixtures are required to obtain satisfactory stability. The HTRF assay is well suited to screen the large number of potential salts, detergents, and lipids. CCR5 retained proper folding in the well-performing buffer, which includes cholesterol hemisuccinate (CHS), even after being heated at >40°C for 30 min, and for up to 48 h at 4°C. CHS has previously been shown to stabilize a number of GPCRs (Chiu et al., 2008). Preincubation with small molecule CCR5 antagonists resulted in a marked shift of the T_M to 59-66°C. These temperatures compare favorably with GPCRs that were successfully crystallized, for example the β_1 -adrenergic receptor (Serrano-Vega et al., 2008).

The thermal stability experiments performed probe the kinetics of denaturation rather than the equilibrium distribution. The experimental results are modeled

accordingly. We hypothesize that the receptor-ligand complex proceeds through a series of conformational states: a “loose” antagonist-bound state, a “tight” antagonist-bound state, and finally, a denatured state. A similar multistep process with a final irreversible step has been previously proposed to describe rhodopsin denaturation using differential scanning calorimetry data (Landin et al., 2001). The authors of that study concluded that the denaturation step is rapid compared to any reversible step and thus that the process is kinetically controlled. The fitting parameters used in this work include thermodynamic quantities necessary to derive an appropriate rate constant for these transitions, but we restrict our interpretation to a single value, the apparent melting temperature, T_M . Thus, there is no sharp inherent transition temperature for a kinetically-controlled process such as GPCR melting, and the length of time the receptor is heat treated was chosen simply so that it is experimentally relevant and informative.

Our thermal stability results were validated in the hands of our collaborators at Heptares Therapeutics, both in a variation of the HTRF assay and in radioligand binding experiments. Further, size-exclusion chromatography runs of heat-treated receptor confirmed that the observed “melting” corresponds to transitions from mostly monomeric populations to higher-order oligomers and finally, aggregates of denatured protein. Heptares used these tools to identify combinations of mutations that resulted in exceptionally stable CCR5 constructs. This work was motivated by the goal to solve the crystal structure of CCR5 either in complex with the HIV envelope glycoprotein gp120 or, at least, in a conformational state relevant to infection. Point mutations perturb the native structure less than large protein insertions, making this an attractive strategy.

The mutations that conferred improved stability were distributed throughout the

extracellular and intracellular loops as well as the transmembrane helices. In order to understand the effects of the mutations on receptor function, a series of expression and pharmacological assays were conducted. Encouragingly, StaRs expressed at even higher levels than wild type CCR5 in HEK-293T cells. The stable mutants may be more resistant to misfolding and degradation. Despite considerable expression at the plasma membrane, as measured by ELISA, the mutants did not induce intracellular mobilization in response to RANTES treatment. This was the case even at very high (100 nM) ligand concentrations. The signal-dead result could be explained several ways: inability to bind chemokine, inability to form an active conformation, and formation of an oligomeric state inconducive to G protein coupling among them. The ligand-binding hypothesis was tested by incubating cells expressing the CCR5 mutants with [¹²⁵I]-RANTES. These experiments showed that none of the StaRs are able to bind chemokine with nanomolar affinity. It is therefore likely that the mutations lock the receptor into an inverse agonist-like state. This would make sense, as it has been shown that GPCR mutants with greater conformational flexibility – and thus reduced thermal stability – exhibit higher constitutive signaling activity (Gether et al., 1997). Despite the StaRs' inability to bind chemokine, it was shown that they are effectively used as HIV co-receptors by both drug-sensitive and drug-resistant viruses (Figure 3-12). This somewhat surprising result has interesting implications. First, if any of these mutants are successfully crystallized, it would probably be in a conformation that supports HIV infection, clearly a desirable characteristic. The data also suggest that a signaling-competent co-receptor is not necessary for viral entry, supporting the prevailing view (Lusso, 2006).

The antagonists maraviroc (Dorr et al., 2005), AD101 (Trkola et al., 2002),

CMPD 167 (Veazey et al., 2003), vicriviroc (Strizki et al., 2005), and TAK-779 (Baba et al., 1999) block interaction of CCR5 with the HIV envelope glycoprotein gp120 and demonstrate high antiviral potency. Maraviroc is the first FDA-approved GPCR-specific HIV entry inhibitor. Key residues in the transmembrane domains that are required for antagonist binding have been identified, but precisely how gp120 inhibition occurs remains unknown (Kondru et al., 2008; Seibert et al., 2006). The melting curves generated demonstrate that ligand-receptor complexes under optimized conditions could be sufficiently stable for high-temperature nuclear magnetic resonance (NMR) or crystallization studies. These structures could be particularly interesting because some HIV variants that are resistant to small molecule inhibitors have been identified (Kuhmann et al., 2004; Marozsan et al., 2005). The denaturation profiles also shed some light on the binding dynamics of the CCR5 antagonists, which appear to consist of two steps. The first state, which induces a decreased HTRF signal, could be due to slightly decreased 2D7-EuK affinity or an alteration of the antibody binding orientation that results in a longer donor-acceptor distance. The second state, characterized by a notable rise, seems to more closely resemble CCR5 in the absence of antagonist. A similar two-step binding profile has been proposed for β_2 -adrenergic receptor ligands (Deupi and Kobilka, 2007). Interestingly, the five antagonists tested inhibit 2D7-EuK binding to varying extents, but none completely (Figure 3-13). It is unsurprising that the antibody and small molecule can co-bind, as the antibody binds an epitope on the EC2 loop and the small molecules bind a more buried transmembrane region. Competition experiments revealed a relationship of noncompetitive antagonism (Figure 3-14). Antibody and small molecule therapeutics can thus be used synergistically, as previously suggested (Watson

et al., 2005). Further, the varying HTRF signals suggest that the small molecules stabilize different receptor conformations with a common inability to support HIV entry. Earlier studies involving ligand binding to whole cells came to similar conclusions (Ji et al., 2007). Such a situation may motivate a sequential treatment strategy to overcome viral resistance, though cross-resistance to drugs has been demonstrated (Pugach et al., 2008). Additionally, the conformational complexity of these GPCR-ligand complexes make them ideal candidates for single molecule fluorescence experiments probing receptor allostery, which will be discussed in the following chapter.

Chapter Four: Incorporation of CCR5 into Membrane Nanoparticles and Single Molecule Fluorescence

Measurements^{*}

4.1 Introduction

GPCRs, like all membrane proteins, are difficult to study outside of their native membrane environment. A solution of membrane proteins in aqueous buffer will not stay monomeric because of the hydrophobic effect, which drives transmembrane helices to interact with each other. Aggregation and precipitation inevitably result. Careful screening of solubilization conditions, using methods such as the one described in the previous chapter, can help identify favorable combinations of lipids and detergents that overcome protein-protein interactions. Nonetheless, the study of GPCRs in detergents has limits even under relatively stabilizing conditions. The best performing detergents for these samples typically have a relatively low critical micelle concentration and a large micelle size, which can lead to aggregation phenomena that complicate interpretation of results (Bartfai et al., 2004). Furthermore, G protein activity is sharply limited by detergent concentration, making the study of reconstituted ligand-receptor-G protein

^{*} Portions of this chapter have been published previously: Knepp AM, Grunbeck A, Banerjee S, Sakmar TP and Huber T (2011) Direct Measurement of Thermal Stability of Expressed CCR5 and Stabilization by Small Molecule Ligands. *Biochemistry* **50**:502-511. Knepp AM, Sakmar TP and Huber T (2013) Homogeneous time-resolved fluorescence assay to probe folded G protein-coupled receptors. *Methods in Enzymology* **522**:169-189.

“signalosomes” in solution impractical (Ernst et al., 2007). Clearly, an ideal platform for functional studies of GPCRs involves purification and reconstitution into a membrane bilayer.

Nanodisc technology has surged in popularity recently (Popot, 2010). These membrane nanoparticles are comprised of phospholipid bilayers encapsulated by helical amphipathic belt proteins derived from high-density lipoprotein apo A-1. The properties of nanodiscs have been studied by techniques such as small-angle X-ray scattering, electron microscopy (EM), atomic force microscopy and size-exclusion chromatography (Nath et al., 2007). Nanodiscs are relatively monodisperse and generally 10-20 nm in diameter, with the size varying depending on the belt protein employed. They bear several advantages for GPCR functional studies. First, the lipid bilayer is highly similar to the native environment, and the lipid composition can be varied. Second, both the extracellular and intracellular faces of the receptor are solvent-accessible. This enables reconstitution of multicomponent signaling complexes involving receptor interactions on both sides of the membrane. Finally, the receptor incorporation rate can be controlled by changing the ratio of receptors to belt proteins. In this way, one can preferentially isolate and study monomers or dimers.

NABBs (nanoscale apolipoprotein bound bilayers) are a type of nanodisc developed in the Sakmar Lab that utilizes zebrafish rather than human apo A-1 (Banerjee et al., 2008). NABBs are especially stable nanodiscs due to the high lipid affinity and salt bridging properties of zebrafish apo A-1 (zap1). The first report of GPCR NABBs described the incorporation and characterization of rhodopsin. Rhodopsin monomers were shown to efficiently activate G proteins in these structures; a similar result was

obtained with β_2 -adrenergic receptor in nanodiscs (Whorton et al., 2007).

We sought to incorporate CCR5 into NABBs for functional studies. Because CCR5 is generally unstable and cannot be expressed in large quantities, we desired a modular and reproducible approach that could be conducted on a microscale. This chapter describes a method that meets these criteria. Purified receptor is first mixed with selected detergents and lipids. NABBs are formed upon detergent extraction. The NABBs preparation is cleaned up by purification on a size-exclusion column and the quality of CCR5 NABBs can be evaluated using the HTRF assay for folded receptor. In this way, a number of conditions were tested. After a satisfactory preparation protocol was achieved, the samples could be used in proof-of-concept experiments for single molecule platforms under development within the lab.

Though single molecule fluorescence techniques are very difficult to master, they also hold great promise. The number of publications employing them is increasing rapidly (Cornish and Ha, 2007). Visualizing individual receptors at work circumvents the problems of time and ensemble averaging, making detailed kinetic information accessible even when reaction trajectories cannot be synchronized. These types of data are crucial for a full understanding of receptor allostery upon binding a native ligand or drug (Huber and Sakmar, 2011). Additionally, the precise stoichiometry of complexes can be directly observed over time, which may resolve fundamental questions about the composition of the signalosome during different stages of the G protein cycle (Nobles et al., 2005; Oldham and Hamm, 2007).

In this chapter, progress toward studying CCR5 by a near single molecule technique is described. Fluorescence correlation spectroscopy (FCS) is based on the

measurement of fluctuations in intensity as a small number of molecules diffuse through a tiny (<1 fL) confocal volume (Lakowicz, 2006). The autocorrelation function between intensity at a given time t and later time $t + \tau$ reveals information about the number of molecules in the observed volume as well as their diffusion coefficient. Larger molecules diffuse more slowly than smaller ones, causing a shift in the correlation curve. FCS has previously been used to evaluate preparations of membrane nanoparticles (Gao et al., 2011; Nath et al., 2010). It has also been applied to monitor small molecule and peptide binding to GPCRs in cells, where the differences in diffusion time between bound and unbound fractions are very large (Briddon et al., 2004; Hegener et al., 2004; Pramanik et al., 2001). However, because diffusion coefficients exhibit weak dependence on molecular weight, FCS does not perform as well in purified systems, especially with larger ligands. Fluorescence cross-correlation spectroscopy (FCCS), which relies on the correlation between two fluorescence channels, circumvents this problem. When both the ligand and receptor are labeled, an FCCS signal will only be observed when the probes are codiffusing (i.e. bound). This improves resolution compared to traditional one color FCS and expands the types of interactions that can be studied effectively.

FCS features several notable advantages and disadvantages that are complementary to total internal reflection fluorescence (TIRF), another single molecule technique under development in the lab. TIRF occurs when a beam of light meets an interface between two media with different refractive indices and the angle of incidence exceeds the critical angle. The resulting evanescent wave decays exponentially along the z -axis, confining the focal volume to a thin slice above the cover slide. This volume is small enough that signal-to-background ratios suitable for single molecule detection can

be achieved. Samples under study must be tethered to the surface, as opposed to the solution-based FCS method. Though this can be technically difficult, immobilized molecules can be observed for very long periods of time – typically until they photobleach. This enables study of dynamic processes, such as ligand binding and dissociation, that may take place over minutes rather than milliseconds.

Because FCS measures samples quickly diffusing through the focal volume, photobleaching does not present the limitation it does in TIRF. The two methods also access different timescales: μ s dynamics (faster than diffusion) for FCS, and ms to minutes for TIRF. TIRF involves “true” single molecule detection, whereas FCS usually measures several molecules at once. Over the course of a single FCS measurement, many molecules pass through the focal volume, so the data set statistics are very good. Taken together, these two methods form a powerful next-generation toolkit for the study of purified GPCRs, signaling partners, and allosteric modulators such as small molecule drugs. The experiments in this chapter report the development of necessary standards as well as preliminary characterization of CCR5 NABBs.

4.2 Results

4.2.1 Incorporation of CCR5 into NABBs

The first studies demonstrating formation of NABBs reported the incorporation of rod outer segment bovine rhodopsin (Banerjee et al., 2008). Unlike rhodopsin, CCR5 cannot be purified in large quantities from natural sources, so we employed a microscale

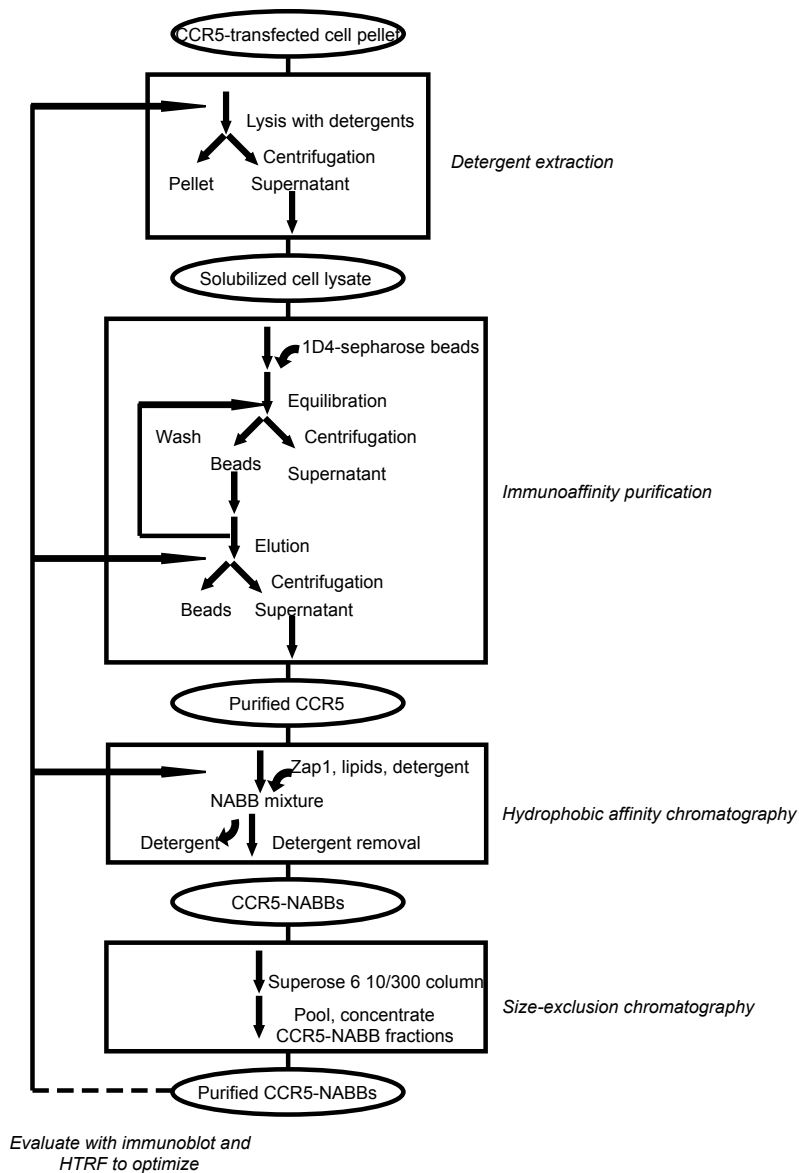


Figure 4-1. Protocol for incorporation of CCR5 into NABBs. Cell pellet is solubilized in detergent buffer and an immunoprecipitation enriches for CCR5. Solubilized CCR5 is mixed with zap1 belt protein, lipids, and detergent. Hydrophobic affinity chromatography removes the detergents and NABBs are formed. CCR5 NABBs are enriched by size-exclusion chromatography. The HTRF assay is used in conjunction with immunoblots to determine the recovery and quality of CCR5 for optimization purposes.

procedure to reconstitute CCR5 in NABBs. The general procedure is outlined in Figure 4-1. CCR5 expressed in HEK-293T cells was immunopurified from solubilized lysate using 1D4-Sepharose beads. After several washing steps, receptor was eluted by addition of 1D5-nonapeptide. Roughly one-half of the receptor is lost in this purification step because of incomplete elution from the beads. The NABB assembly mixture was formed by combining purified zebrafish Apo-A1 (zap1) and lipids at a molar ratio of 1:75. This ratio was shown to yield 10-12 nm diameter disks in the earlier rhodopsin study. Purified CCR5 elution was added to the mixture and, after incubation on ice, applied to a detergent-removal resin. NABBs were eluted under gravity flow by addition of detergent-free buffer, and fractions were collected. Protein-containing fractions were determined by measurement of 280 nm absorbance and pooled. UV-Vis spectra of NABBs with and without rhodamine-labeled DOPE doped into the lipid mixture are shown in Figure 4-2A. As a reference, NABBs containing opsin labeled with Alexa 647 according to a previously reported procedure are also shown (Figure 4-2B). As mentioned above, CCR5 cannot be purified in large quantities like rhodopsin, so it is difficult to obtain UV-Vis spectra showing incorporation of labeled receptor.

Combined elutions from the detergent removal resin were run on a gel filtration column for characterization and purification (Figure 4-3A). Co-elution of protein and lipids was monitored by measuring absorption at 280 and 570 nm, which detected rhodamine-labeled DOPE doped into the lipid mixture. Immunoblots showed the relative content of CCR5 (1D4 mAb detection) and zap1 (α -His6 mAb detection) in each fraction. The majority of the CCR5 NABBs elute at 15.6 mL in the shoulder of the first peak, which is centered at ~16.1 mL. The second peak, at ~17 mL, contains mainly empty

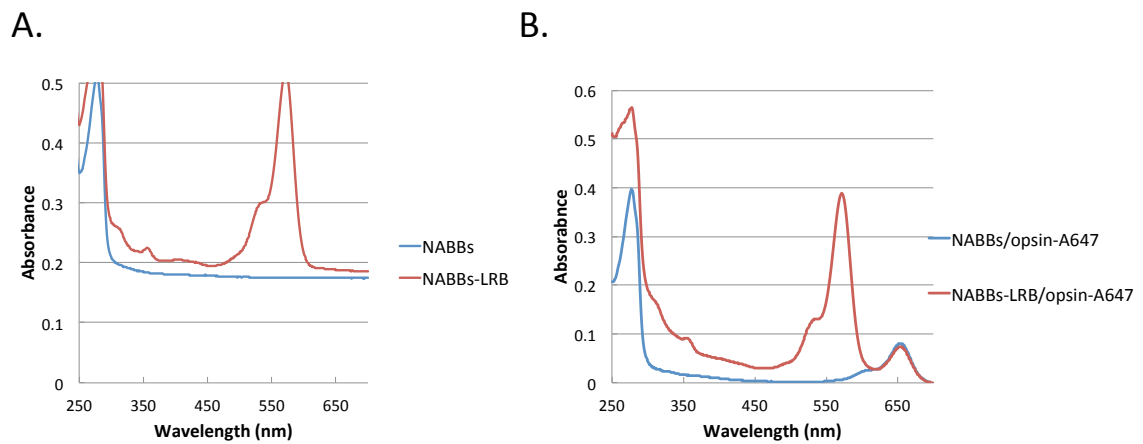


Figure 4-2. UV-Vis spectra of NABBs formed by detergent removal over a hydrophobic affinity resin. (A) NABBs with and without Lissamine-Rhodamine B-labeled lipids doped into the lipid mixture. (B) NABBs containing opsin labeled with Alexa 647 show that the procedure results in GPCR-containing NABBs.

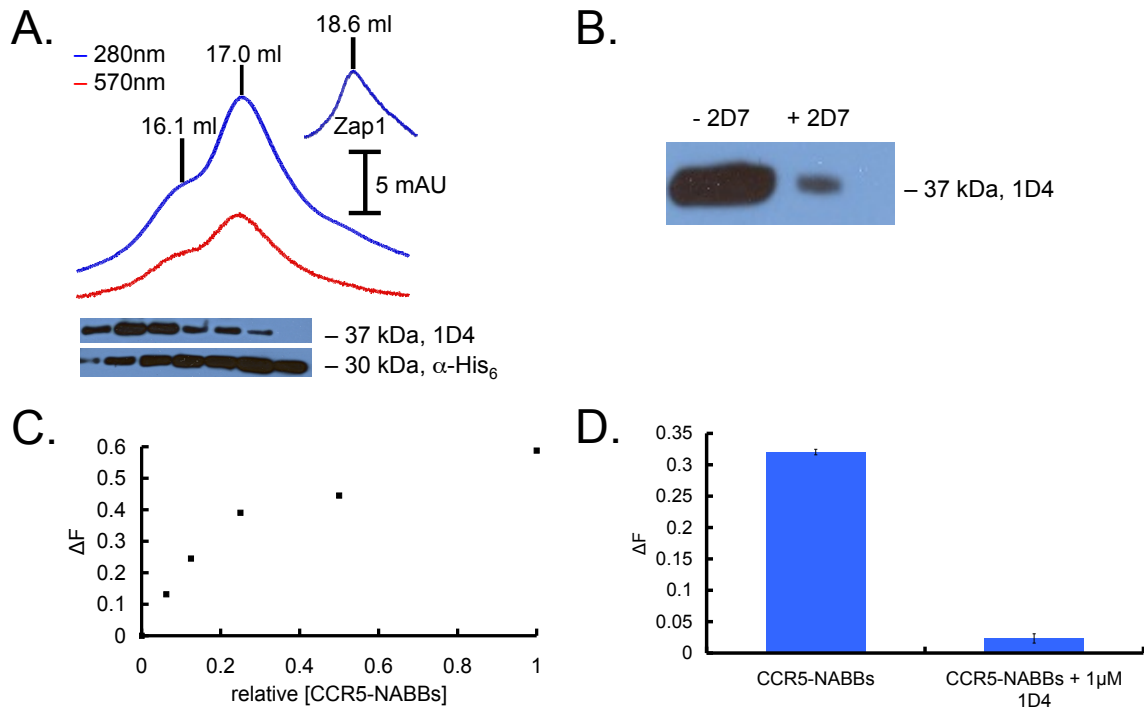


Figure 4-3. (A) Chromatogram showing co-elution of NABBs protein (blue; 280 nm) and fluorescent lipids (red; 570 nm). The 1D4 immunoblot below shows that CCR5 NABBs elute in the peak centered at 15.6 mL, exhibiting a larger hydrodynamic radius than the majority of the NABBs at 16.1 and 17.0 mL. The anti-His₆ blot detects His-tagged zap1 belt protein. Free zap1 elutes at 18.6 mL (inset). (B) CCR5 NABBs were incubated with Protein G beads and 2D7, and the supernatant fraction was probed with a 1D4 immunoblot. The majority of CCR5 in NABBs is immunoprecipitated by 2D7, indicating properly folded receptor. (C) HTRF signal from a serial dilution of CCR5 NABBs, demonstrating the ability to quantify properly folded CCR5 in NABBs. (D) The HTRF signal is efficiently competed with 1 μ M 1D4, showing signal specificity.

NABBs. In the previous study of rhodopsin NABBs reconstituted at a similar ratio, it was also observed that the receptor-containing NABBs elute ~0.5 mL earlier than the majority of empty NABBs. Note that the ratio of CCR5 to NABBs is approximately 1:100. This reduces the likelihood of incorporating more than one receptor per NABB and favors a relatively homogeneous CCR5 NABB preparation. Free zap1, which elutes at ~18.6 mL (Figure 4-3A, inset), likely constitutes the right peak shoulder that is rather lipid-poor as judged by the 570 nm absorbance. The CCR5 NABBs were mixed with Protein G beads with (left) and without (right) 2D7, and the supernatant fractions were subjected to 1D4 immunoblot analysis (Figure 4-3B). The near-quantitative immunoprecipitation of CCR5 NABBs with the conformationally sensitive 2D7 antibody suggests that most of the receptor is properly folded.

The HTRF assay was used in conjunction with gel filtration chromatography and immunoblot analysis to facilitate optimization of preparation conditions. The HTRF assay complements immunoblots because it reports on receptor folding, not just the total amount of receptor protein. Moreover, the HTRF assay is much more quantitative and reproducible. 2D7-EuK and 1D4-biotin bind to CCR5 in NABBs, resulting in a dynamic range for the HTRF assay as with the detergent-solubilized receptor (Figure 4-3C). Competition with 1 μ M 1D4 ablates the signal, demonstrating signal specificity as in detergent solution (Figure 4-3D). Assay conditions were identical to those in detergent experiments, except that phosphate-buffered saline (PBS) was used as the starting buffer.

Using the HTRF signal as a guide, a number of conditions were screened for optimal formation of CCR5 NABBs containing correctly folded receptor. Variables included changing the detergents used, the zap1:lipid ratio, the lipid composition, and the

detergent-removal resin elution buffer. We found that several factors were particularly important for optimal CCR5 recovery. Elution of CCR5 from 1D4-Sepharose beads in buffer N and inclusion of 0.3% (w/v) *n*-dodecyl β -D-maltopyranoside (DM) in the final NABB mixture enhanced stability. Notably, the detergent removal resin adequately extracted DM despite its low critical micelle concentration (CMC). Additionally, equilibrating and eluting from the detergent removal resin with buffer S, 20 mM Tris-HCl (pH 7.0), 0.1 M (NH₄)₂SO₄, and 10% (v/v) glycerol further increased recovery. Comparing the HTRF signal from CCR5 NABBs to that of the solubilized CCR5 starting material, the overall yield of correctly folded receptor in the optimized procedure was >15%. This estimate likely represents a lower bound because the NABB might prevent head-to-tail donor-acceptor interactions that theoretically may cause a reduction in the donor-acceptor distance and an increase in HTRF signal intensity in detergent. Indeed, it appears that the HTRF signal at a saturating concentration of CCR5 NABBs is weaker than the maximal signal in detergent solution (Figure 3-5B).

Thermal stability measurements were made for CCR5 NABBs using the HTRF assay (Figure 4-4). There are several notable features of the CCR5 NABB melting curve. The T_M was $54.5 \pm 3.4^\circ\text{C}$, suggesting that incorporation into the native membrane-like environment of NABBs improves the thermal stability of CCR5. Additionally, the temperature range over which the magnitude of the signal decreases is significantly broadened compared with that of solubilized CCR5, suggesting some sample heterogeneity or a lower activation energy associated with denaturation. It is also possible that heat treatment results in melting of the NABB before unfolding of CCR5, which would cause the receptor to aggregate.

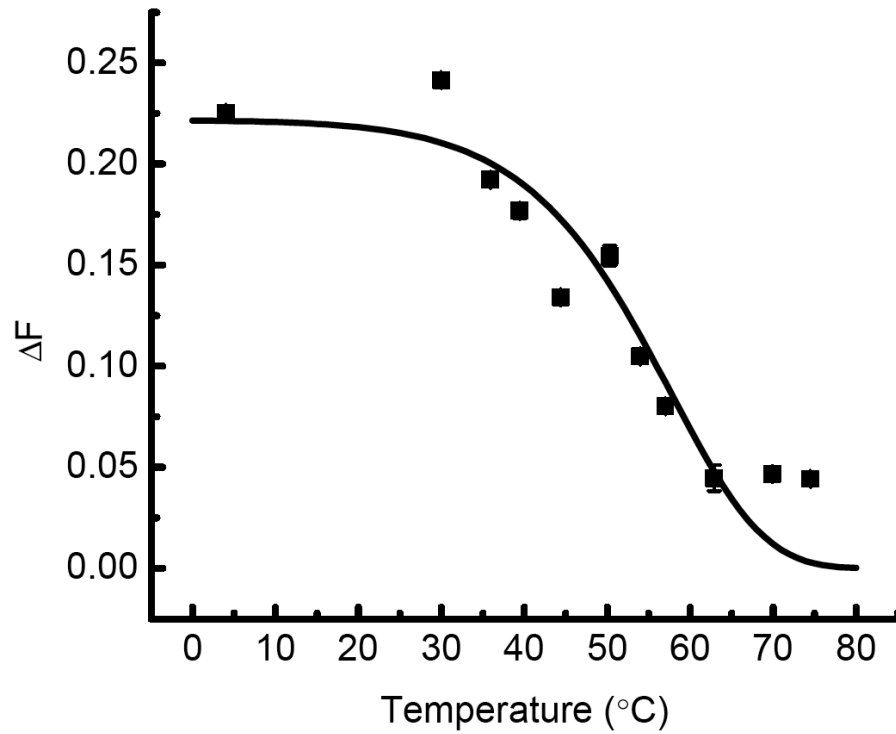


Figure 4-4. Melting curve of CCR5 NABBs. The assembly denatures at 54.5°C. CCR5 NABBs melt over a much broader range than CCR5 in detergent solution, suggesting some sample heterogeneity or a distinct denaturation pathway.

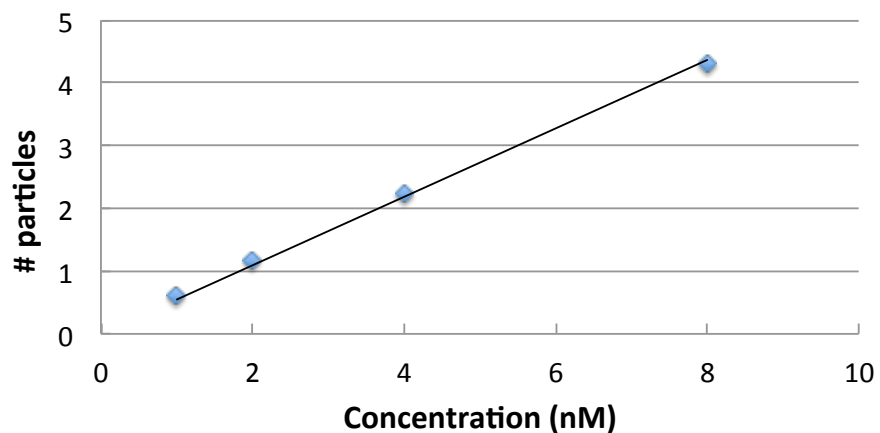
4.2.2 Fluorescence Correlation Spectroscopy Measurements of Oligonucleotide

Standards and CCR5 NABBs

Fluorescence correlation spectroscopy (FCS) is a sensitive microscopy technique that relies on the fluctuating intensity from small numbers of molecules diffusing through a confocal volume. The autocorrelation function of the intensity trace reveals information about the concentration, size, and dynamics of the diffusing species. Additionally, ligand-receptor interactions can be quantitatively measured, especially when a second color is used and the two channels are cross-correlated. This technique is called fluorescence cross-correlation spectroscopy (FCCS) and the same general principles apply. We sought to characterize CCR5 NABBs using these approaches. NABBs are a particularly advantageous platform for FCS studies because the particles are freely diffusing and relatively small.

Prior to studies with NABBs, we developed a system of standards to calibrate the microscope system, ensure the reproducibility of measurements, and determine ideal fitting models. Serial dilutions of free dyes, Alexa 488 and Alexa 647, were first measured to determine the dynamic range of the FCS system. The average number of particles in the confocal volume is determined by the y-intercept of a fit to the autocorrelation function (Ferrand et al., 2011). Plotting this number against the dye concentration produces the FCS standard curves (Figure 4-5). The curves are linear, indicating that the nanomolar concentration range is suitable. Further, the slopes can be used to determine the effective focal volume for each laser excitation line (from Eq. 16 in Chapter 2.16). The focal volumes at 488 nm and 633 nm were calculated to be 0.32 fL and 0.51 fL, respectively. These sub-femtoliter volumes are within the range expected

A.



B.

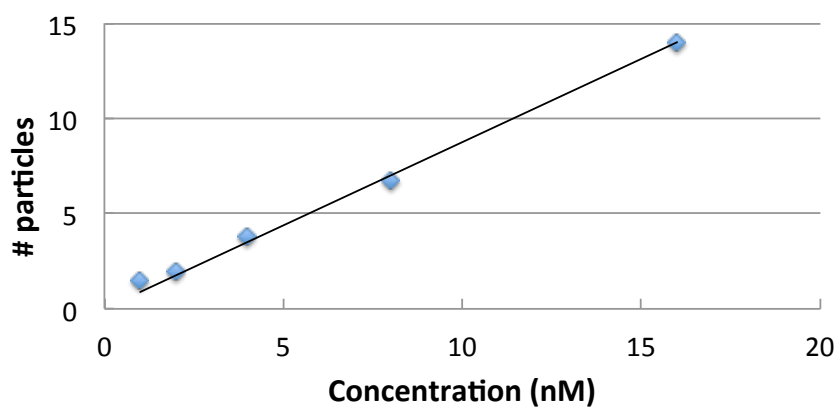


Figure 4-5. FCS standard curves for Alexa 488 (A) and Alexa 647 (B). The calculated average number of particles in the focal volume is plotted against the dye concentration. The slope of this curve was used to calculate focal volumes of 0.32 fL and 0.51 fL for the two dyes.

and acceptable for FCS studies. Average diffusion correlation times for Alexa 488 and Alexa 647 were 42 μs and 63 μs in the setup. These values, along with known reference diffusion coefficients (Kapusta, 2010; Petrasek and Schwille, 2008), can be inputted into Eq. 17 and Eq 18 of Chapter 2.16 to calculate the lateral radius and translational structural parameter, which is defined as the ratio of the axial radius to the lateral radius. The lateral radius and structural parameter of Alexa 488 were 270 nm and 2.9; for Alexa 647, the figures were 290 nm and 3.8.

Because complementary oligonucleotides anneal with high efficiency, we reasoned that they would serve as useful codiffusion probes. Oligos carrying Alexa 488 and Alexa 647 were custom synthesized (Fisher Operon) to generate standards for FCCS. The sequences were 40 base pairs – long enough to avoid FRET – and were chosen based on a previous study (Schwille et al., 1997). These reagents are depicted in Figure 4-6A. The autocorrelation curves for the oligos are presented in Figure 4-6B alongside those of the free dyes. As expected, the larger oligos diffuse through the confocal volume more slowly, with calculated diffusion times of 380 μs (Oligo 1) and 320 μs (Oligo 3). Note that in this plot, the correlations were normalized so that shifts in diffusion time could be easily visualized. For FCCS measurements, the oligos were annealed with a slow cool from 77°C to 55°C. Binding causes the Alexa 488 and Alexa 647 dyes to diffuse through the focal volume together, which we expected to result in cross-correlation between the 488 nm and 633 nm excitation lines. In contrast, a mixture of the two free dyes should show no cross-correlation. Indeed, this was the case. The results of the FCCS experiments are shown in Figure 4-6C. As predicted, the annealed oligos diffuse together with a longer diffusional correlation time, 510 μs , compared to the individual oligos.

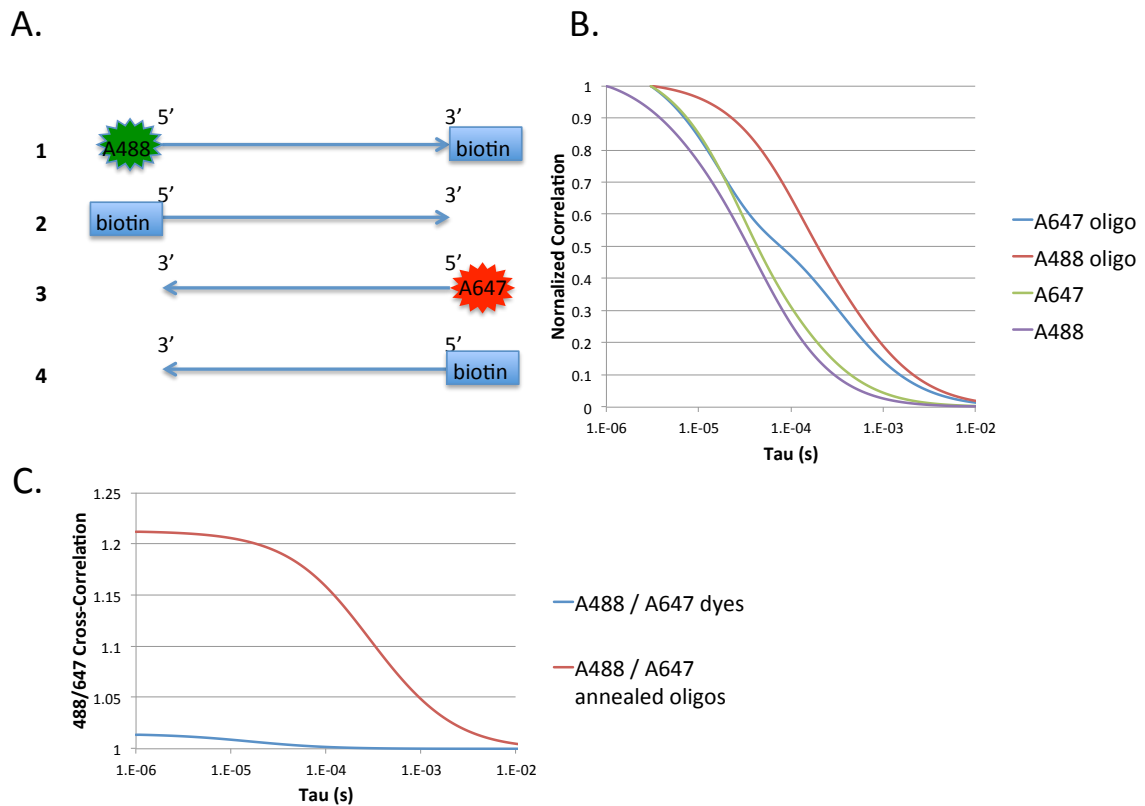


Figure 4-6. (A) Cartoon diagram of the oligonucleotides synthesized as FCS and FCCS standards. Oligos 3-4 are the reverse complement sequence of oligos 1-2. The biotin handles were included so the oligos could be captured in future total internal reflection fluorescence experiments. (B) Correlation curves of Alexa 488 and Alexa 647 dyes (purple, green) and oligos (red, blue). The oligos are larger species and therefore diffuse through the focal volume more slowly, hence curves shift to the right. (C) Cross-correlation experiments with a mixture of Alexa 488 and Alexa 647 dyes as well as annealed oligos carrying the two labels. Significant cross-correlation between the two channels is observed for the annealed oligos, in which the dyes co-diffuse. In contrast, the mixed dyes do not cross-correlate.

NABBs were first characterized by FCS with Lissamine Rhodamine B-labeled lipids doped in, as shown in Figure 4-2A. The labeled lipids enabled tracing of the particles through the confocal volume and evaluation of the preparation's monodispersity. Correlation curves of NABB-LRB samples are presented in Figure 4-7A. Two different concentrations of the LRB lipids are shown. The higher concentration has a lower y-intercept, as predicted by FCS theory (Chapter 2.16 Eq. 11). There was some variability from experiment to experiment in the diffusion time of NABB samples, but the profiles were typically best fit to two components. A faster component of $\sim 500\text{-}700\ \mu\text{s}$ likely corresponded to NABBs; a slower component of $1000\text{-}2000\ \mu\text{s}$ was probably a small number of aggregates or vesicles. The variations suggested some sample heterogeneities, which increased over time. For example, NABBs left at 4°C for one week after preparation showed a large number of vesicles, which were indicated by large spikes in the intensity trace (Figure 4-7B). Traces with these abnormalities had to be discarded because they skewed the average intensity. We found that dilution of NABBs to $100\ \text{nM}$, rather than a more typical $>1\ \mu\text{M}$, resulted in significantly more aggregates. It appears that dilution of the particles favors their fusion. In addition, qualitative assessment of the traces for vesicle spikes allowed us to determine suitable storage conditions for NABBs. NABBs supplemented with 50% glycerol and stored at -20°C displayed few aggregates for at least a week.

Opsin labeled with Alexa 647 was incorporated into NABBs (as in Figure 4-2B) and subjected to FCS measurements. Compared to freely diffusing dye, the curve is significantly shifted to longer correlation times (Figure 4-7C). In addition, the NABBs curve is more complex, reflecting the sample heterogeneity mentioned above. In some

cases, the receptor-loaded profiles were better fit when a rotational diffusion component was included, a feature that has been mentioned previously (Gao et al., 2011). However, this was not always the case and, in general, the simplest possible model was used to fit the data. To demonstrate a binding experiment, Alexa 647-labeled 2D7 mAb (prepared as described in Chapter 3.1) was incubated with empty NABBs and CCR5 NABBs (Figure 4-7D). The expectation that binding to CCR5 would cause a shift in the diffusion time was borne out. While the change is fairly small, as predicted, future experiments with both a labeled receptor and labeled antibody or ligand should show significant signal above a negative control in FCCS measurements. In addition, they should enable measurement of binding constants because both free and bound ligand can be quantified.

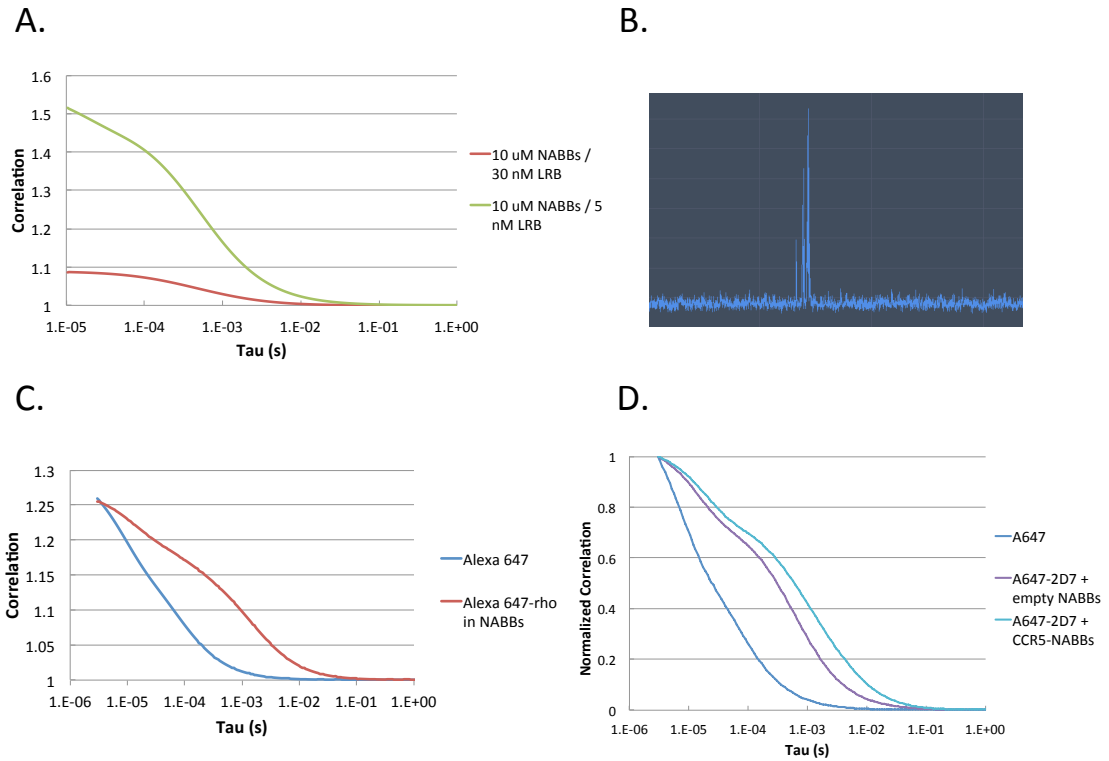


Figure 4-7. FCS experiments with NABBs. (A) Correlation curves of NABBs carrying 30 nM (red) and 5 nM (green) LRB-labeled lipids. The difference in y-intercept reflects the difference in lipid concentration. (B) Example of a spike in intensity due to diffusion of an aggregate through the focal volume. Traces with features like this were not included in the data fits. (C) Alexa 647 dye (blue) and Alexa 647-labeled opsin in NABBs. The NABBs are best fit to a two-component translational diffusion model. (D) Alexa 647 dye (blue) and Alexa 647 labeled 2D7 incubated with empty NABBs (purple) and CCR5 NABBs (cyan). The shift in diffusion time indicates that the antibody binds the receptor in NABBs.

4.3 Discussion

We report a rapid, microscale procedure to incorporate purified CCR5 into membrane nanoparticles called NABBs. NABBs possess a lipid bilayer defined by the experimental conditions, which can be optimized using the HTRF immunosandwich assay described in Chapter 3. The best procedure results in a >15% overall yield of CCR5 with the majority of the receptor able to bind 2D7. Furthermore, incorporation of CCR5 into NABBs confers improved thermal stability compared to detergent solution, an effect that was also observed with rhodopsin in NABBs. (Banerjee et al., 2008). The native-like lipid bilayer of NABBs could be a particularly attractive platform for studies of receptor activation because GPCR aggregation phenomena endemic to detergents are of less concern (Jastrzebska et al., 2004). In addition, because the expression, purification, and NABB formation steps can be scaled, adequate quantities of CCR5 NABBs for structural and biochemical studies should be attainable, especially using inducible suspension-adapted stable cell lines or Sf9 insect cells.

FCS is a versatile technique for obtaining dynamic information from systems in solution, such as NABBs. Though the theory of FCS was largely worked out in the 1970s (Magde et al., 1972), the technical difficulties associated with the method rendered it largely inaccessible to non-specialists until more recently. FCS has been applied to the study of GPCRs, primarily to study the diffusion of receptors in membranes or in screens to identify ligand-receptor interactions (Bridson and Hill, 2007). We first developed a set of standards for our microscope system that included free Alexa Fluor dyes as well as labeled oligonucleotides. These simple samples enabled calibration of the system, measurement of the dynamic range and focal volume, and identification of fluorophores

suitable for these techniques. Alexa 488 performed particularly well, displaying high photon counts rates at nanomolar concentrations. Alexa 647 was slightly less satisfactory due to a high fraction of molecules excited to the triplet state, which complicated fits at short delay times. However, these two dyes proved to be a solid pair for FCCS work, with little leakage between channels. The volume parameters we extracted correspond well with values reported in practical guides to the method (Elson, 2011; Ferrand et al., 2011).

CCR5 NABBs were characterized by FCS to determine sample homogeneity, size, and, suitable storage conditions. Most samples were best fit to two-component models, indicating some vesicle formation even in optimized preparations. Large aggregates were observed rarely, however, and the resulting large deviations from mean fluorescent intensities were easily identified so those experiments could be removed from averages. Aggregates could be prevented for days after initial sample preparation by supplementing NABBs with 50% glycerol and storing at -20°C. The inclusion of glycerol prevents complete freezing, which may drive aggregation of NABBs. The faster diffusing NABBs component in our experiments (500-700 μ s) aligns well with previous FCS reports of ~10 nm nanodiscs (Gao et al., 2011). We also demonstrate binding of a labeled, conformationally sensitive antibody to CCR5 in NABBs, further indicating that the samples include properly folded receptor. Future experiments with a range of antibody and ligand concentrations will allow quantitative study of these binding interactions in the presence and absence of small molecule drugs. Two color FCCS with Alexa 488 and Alexa 647 should facilitate this work.

Chapter Five: Chemical Crosslinking of Rhodopsin in Native Membranes to Identify a Primary Dimerization Interface*

5.1 Introduction

Like many other membrane receptors, GPCRs are known to form dimers and higher-order oligomers in membranes. Functional *trans*-complementation assays, such as one employing chimeric α_2 -adrenergic/M3 muscarinic receptors (Maggio et al., 1993), have provided examples where intermolecular interactions are required for signaling. Immunoprecipitation (Hebert et al., 1996) and bioluminescence resonance energy transfer (Angers et al., 2000) have also demonstrated the presence of β_2 -adrenergic receptor dimers. There are fewer reports describing the functional consequences of dimerization, but they are known in some cases. GABA(B) receptor subtype heterodimerization is required for trafficking to the plasma membrane (White et al., 1998). It has also been shown that the chemokine receptors CXCR7 and CXCR4 form a heterodimer that preferentially recruits β -arrestin rather than heterotrimeric G protein (Decailot et al., 2011). Still, both rhodopsin (Banerjee et al., 2008) and β_2 -adrenergic receptor (Whorton

* Portions of this chapter have been published previously: Knepp AM, Periole X, Marrink SJ, Sakmar TP and Huber T (2012) Rhodopsin Forms a Dimer with Cytoplasmic Helix 8 Contacts in Native Membranes. *Biochemistry* **51**:1819-1821. Periole X, Knepp AM, Sakmar TP, Marrink SJ and Huber T (2012) Structural Determinants of the Supramolecular Organization of G Protein-Coupled Receptors in Bilayers. *J Am Chem Soc* **134**:10959-10965.

et al., 2007) monomers can activate G proteins when segregated in membrane nanoparticles. Another study showed that a 1:1 complex of rhodopsin:transducin resulted in G protein activation at a rate near the diffusion limit (Ernst et al., 2007). This suggests that a monomer is in fact the minimal functional unit for G protein signaling.

The concept of rhodopsin dimerization garnered increased attention upon publication of atomic force microscopy (AFM) images of native rod outer segment (ROS) disk membranes that showed rows of rhodopsin dimers (Fotiadis et al., 2003). This provided perhaps the most striking demonstration yet of the visual system's possible supramolecular organization. The burst in GPCR structural biology over the past several years has also contributed to the dimer debate. While the first crystal structure of rhodopsin showed nonphysiological, antiparallel dimers (Palczewski et al., 2000), some more recent structures, such as those of CXCR4 (Wu et al., 2010) and κ -opioid receptor (Wu et al., 2012), showed physiologically plausible dimers. Despite these advances, the precise interface(s) mediating receptor–receptor contacts remains controversial (Palczewski, 2010). Spatial constraints from the AFM images were used to predict that the primary rhodopsin dimer interface involved transmembrane (TM) helices 4 (H4) and 5 (H5) (Liang et al., 2003). However, two-dimensional (Schertler and Hargrave, 1995) and three-dimensional (Ruprecht et al., 2004) densities obtained from electron microscopy (EM) as well as X-ray data for packing of rhodopsin crystals (Salom et al., 2006) show that dimer contacts involve TM H1 and cytoplasmic H8. Interestingly, the κ -opioid receptor crystal structure revealed dimers that almost exactly match those in the 3D EM densities. It is possible that solubilization conditions drive these dimers – indeed, it has been shown that the choice of detergents greatly affects the oligomeric state of

rhodopsin (Jastrzebska et al., 2006). However, a recent cross-linking study suggests the H1/H8 interface exists for dopamine D2 receptors heterologously expressed at physiological densities in membranes (Guo et al., 2008). The authors interpreted their results in the context of an oligomeric model in which both the H4/H5 and H1/H8 symmetrical interfaces are simultaneously present.

We set out to demonstrate the possibility of the H1/H8 dimer in native disk membranes by cross-linking the endogenous cysteines of rhodopsin and identifying the site(s) involved. Here we go beyond previous studies of rhodopsin in that we identify additional intermolecular cross-linking sites (Jastrzebska et al., 2004). Working with receptors in the native membrane environment eliminates artifacts associated with dimerization in detergent.

5.2 Results

5.2.1 Chemical Crosslinking and Partial Proteolysis Analysis

Rhodopsin contains two primary reactive cysteines (positions 140 and 316), and two additional cysteine residues in H8 (positions 322 and 323) may also be reactive because of incomplete palmitoylation. Structural evidence suggests that the Cys316–Cys316 distance in an H1/H8 interface would be 2–3 nm. (Ruprecht et al., 2004) (Salom et al., 2006). In contrast, these side chains are on opposite faces and thus farther from each other in an H4/H5 dimer arrangement. We hypothesized that a Cys316–Cys316 cross-link using a reagent with a spacer length close to the predicted distance would support the presence of the H1/H8–H1/H8 dimer.

Dark state ROS membranes were first cross-linked with two homobifunctional bis-maleimide reagents containing polyethylene glycol (PEG) spacers of different lengths (Figure 5-1A-B). The cross-linker:rhodopsin stoichiometry was controlled to optimize cross-linking. If an overly large excess is used, the reactive cysteines saturate with the reagent rather than cross-linking to a neighboring receptor. We found that a 5:1 excess of cross-linker resulted in appreciable formation of dimers and higher-order oligomers that could be observed on a gel. Addition of either BM(PEG)₃ (2.1 nm, the sulfur–sulfur distance in the extended conformation of the cross-link) or Bis-MAL-dPEG₃ (3.1 nm) reduced the amount of monomer present relative to a negative control.

To identify the region of the cross-link, we employed a partial proteolysis procedure with thermolysin. Thermolysin cleaves rhodopsin at several C-terminal sites in addition to a primary cut site in the third intracellular loop (Poerber, 1982). The C-terminal

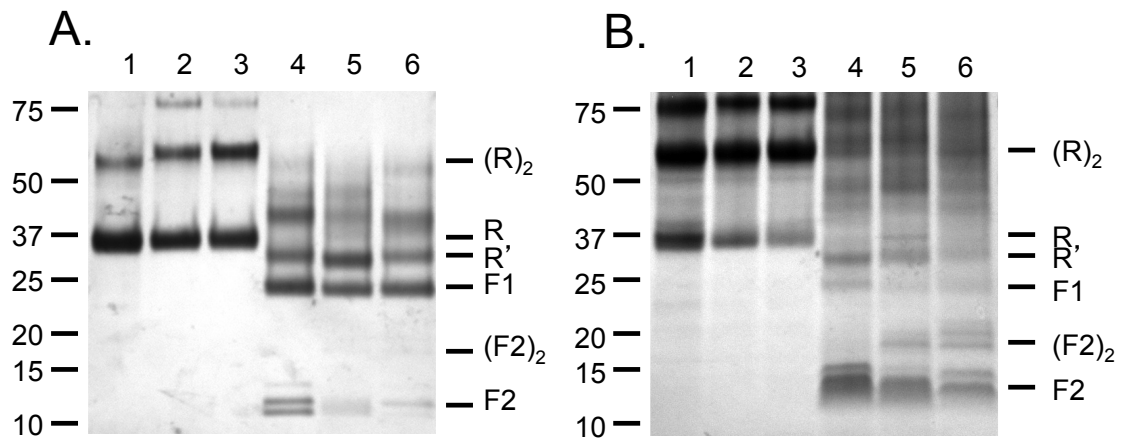


Figure 5-1. Chemical cross-linking of rhodopsin in ROS disk membranes followed by limited proteolysis and SDS-PAGE analysis with silver (A) and Coomassie (B) staining. Samples were analyzed before (lanes 1–3) and after (lanes 4–6) thermolysin treatment (proteolysis) in the absence of cross-linker (lanes 1 and 4), after cross-linking with BM(PEG)₃ (lanes 2 and 5), and after cross-linking with Bis-MAL-dPEG₃ (lanes 3 and 6). The cross-linkers are noncleavable homobifunctional cysteine-reactive reagents with different spacer lengths. R' results from cleavage of short C-terminal peptides; F1 is an ~28 kDa N-terminal peptide, and F2 is an ~12 kDa C-terminal peptide. The appearance of the cross-linker-dependent band (F2)₂ in lanes 5 and 6 of panel B demonstrates the proximity of H8 in adjacent rhodopsin monomers in ROS, as described in the text. This result is consistent with an H1/H8–H1/H8 dimer model.

cuts result in a slightly shorter peptide, R'. Further proteolysis results in two predominant fragments: an ~28 kDa N-terminal peptide (F1) and an ~12 kDa C-terminal peptide (F2). The F1 peptide contains Cys140, and the F2 peptide contains Cys316, Cys322, and Cys323. Because these fragments are easily resolved on a gel, the region of the cysteine cross-link can be determined by observing which of them oligomerize upon addition of the bis-maleimide reagent. As shown in lane 4 of panels A and B of Figure 5-1, R', F1, and several forms of F2 (depending on the extent of C-terminal proteolysis) are the only lower-molecular mass bands observed in a control sample. The F1 band stains relatively poorly with Coomassie, likely because it is glycosylated, so it is clearer in the silver-stained gel. On the other hand, the modified F2 bands are almost invisible with silver staining, but prominent with Coomassie. Upon addition of either cross-linker (Figure 5-1B, lanes 5 and 6), the intensities of the F2 bands decrease and new bands appear near 20 kDa. These bands can correspond to only an F2 dimer, so we conclude that the H8 regions cross-link to each other and are thus in the proximity of each other in neighboring receptors in ROS.

Next, we demonstrated the chemical specificity of the Cys cross-linking with two methanethiosulfonate (MTS) reagents, MTS-O4-MTS (2.2 nm) and MTS-O5-MTS (2.6 nm). The MTS groups are extremely reactive, and cross-linking is observed after just 5 min (Figure 5-2). These reagents have an advantage in the fact that the covalent linkage formed can be cleaved with a reducing agent. Treatment of cross-linked samples with DTT before running a gel collapsed the higher-molecular mass bands back down to primarily monomer, as observed in negative controls. This shows that the cross-linker-dependent bands are the result of thiol reactions and not nonspecific oligomerization.

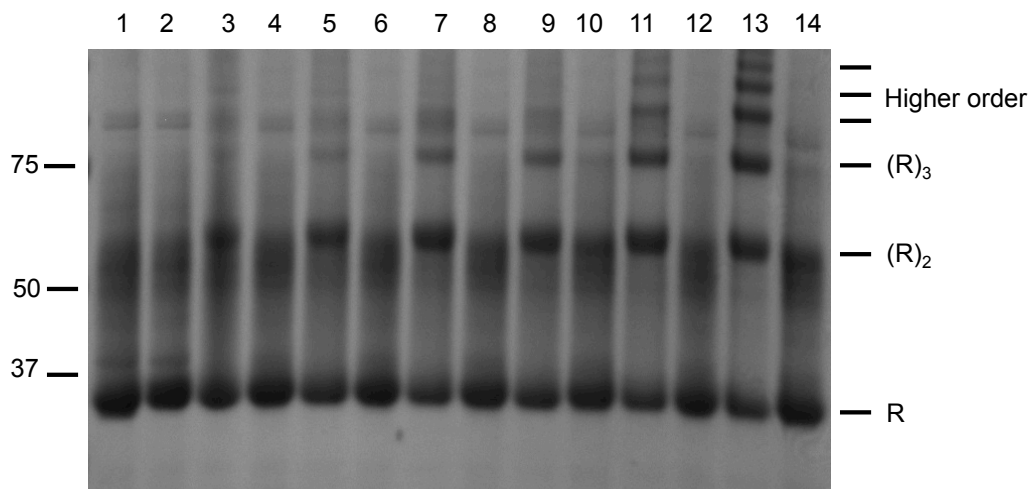


Figure 5-2. Chemical crosslinking of rhodopsin in ROS disc membranes with a cleavable reagent. Samples were analyzed by SDS-PAGE with Coomassie staining in the absence of crosslinker (lanes 1 and 2), in the presence of MTS-O4-MTS for 5 (lanes 3 and 4), 15 (lanes 5 and 6), and 60 min (lanes 7 and 8), and in the presence of MTS-O5-MTS for 5 (lanes 9 and 10), 15 (lanes 11 and 12), and 60 min (lanes 13 and 14). The even numbered lanes were treated with DTT before running the gel. The reduction of crosslinked samples to profiles resembling the negative control in lane 1 demonstrates the chemical specificity of the crosslink.

5.2.2 Liquid Chromatography-Mass Spectrometry Identification of Crosslinked Peptides

We used liquid chromatography and mass spectrometry (LC-MS) to demonstrate definitively the presence of a Cys316-Cys316 dimer cross-link. ROS samples were solubilized, alkylated, and precipitated with trichloroacetic acid. The precipitate was then digested with cyanogen bromide (CNBr), which cleaves after methionines at positions 309 and 317 to yield a small peptide that can be detected by LC-MS. The C-terminal methionine is modified to a homoserine lactone as a result of the chemical cleavage, and iodoacetamide treatment adds a carbamidomethyl group to Cys316 if it has not been substituted with a cross-linker.

In cross-linked samples, the carbamidomethyl-modified 310-317 peptide was identified first (Table 5-1) It appears as several isotopes, and its mass is accurate to several parts per million with respect to theoretical monoisotopic masses. For Bis-MAL-dPEG3 samples, the cross-linked product is simply two 310-317 peptides plus the mass of the reagent. This product appeared as a $z = 4$ ion (Figure 5-3A). For MTS peaks, we identified the 310-317 peptide with carbamidomethyl and N-ethylmaleimide (NEM) (resulting from reaction quenching) and then found the peptide substituted with a cross-linker. Monosubstituted MTS reagents have their second reactive group hydrolyzed to a thiol, which can then be modified with NEM, and this peak was also present. Finally, the cross-linked product was found, again with roughly parts per million accuracy (Figure 5-3B). Crucially, in samples treated with DTT prior to precipitation and digestion, the peaks corresponding to the peptide substituted with the MTS cross-linker were not observed. This additional control confirms the peak assignments. The mass spectrometry

Table 5-1. Mass spectrometry peaks identified in analysis. The masses were calculated by multiplying the peak m/z ratio by its assigned charge. The abbreviations are the following. H: homoserine lactone (position 317 modified by CNBr treatment); C: carbamidomethyl; B: Bis-MAL-dPEG₃; N: N-ethylmaleimide; M: MTS- O5-MTS

Sample	Obs. Mass	Theor. mass	Error (ppm)	Sequence ID	Ion
Bis-MAL-dPEG ₃	1050.508	1050.5029	4.85	310-316-H+C	M+2H
Bis-MAL-dPEG ₃	1051.512	1051.5029	8.65	310-316-H+C	M+2H+1
Bis-MAL-dPEG ₃	1052.514	1052.5029	10.55	310-316-H+C	M+2H+2
Bis-MAL-dPEG ₃	1053.514	1053.5029	10.54	310-316-H+C	M+2H+3
Bis-MAL-dPEG ₃	2510.216	2510.1954	8.21	2*(310-316-H)+B	M+4H+1
Bis-MAL-dPEG ₃	2511.212	2511.1954	6.61	2*(310-316-H)+B	M+4H+2
MTS-O5-MTS	1048.4836	1048.4872	3.43	310-316-H+C	M
MTS-O5-MTS	1118.5264	1118.5291	2.41	310-316-H+C+N	M+2H
MTS-O5-MTS	1119.5276	1119.5291	1.34	310-316-H+C+N	M+2H+1
MTS-O5-MTS	1120.5276	1120.5291	1.34	310-316-H+C+N	M+2H+2
MTS-O5-MTS	1121.529	1121.5291	0.09	310-316-H+C+N	M+2H+3
MTS-O5-MTS	1304.5999	1304.5801	15.18	310-316-H+M	M+H
MTS-O5-MTS	1305.6111	1305.5801	23.74	310-316-H+M	M+H+1
MTS-O5-MTS	1428.6198	1428.6199	0.07	310-316-H+M+N	M+H
MTS-O5-MTS	1429.6204	1429.6199	0.35	310-316-H+M+N	M+H+1
MTS-O5-MTS	1430.6214	1430.6199	1.05	310-316-H+M+N	M+H+2
MTS-O5-MTS	1431.6228	1431.6199	2.03	310-316-H+M+N	M+H+3
MTS-O5-MTS	2293.9846	2294.0223	16.43	2*(310-316-H)+M	M+1
MTS-O5-MTS	2294.9864	2295.0223	15.64	2*(310-316-H)+M	M+2

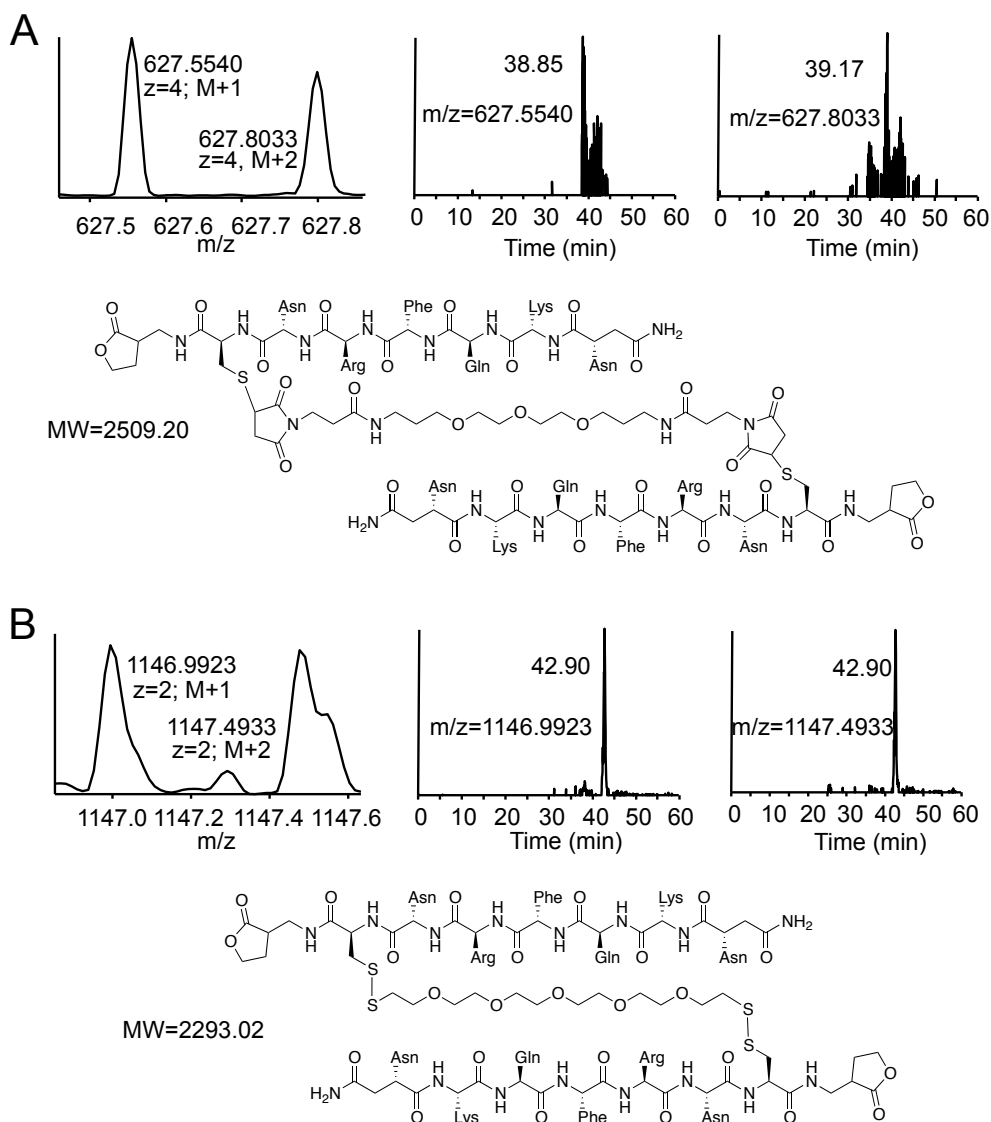


Figure 5-3. LC-MS analysis of Cys316-Cys316 cross-linked peptides. (A) Two 310-317 peptides cross-linked with Bis-MAL-dPEG3. The monoisotopic peaks are $z = 4$ ions. Liquid chromatograms integrated across the two MS peaks show that the species elute at similar times. (B) Two 310-317 peptides cross-linked with MTS-O5-MTS. The monoisotopic peaks are $z = 2$ ions and disappear from samples treated with DTT prior to precipitation. Liquid chromatograms integrated across the MS peaks show that they elute simultaneously.

data conclusively demonstrate the existence of Cys316–Cys316 cross-links. It is notable that this cross-link was only observed with the longer reagents (≥ 2.6 nm) but not with the shorter reagents (≤ 2.2 nm), suggesting the distance between the side chains is less than 2.6 nm. However, the thermal mobility and other factors limit the accuracy of such estimates.

The partial proteolysis and LC–MS data are complementary, highlighting the importance of integrating diverse experimental data to identify cross-linking sites. The gels in Figures 5-1 and 5-2 show extensive oligomerization, so more than one dimerization interface must be relevant. The presence of the (F2)₂ band demonstrates that one of them involves the proximity of H8 regions on adjacent receptors. The LC–MS experiments allow precise identification of the Cys316–Cys316 cross-linking site. The results are especially convincing because the assigned MTS peaks disappear upon addition of DTT, which cleaves the cross-link disulfide bond. Further, because the MTS reagent hydrolyzes so quickly, it is likely that the cross-links result from prearranged dimers and not from random collisions over extended periods of time. Interestingly, the partial proteolysis data show H8 cross-links for all four reagents employed, but the Cys316–Cys316 peaks were identified with only the two longer (Bis- MAL-dPEG₃ and MTS-O5-MTS) cross-linkers. It is possible that either Cys322 or Cys323 cross-links are responsible for the gel shift with the shorter reagents. As with Cys140-containing fragments, we were not able to identify these sites with our CNBr cleavage strategy.

5.3 Discussion

Dimerization of transmembrane receptors is a common theme in signal transduction (Heldin, 1995). GPCRs are no exception – a wealth of biochemical, cell biology, and structural data suggest the presence of dimers (Bouvier, 2001). A particularly compelling, though controversial, example is the report of AFM images of rhodopsin dimers aligned into rows (Fotiadis et al., 2003). While earlier studies demonstrated that rhodopsin could be cross-linked into dimers, the sites were not identified (Jastrzebska et al., 2004). We set out to test the hypothesis that rhodopsin forms dimers mediated by contacts in transmembrane helix 1 and cytoplasmic helix 8. The cross-linking methods used were adapted from the work of earlier groups, in which intramolecular cross-links were identified (Jacobsen et al., 2006; Suda et al., 2004). Here we extend this work and report a Cys316-Cys316 intermolecular cross-link. The cross-link was identified by complementary partial proteolysis and LC-MS approaches and with multiple cross-linkers, strongly supporting a H1/H8 dimer interface. Despite earlier structural evidence suggesting the presence of this interface, its small protein burial raised doubts about its relevance (Lodowski et al., 2007). Buried accessible surface area is often used as a predictor of protein-protein interfaces in aqueous solution, but it seems likely that additional forces, such as lipid-protein interactions, drive associations in bilayers.

To further probe rhodopsin dimerization in membranes, coarse-grained molecular dynamics (CGMD) studies of spontaneous rhodopsin assembly were conducted by our collaborators (Periole et al., 2012). The second most frequently populated dimer cluster

involved an H1/H8 interface similar to structures observed via X-ray crystallography and EM (Figure 5-4). The Cys316–Cys316 side chain bead distance of this cluster (Figure 5-4C) was 2.3 nm (2.6 nm when fitting residues 310–322 of PDB entry 1U19). Notably, a similar but less populated cluster (Figure 5-4D) showed a Cys316–Cys316 distance closer to 1.9 nm (2.1 nm from the local fit of 1U19). It should be noted that the analysis of the CGMD self-assembly simulations on a microsecond time scale does not predict thermodynamic stability, and consequently, cluster populations do not reflect equilibrium distributions. The two structures are spatiotemporally mutually exclusive, but it is difficult to determine which of these arrangements is responsible for the cross-links presented here. If the monomer–dimer exchange is slow on the time scale of the cross-linking experiment, the more stable interface may predominate and thereby exclude the other possible orientation. On the other hand, if the dimers are more transient, then the structure that brings Cys316 residues closer and thus increases the likelihood of cross-linking could account for the data presented.

Note that several distances between Cys316 residues in dimer structures are cited. The Cys316–Cys316 distances generally refer to the distances measured between the $S\gamma$ atoms in the corresponding residue in the two protomers. For the CGMD dimers, we report distances of the side chain beads in the coarse grained model together with fits of crystallographic structures to the coarse grained representations. The first distances mentioned correspond to the distance between Cys316–Cys316 side chain beads in the CGMD dimer clusters: 2.3 nm for the cluster in Figure 5-4C and 1.9 nm for the cluster in Figure 5-4D. The dimer images in the figure panels were generated from a complete fit of $C\alpha$ 1-326 of PDB 1U19 to the CGMD beads. The Cys316–Cys316 distances of the $S\gamma$

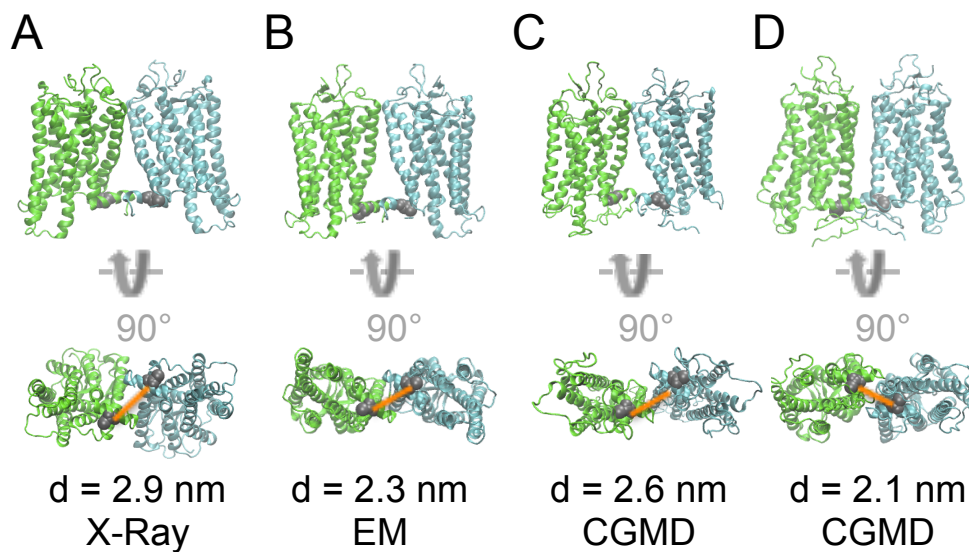


Figure 5-4. Structural and CGMD analysis of H1/H8 dimer orientations. (A) Two symmetry-related promoters from the crystal structure of photoactivated rhodopsin [Protein Data Bank (PDB) entry 2I35]. (B) Crystal structure of rhodopsin (PDB entry 1GZM) fit to the electron density of a metarhodopsin I dimer observed in an EM image (Ruprecht et al., 2004). (C and D) Crystal structure of rhodopsin (PDB entry 1U19) fit to two distinct H1/H8–H1/H8 dimer clusters observed via CGMD analysis.

atoms in these two dimer structures are 2.8 nm and 1.9 nm for 5.4C and 5.4D, respectively. The local fits were generated in a similar manner, except that only Ca 310-322 of PDB 1U19 was fit to the CGMD beads. This resulted in distances of 2.6 nm and 2.1 nm for Figure 5-4C and 5-4D, respectively, which are the distances noted in the figure. Local fitting reduces the effects of distortions in other regions of the receptor that otherwise might result in unsatisfactory fits.

The dimer interfaces observed in the CGMD studies were synthesized with structural information obtained from the AFM images to build a supramolecular model of the rod cell disc membrane (Figure 5-5). In this model, dimers interacting through the H1/H8 interface are stabilized by lipid-lubricated contacts at a second interface involving H4, H5, and H6. This arrangement was stable in further simulations over a μ s time scale. Despite studies that have demonstrated a single receptor is sufficient for full G protein activation, the extremely high density of rhodopsin in disk membranes hints that a dimer may be the primary structural unit that interacts with the heterotrimer. Recent EM images of purified rhodopsin-transducin complexes display densities that favor modeling a receptor dimer (Jastrzebska et al., 2011). It is tempting to speculate that the $G\alpha$ subunit may slide along the rows of dimers in a one-dimensional search for activated receptors. This could explain the very fast temporal response of the system, which exceeds that predicted by free diffusion (Dell'Orco and Schmidt, 2008). In this case, $G\beta\gamma$ would ride in the bilayer slot between rows.

Taken together, the biochemical cross-linking experiments strongly suggest a rhodopsin dimer interface mediated by H1/H8 contacts. This structure has been suggested by previous cross-linking, EM, and crystallography data. Encouragingly, this interface

was also observed in CGMD simulations of rhodopsin monomers in a bilayer. Because cross-linking caused the formation of oligomers, a second interface, perhaps involving H4/H5 contacts, must also be present. The high degree of homology in class A GPCRs suggests that the results reported here might be relevant for other receptors that are known to oligomerize.

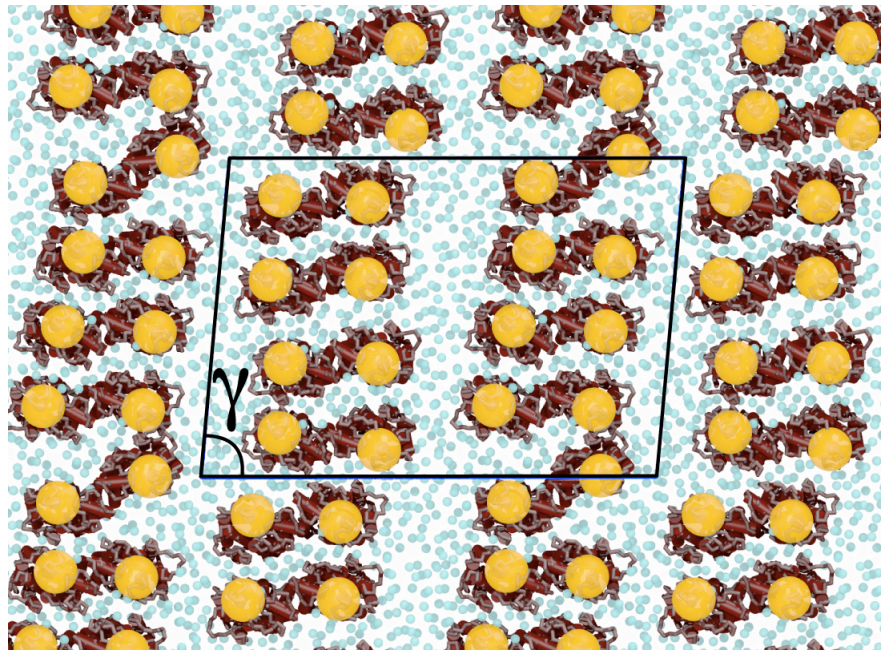


Figure 5-5. Model of the rows-of-dimers organization of rhodopsin molecules after a 16- μs CGMD simulation. The starting conformation was built according to the cell dimensions determined from AFM images of rhodopsin in disk membranes prepared from mouse retinas (Fotiadis et al., 2003; Liang et al., 2003). The lipid molecules are shown as cyan dots placed at the location of the phosphate groups. Rhodopsins are shown in deep red using cylinders for the helices and gray tubes for the backbone trace. The large orange spheres are centered on Thr242 to show the H6 protrusion. The monoclinic unit cell ($\gamma = 85^\circ$) is outlined by a black box; the view is from the cytoplasmic surface. Figure taken from (Periole et al., 2012).

Chapter Six: Future Perspectives

The present is an exciting time in GPCR research. Advances in structural biology, biophysical methods, and chemical biology have energized the field and enabled unprecedented insights into the structure-function relationships of these remarkably important receptors. As described throughout this thesis, much work remains to be done to unite high-resolution structural information with the observed complex signaling phenomena. The technologies and findings herein lend themselves to several threads of ongoing work that support these efforts.

The rate of new crystal structures has rapidly increased in the past several years. Nonetheless, many therapeutically important receptors have yet to yield to crystallization, including CCR5. Since the role of CCR5 in HIV infection was discovered, it has attracted a tremendous amount of attention, and a number of small molecules and biologics have been developed with the aim of blocking viral entry. Though extensive mutagenesis (Maeda et al., 2006; Seibert et al., 2006) and more recent targeted photocrosslinking (Grunbeck et al., 2012) studies have identified the putative binding pockets of some of these drugs, a high-resolution structure would provide new insights that inform existing therapies and perhaps facilitate development of new ones. The HTRF analytical assay has enabled identification of exceptionally stable CCR5 mutants (StaRs), a key step toward crystallization. Intriguingly, though these mutants were shown to be G protein-signaling-dead, they are capable of mediating viral entry. This suggests that a high-resolution structure of one of the StaRs would display an infection-relevant conformation of the

extracellular loops. Though co-crystallization with viral envelope glycoproteins may not be feasible, a combination of docking models and molecular dynamics simulations could shed light on the structural basis of co-receptor activity. Additionally, because CCR5 plays a central role in the immune response, antagonists developed with the initial aim of preventing HIV infection may also find a role in different indications such as rheumatoid arthritis (Horuk, 2009). Detailed structural information of this receptor would advance this ongoing progress. Moreover, the HTRF immunosandwich assay represents a useful new tool for GPCRs and other relatively intractable membrane proteins. Though the formulation developed in this work used a conformationally sensitive antibody, even antibodies to linear epitopes may be sensitive to receptor aggregation upon heat treatment. If this is indeed the case, the approach would be seemingly generalizable to any target of interest that can be appropriately tagged.

The unique properties of the stabilized CCR5 mutants make them interesting candidates for further studies aiming to tease out complicated allosteric behavior. Competition experiments with wild type receptor strongly suggested that small molecule antagonists promote unique conformations (Figure 3-13). Though these data are compelling, the FRET-based experiment cannot distinguish between two plausible explanations for why the signals are lower than unliganded receptor. The small molecules could shift the antibody-receptor equilibrium, resulting in fewer receptors binding both labeled antibodies. Alternatively, the molecules could induce subtle changes in loop conformation that cause the antibody to bind in a different orientation, which would change the distance between donor and acceptor fluorophores. Single molecule fluorescence experiments are capable of ascertaining the correct explanation. Chapter 4

describes a method to incorporate CCR5 into membrane nanoparticles called NABBs, which are useful platforms for single molecule studies. The resultant structures are thermally stable, and the membrane bilayer environment should support folded, functional receptors.

A capture method and TIRF system, in conjunction with site-specific labeling methods, enable long timescale observations of receptors. A capturing surface comprising several layers has already been developed in the Sakmar Lab. The glass surface of a 384-well plate is first silanated to increase its binding capacity. Sequential incubations and washes are then carried out with biotinylated BSA, NeutrAvidin, and biotinylated 1D4 antibody. Remaining biotin binding sites are saturated with biotin prior to addition of fluorescent samples. With labeled CCR5 and labeled 2D7, one could measure the number of receptors bound and not bound to antibodies through fluorescence colocalization. The effects of the small molecules on equilibrium distributions could be tested by adding them at a range of concentrations. On- and off-rates are also accessible by building histograms of the time receptors spend in bound and unbound states before dissociation and association, respectively. The theory and practice of these types of experiments has been well-described (Lakowicz, 2006), and the fluorescently labeled oligonucleotides described in Chapter 4 will serve as useful standards.

With labeled GPCRs, chemokines and G protein subunits, single molecule fluorescence can be applied to address some fundamental questions. Examples include: whether one or two receptors bind the heterotrimer, the precise sequence of signalosome assembly and disassembly, and whether G proteins precouple to receptors (Nobles et al., 2005; Oldham and Hamm, 2007). The stabilized receptor mutants may prove to be

especially interesting tools here – though they do not appear to bind RANTES with measurable affinity, they may bind other chemokines or couple to G proteins in an unproductive manner. Recombinant chemokine analogues with unique antiviral and signaling properties could also be tested (Gaertner et al., 2008). Because the experimental platforms have been designed to handle very small amounts of sample, the numerous combinatorial possibilities can be explored without becoming prohibitively laborious and/or expensive.

FCS represents a valuable complementary method to TIRF. While not strictly a single molecule technique, samples are observed in solution so any artifacts associated with surface immobilization are bypassed. Applying two color FCCS to these problems enables many of the same binding events to be monitored quantitatively. This method is not merely confirmatory, however. FCCS may be a superior approach for bringing these studies *in vivo*, as previous work has demonstrated its potential for studying interactions within signaling networks (Slaughter et al., 2007). The development of standards and analysis methods described in Chapter 4 should facilitate work along these lines. Like TIRF, FCS is a very sensitive technique that requires small sample quantities.

The functional consequences of GPCR dimerization might also be accessible through these methods. NABBs are a particularly attractive system for this application because dimers can be isolated. Though earlier work showed that GPCR monomers efficiently activate G proteins, it is possible that a dimerization results in preferential recruitment of certain cytoplasmic proteins over others. To use CXCR4-CXCR7 heterodimerization as an example (Decaillet et al., 2011), one could label both receptors and look for differences in binding to G protein subunits between monomers and

colocalized receptors.

A variety of data will be needed to advance our understanding of the structural basis of GPCR dimerization. Crystallography serves an integral role, especially if physiologically relevant structures can be trapped. This might be accomplished by strategically crosslinking receptors prior to purification, or by assessing the effect of detergents and lipids on the oligomeric state of the receptor. Chemical crosslinking experiments combined with methods to identify the site(s) should be applied to receptors other than rhodopsin, especially in cases where dimers have been suggested to play a functional role. Because heterologous expression systems will be necessary for other receptors, maintaining a physiological receptor density will be crucial to the obtainment of meaningful results (Guo et al., 2008). Finally, a combination of computational approaches (Periole et al., 2012) and structural methods such as AFM and cryo-EM will be needed to construct supramolecular models of GPCRs oligomers and other binding partners. Though extremely high receptor densities make the visual system a special case, it is possible that GPCRs form higher-order structures in plasma membrane regions with certain lipid compositions, resulting in a similar improvement of temporal response to a stimulus.

In sum, GPCRs will continue to be one of the more challenging and important research foci in human biology. Their central role in physiology and therapeutics mandate attention, and their complex signaling behavior ensures there will be no shortage of open questions to pursue. Though these receptors present considerable obstacles, the many recent technical advances have made the most interesting problems more tractable than ever before.

References

- Albizu L, Teppaz G, Seyer R, Bazin H, Ansanay H, Manning M, Mouillac B and Durroux T (2007) Toward efficient drug screening by homogeneous assays based on the development of new fluorescent vasopressin and oxytocin receptor ligands. *J Med Chem* **50**:4976-4985.
- Alexandrov AI, Mileni M, Chien EYT, Hanson MA and Stevens RC (2008) Microscale fluorescent thermal stability assay for membrane proteins. *Structure* **16**:351-359.
- Allen SJ, Crown SE and Handel TM (2007) Chemokine: Receptor structure, interactions, and antagonism, in *Annual Review of Immunology* pp 787-820, Annual Reviews, Palo Alto.
- Angers S, Salahpour A, Joly E, Hilairet S, Chelsky D, Dennis M and Bouvier M (2000) Detection of beta(2)-adrenergic receptor dimerization in living cells using bioluminescence resonance energy transfer (BRET). *Proc Natl Acad Sci U S A* **97**:3684-3689.
- Baba M, Nishimura O, Kanzaki N, Okamoto M, Sawada H, Iizawa Y, Shiraishi M, Aramaki Y, Okonogi K, Ogawa Y, Meguro K and Fujino M (1999) A small-molecule, nonpeptide CCR5 antagonist with highly potent and selective anti-HIV-1 activity. *Proc Natl Acad Sci U S A* **96**:5698-5703.

- Banerjee S, Huber T and Sakmar TP (2008) Rapid incorporation of functional rhodopsin into nanoscale apolipoprotein bound bilayer (NABB) particles. *J Mol Biol* **377**:1067-1081.
- Bartfai T, Benovic JL, Bockaert J, Bond RA, Bouvier M, Christopoulos A, Civelli O, Devi LA, George SR, Inui A, Kobilka B, Leurs R, Neubig R, Pin JP, Quirion R, Roques BP, Sakmar TP, Seifert R, Stenkamp RE and Strange PG (2004) The state of GPCR research in 2004. *Nat Rev Drug Discov* **3**:574-626.
- Bazin H, Preaudat M, Trinquet E and Mathis G (2001) Homogeneous time resolved fluorescence resonance energy transfer using rare earth cryptates as a tool for probing molecular interactions in biology. *Spectrosc Acta Pt A-Molec Biomolec Spectr* **57**:2197-2211.
- Bigay J and Chabre M (1994) Purification of transducin. *Methods Enzymol* **237**:139-146.
- Blanpain C, Doranz BJ, Vakili J, Rucker J, Govaerts C, Baik SSW, Lorthioir O, Migeotte I, Libert F, Baleux F, Vassart G, Doms RW and Parmentier M (1999) Multiple charged and aromatic residues in CCR5 amino-terminal domain are involved in high affinity binding of both chemokines and HIV-1 Env protein. *J Biol Chem* **274**:34719-34727.
- Bockaert J and Pin JP (1999) Molecular tinkering of G protein-coupled receptors: an evolutionary success. *Embo J* **18**:1723-1729.
- Bouvier M (2001) Oligomerization of G-protein-coupled transmitter receptors. *Nat Rev Neurosci* **2**:274-286.
- Brady AE and Limbird LE (2002) G protein-coupled receptor interacting proteins: Emerging roles in localization and signal transduction. *Cell Signal* **14**:297-309.

- Bridson SJ and Hill SJ (2007) Pharmacology under the microscope: the use of fluorescence correlation spectroscopy to determine the properties of ligand-receptor complexes. *Trends Pharmacol Sci* **28**:637-645.
- Bridson SJ, Middleton RJ, Yates AS, George MW, Kellam B and Hill SJ (2004) Application of fluorescence correlation spectroscopy to the measurement of agonist binding to a G-protein coupled receptor at the single cell level. *Faraday Discuss* **126**:197-207.
- Cherezov V, Rosenbaum DM, Hanson MA, Rasmussen SGF, Thian FS, Kobilka TS, Choi HJ, Kuhn P, Weis WI, Kobilka BK and Stevens RC (2007) High-resolution crystal structure of an engineered human beta(2)-adrenergic G protein-coupled receptor. *Science* **318**:1258-1265.
- Chien EYT, Liu W, Zhao QA, Katritch V, Han GW, Hanson MA, Shi L, Newman AH, Javitch JA, Cherezov V and Stevens RC (2010) Structure of the Human Dopamine D3 Receptor in Complex with a D2/D3 Selective Antagonist. *Science* **330**:1091-1095.
- Chiu ML, Tsang C, Grihalde N and MacWilliams MP (2008) Over-expression, solubilization, and purification of G protein-coupled receptors for structural biology. *Comb Chem High Throughput Screen* **11**:439-462.
- Choe HW, Kim YJ, Park JH, Morizumi T, Pai EF, Krauss N, Hofmann KP, Scheerer P and Ernst OP (2011) Crystal structure of metarhodopsin II. *Nature* **471**:651-U137.
- Cornish PV and Ha T (2007) A survey of single-molecule techniques in chemical biology. *ACS Chem Biol* **2**:53-61.

- Cummings RT, McGovern HM, Zheng S, Park YW and Hermes JD (1999) Use of a phosphotyrosine-antibody pair as a general detection method in homogeneous time-resolved fluorescence: Application to human immunodeficiency viral protease. *Anal Biochem* **269**:79-93.
- Decaillot FM, Kazmi MA, Lin Y, Ray-Saha S, Sakmar TP and Sachdev P (2011) CXCR7/CXCR4 Heterodimer Constitutively Recruits beta-Arrestin to Enhance Cell Migration. *J Biol Chem* **286**:32188-32197.
- Dell'Orco D and Schmidt H (2008) Mesoscopic Monte Carlo simulations of stochastic encounters between photoactivated rhodopsin and transducin in disc membranes. *J Phys Chem B* **112**:4419-4426.
- Deupi X and Kobilka B (2007) Activation of G Protein Coupled Receptors. *Adv Protein Chem* **74**:137-166.
- Devigny C, Perez-Balderas F, Hoogeland B, Cuboni S, Wachtel R, Mauch CP, Webb KJ, Deussing JM and Hausch F (2011) Biomimetic Screening of Class-B G Protein-Coupled Receptors. *J Am Chem Soc* **133**:8927-8933.
- Dore AS, Robertson N, Errey JC, Ng I, Hollenstein K, Tehan B, Hurrell E, Bennett K, Congreve M, Magnani F, Tate CG, Weir M and Marshall FH (2011) Structure of the Adenosine A(2A) Receptor in Complex with ZM241385 and the Xanthines XAC and Caffeine. *Structure* **19**:1283-1293.
- Dorr P, Westby M, Dobbs S, Griffin P, Irvine B, Macartney M, Mori J, Rickett G, Smith-Burchnell C, Napier C, Webster R, Armour D, Price D, Stammen B, Wood A and Perros M (2005) Maraviroc (UK-427,857), a potent, orally bioavailable, and selective small-molecule inhibitor of chemokine receptor CCR5 with broad-

- spectrum anti-human immunodeficiency virus type 1 activity. *Antimicrob Agents Chemother* **49**:4721-4732.
- Dorsam RT and Gutkind JS (2007) G-protein-coupled receptors and cancer. *Nat Rev Cancer* **7**:79-94.
- Elson EL (2011) Fluorescence Correlation Spectroscopy: Past, Present, Future. *Biophys J* **101**:2855-2870.
- Ernst OP, Gramse V, Kolbe M, Hofmann KP and Heck M (2007) Monomeric G protein-coupled receptor rhodopsin in solution activates its G protein transducin at the diffusion limit. *Proc Natl Acad Sci U S A* **104**:10859-10864.
- Farrens DL, Altenbach C, Yang K, Hubbell WL and Khorana HG (1996) Requirement of rigid-body motion of transmembrane helices for light activation of rhodopsin. *Science* **274**:768-770.
- Farzan M, Mirzabekov T, Kolchinsky P, Wyatt R, Cayabyab M, Gerard NP, Gerard C, Sodroski J and Choe H (1999) Tyrosine sulfation of the amino terminus of CCR5 facilitates HIV-1 entry. *Cell* **96**:667-676.
- Ferrand P, Wenger J and Rigneault H (2011) Fluorescence Correlation Spectroscopy, in *Single Molecule Analysis: Methods and Protocols* (Peterman EJG and Wuite GJL eds) pp 181-195, Humana Press Inc, 999 Riverview Dr, Ste 208, Totowa, Nj 07512-1165 USA.
- Foord SM, Bonner TI, Neubig RR, Rosser EM, Pin JP, Davenport AP, Spedding M and Harmar AJ (2005) International Union of Pharmacology. XLVI. G protein-coupled receptor list. *Pharmacol Rev* **57**:279-288.

- Fotiadis D, Liang Y, Filipek S, Saperstein DA, Engel A and Palczewski K (2003)
Atomic-force microscopy: Rhodopsin dimers in native disc membranes. *Nature*
421:127-128.
- Fredriksson R and Schioth HB (2005) The repertoire of G-protein-coupled receptors in
fully sequenced genomes. *Mol Pharmacol* **67**:1414-1425.
- Gaertner H, Cerini F, Escola JM, Kuenzi G, Melotti A, Offord R, Rossitto-Borlat I,
Nedellec R, Salkowitz J, Gorochov G, Mosier D and Hartley O (2008) Highly
potent, fully recombinant anti-HIV chemokines: Reengineering a low-cost
microbicide. *Proc Natl Acad Sci U S A* **105**:17706-17711.
- Gao TJ, Blanchette CD, He W, Bourguet F, Ly S, Katzen F, Kudlicki WA, Henderson
PT, Laurence TA, Huser T and Coleman MA (2011) Characterizing diffusion
dynamics of a membrane protein associated with nanolipoproteins using
fluorescence correlation spectroscopy. *Protein Sci* **20**:437-447.
- Gether U, Ballesteros JA, Seifert R, SandersBush E, Weinstein H and Kobilka BK (1997)
Structural instability of a constitutively active G protein-coupled receptor -
Agonist-independent activation due to conformational flexibility. *J Biol Chem*
272:2587-2590.
- Ghanouni P, Gryczynski Z, Steenhuis JJ, Lee TW, Farrens DL, Lakowicz JR and Kobilka
BK (2001) Functionally different agonists induce distinct conformations in the G
protein coupling domain of the beta(2) adrenergic receptor. *J Biol Chem*
276:24433-24436.

- Grunbeck A, Huber T, Abrol R, Trzaskowski B, Goddard WA and Sakmar TP (2012)
Genetically Encoded Photo-cross-linkers Map the Binding Site of an Allosteric
Drug on a G Protein-Coupled Receptor. *ACS Chem Biol* **7**:967-972.
- Guo W, Urizar E, Kralikova M, Mobarec JC, Shi L, Filizola M and Javitch JA (2008)
Dopamine D2 receptors form higher order oligomers at physiological expression
levels. *Embo J* **27**:2293-2304.
- Haga K, Kruse AC, Asada H, Yurugi-Kobayashi T, Shiroishi M, Zhang C, Weis WI,
Okada T, Kobilka BK, Haga T and Kobayashi T (2012) Structure of the human
M2 muscarinic acetylcholine receptor bound to an antagonist. *Nature* **482**:547-
U147.
- Hebert TE, Moffett S, Morello JP, Loisel TP, Bichet DG, Barret C and Bouvier M (1996)
A peptide derived from a beta(2)-adrenergic receptor transmembrane domain
inhibits both receptor dimerization and activation. *J Biol Chem* **271**:16384-16392.
- Hegener O, Prenner L, Runkel F, Baader SL, Kappler J and Haberlein H (2004)
Dynamics of beta(2)-adrenergic receptor - Ligand complexes on living cells.
Biochemistry **43**:6190-6199.
- Heldin CH (1995) Dimerization of cell-surface receptor in signal-transduction. *Cell*
80:213-223.
- Hofmann KP, Scheerer P, Hildebrand PW, Choe HW, Park JH, Heck M and Ernst OP
(2009) A G protein-coupled receptor at work: the rhodopsin model. *Trends*
BiochemSci **34**:540-552.
- Horuk R (2009) OPINION Chemokine receptor antagonists: overcoming developmental
hurdles. *Nat Rev Drug Discov* **8**:23-33.

- Hubbard R (1958) The thermal stability of rhodopsin and opsin. *J Gen Physiol* **42**:259-280.
- Huber T and Sakmar TP (2011) Escaping the flatlands: new approaches for studying the dynamic assembly and activation of GPCR signaling complexes. *Trends Pharmacol Sci* **32**:410-419.
- Insel PA, Tang CM, Hahntow I and Michel MC (2007) Impact of GPCRs in clinical medicine: Monogenic diseases, genetic variants and drug targets. *Biochim Biophys Acta-Biomembr* **1768**:994-1005.
- Jaakola VP, Griffith MT, Hanson MA, Cherezov V, Chien EYT, Lane JR, Ijzerman AP and Stevens RC (2008) The 2.6 Angstrom Crystal Structure of a Human A(2A) Adenosine Receptor Bound to an Antagonist. *Science* **322**:1211-1217.
- Jacobsen RB, Sale KL, Ayson MJ, Novak P, Hong JH, Lane P, Wood NL, Kruppa GH, Young MM and Schoeniger JS (2006) Structure and dynamics of dark-state bovine rhodopsin revealed by chemical cross-linking and high-resolution mass spectrometry. *Protein Sci* **15**:1303-1317.
- Jastrzebska B, Fotiadis D, Jang GF, Stenkamp RE, Engel A and Palczewski K (2006) Functional and structural characterization of rhodopsin oligomers. *J Biol Chem* **281**:11917-11922.
- Jastrzebska B, Maeda T, Zhu L, Fotiadis D, Filipek S, Engel A, Stenkamp RE and Palczewski K (2004) Functional characterization of rhodopsin monomers and dimers in detergents. *J Biol Chem* **279**:54663-54675.
- Jastrzebska B, Ringler P, Lodowski DT, Moiseenkova-Bell V, Golczak M, Muller SA, Palczewski K and Engel A (2011) Rhodopsin-transducin heteropentamer: Three-

- dimensional structure and biochemical characterization. *J Struct Biol* **176**:387-394.
- Ji C, Zhang J, Dioszegi M, Chiu S, Rao E, deRosier A, Cammack N, Brandt M and Sankuratri S (2007) CCR5 small-molecule antagonists and monoclonal antibodies exert potent synergistic antiviral effects by cobinding to the receptor. *Mol Pharmacol* **72**:18-28.
- Kane SA, Fleener CA, Zhang YS, Davis LJ, Musselman AL and Huang PS (2000) Development of a binding assay for p53/HDM2 by using homogeneous time-resolved fluorescence. *Anal Biochem* **278**:29-38.
- Kapusta P (2010) Absolute Diffusion Coefficients: Compilation of Reference Data for FCS Calibration, in *Application Notes*, PicoQuant GmbH.
- Kenakin T (1997) Protean agonists - Keys to receptor active states?, in *Receptor Classification: The Integration of Operational, Structural, and Transductional Information* (Trist DG, Humphrey PPA, Leff P and Shankley NP eds) pp 116-125, New York Acad Sciences, New York.
- Kenakin T (2003) Ligand-selective receptor conformations revisited: the promise and the problem. *Trends Pharmacol Sci* **24**:346-354.
- Khurana S, Kennedy M, King LR and Golding H (2005) Identification of a linear peptide recognized by monoclonal antibody 2D7 capable of generating CCR5-Specific antibodies with human immunodeficiency virus-neutralizing activity. *J Virol* **79**:6791-6800.

- Knepp AM, Grunbeck A, Banerjee S, Sakmar TP and Huber T (2011) Direct Measurement of Thermal Stability of Expressed CCR5 and Stabilization by Small Molecule Ligands. *Biochemistry* **50**:502-511.
- Knepp AM, Periole X, Marrink SJ, Sakmar TP and Huber T (2012) Rhodopsin Forms a Dimer with Cytoplasmic Helix 8 Contacts in Native Membranes. *Biochemistry* **51**:1819-1821.
- Knepp AM, Sakmar TP and Huber T (2013) Homogeneous time-resolved fluorescence assay to probe folded G protein-coupled receptors. *Methods in Enzymology* **522**:169-189.
- Kondru R, Zhang J, Ji C, Mirzadegan T, Rotstein D, Sankuratri S and Dioszegi M (2008) Molecular interactions of CCR5 with major classes of small-molecule anti-HIV CCR5 antagonists. *Mol Pharmacol* **73**:789-800.
- Kraft P, Mills J and Dratz E (2001) Mass spectrometric analysis of cyanogen bromide fragments of integral membrane proteins at the picomole level: Application to rhodopsin. *Anal Biochem* **292**:76-86.
- Krupnick JG and Benovic JL (1998) The role of receptor kinases and arrestins in G protein-coupled receptor regulation. *Annu Rev Pharmacol Toxicol* **38**:289-319.
- Kuhmann SE and Hartley O (2008) Targeting chemokine receptors in HIV: A status report, in *Annu Rev Pharmacol Toxicol* pp 425-461, Annual Reviews, Palo Alto.
- Kuhmann SE, Pugach P, Kunstman KJ, Taylor J, Stanfield RL, Snyder A, Strizki JM, Riley J, Baroudy BM, Wilson IA, Korber BT, Wolinsky SM and Moore JP (2004) Genetic and phenotypic analyses of human immunodeficiency virus type 1 escape from a small-molecule CCR5 inhibitor. *J Virol* **78**:2790-2807.

- Lagerstrom MC and Schioth HB (2008) Structural diversity of G protein-coupled receptors and significance for drug discovery. *Nat Rev Drug Discov* **7**:339-357.
- Lakowicz JR (2006) *Principles of Fluorescence Spectroscopy, Third Edition*, Springer, New York, NY.
- Landin JS, Katragadda M and Albert AD (2001) Thermal destabilization of rhodopsin and opsin by proteolytic cleavage in bovine rod outer segment disk membranes. *Biochemistry* **40**:11176-11183.
- Lebon G, Warne T, Edwards PC, Bennett K, Langmead CJ, Leslie AGW and Tate CG (2011) Agonist-bound adenosine A(2A) receptor structures reveal common features of GPCR activation. *Nature* **474**:521-U154.
- Lee B, Sharron M, Blanpain C, Doranz BJ, Vakili J, Setoh P, Berg E, Liu G, Guy HR, Durell SR, Parmentier M, Chang CN, Price K, Tsang M and Doms RW (1999) Epitope mapping of CCR5 reveals multiple conformational states and distinct but overlapping structures involved in chemokine and coreceptor function. *J Biol Chem* **274**:9617-9626.
- Liang Y, Fotiadis D, Filipek S, Saperstein DA, Palczewski K and Engel A (2003) Organization of the G protein-coupled receptors rhodopsin and opsin in native membranes. *J Biol Chem* **278**:21655-21662.
- Lodowski DT, Salom D, Le Trong I, Teller DC, Ballesteros JA, Palczewski K and Stenkamp RE (2007) Crystal packing analysis of Rhodopsin crystals. *J Struct Biol* **158**:455-462.

- Lopez-Crapez E, Malinge JM, Gatchitch F, Casano L, Langlois T, Pugnieri M, Roquet F, Mathis G and Bazin H (2008) A homogeneous resonance energy transfer-based assay to monitor MutS/DNA interactions. *Anal Biochem* **383**:301-306.
- Lundstrom K, Wagner R, Reinhart C, Desmyter A, Cherouati N, Magnin T, Zeder-Lutz G, Courtot M, Prual C, Andre N, Hassaine G, Michel H, Cambillau C and Pattus F (2006) Structural genomics on membrane proteins: comparison of more than 100 GPCRs in 3 expression systems. *Journal of Structural and Functional Genomics* **7**:77-91.
- Lusso P (2006) HIV and the chemokine system: 10 years later. *Embo J* **25**:447-456.
- Maeda K, Das D, Ogata-Aoki H, Nakata H, Miyakawa T, Tojo Y, Norman R, Takaoka Y, Ding JP, Arnold GF, Arnold E and Mitsuya H (2006) Structural and molecular interactions of CCR5 inhibitors with CCR5. *J Biol Chem* **281**:12688-12698.
- Magde D, Webb WW and Elson E (1972) Thermodynamic fluctuations in a reacting system - measurement by fluorescence correlation spectroscopy. *Phys Rev Lett* **29**:705-&.
- Maggio R, Vogel Z and Wess J (1993) Coexpression studies with mutant muscarinic adrenergic-receptors provide evidence for intermolecular cross-talk between G-protein-linked receptors. *Proc Natl Acad Sci U S A* **90**:3103-3107.
- Manglik A, Kruse AC, Kobilka TS, Thian FS, Mathiesen JM, Sunahara RK, Pardo L, Weis WI, Kobilka BK and Granier S (2012) Crystal structure of the mu-opioid receptor bound to a morphinan antagonist. *Nature* **485**:321-U170.
- Marozsan AJ, Kuhmann SE, Morgan T, Herrera C, Rivera-Troche E, Xu S, Baroudy BM, Strizki J and Moore JP (2005) Generation and properties of a human

- immunodeficiency virus type I isolate resistant to the small molecule CCR5 inhibitor, SCH-417690 (SCH-D). *Virology* **338**:182-199.
- Mathis G (1995) Probing molecular-interactions with homogeneous techniques based on rare-earth cryptates and fluorescence energy-transfer. *Clin Chem* **41**:1391-1397.
- Mendes HF, van der Spuy J, Chapple JP and Cheetham ME (2005) Mechanisms of cell death in rhodopsin retinitis pigmentosa: implications for therapy. *Trends Mol Med* **11**:177-185.
- Menon ST, Han M and Sakmar TP (2001) Rhodopsin: Structural basis of molecular physiology. *Physiol Rev* **81**:1659-1688.
- Mirzabekov T, Bannert N, Farzan M, Hofmann W, Kolchinsky P, Wu LJ, Wyatt R and Sodroski J (1999) Enhanced expression, native purification, and characterization of CCR5, a principal HIV-1 coreceptor. *J Biol Chem* **274**:28745-28750.
- Molday RS and Mackenzie D (1983) Monoclonal-antibodies to rhodopsin - characterization, cross-reactivity, and application as structural probes. *Biochemistry* **22**:653-660.
- Nath A, Atkins WM and Sligar SG (2007) Applications of phospholipid bilayer nanodiscs in the study of membranes and membrane proteins. *Biochemistry* **46**:2059-2069.
- Nath A, Trexler AJ, Koo P, Miranker AD, Atkins WM and Rhoades E (2010) Single-molecule fluorescence spectroscopy using phospholipid bilayer nanodiscs, in *Methods in Enzymology, Vol 472: Single Molecule Tools, Pt A: Fluorescence Based Approaches* (Walter NG ed) pp 89-117, Elsevier Academic Press Inc, San Diego.

- Navratilova I, Dioszegi M and Myszka DG (2006) Analyzing ligand and small molecule binding activity of solubilized GPCRs using biosensor technology. *Anal Biochem* **355**:132-139.
- Navratilova I, Sodroski J and Myszka DG (2005) Solubilization, stabilization, and purification of chemokine receptors using biosensor technology. *Anal Biochem* **339**:271-281.
- Nisius L, Rogowski M, Vangelista L and Grzesiek S (2008) Large-scale expression and purification of the major HIV-1 coreceptor CCR5 and characterization of its interaction with RANTES. *Protein Expr Purif* **61**:155-162.
- Nobles M, Benians A and Tinker A (2005) Heterotrimeric G proteins precouple with G protein-coupled receptors in living cells. *Proc Natl Acad Sci U S A* **102**:18706-18711.
- Nygaard R, Frimurer TM, Holst B, Rosenkilde MM and Schwartz TW (2009) Ligand binding and micro-switches in 7TM receptor structures. *Trends Pharmacol Sci* **30**:249-259.
- Okada T, Sugihara M, Bondar AN, Elstner M, Entel P and Buss V (2004) The retinal conformation and its environment in rhodopsin in light of a new 2.2 angstrom crystal structure. *J Mol Biol* **342**:571-583.
- Oldham WM and Hamm HE (2007) How do receptors activate g proteins? *AdvProtein Chem* **74**:67-93.
- Overington JP, Al-Lazikani B and Hopkins AL (2006) Opinion - How many drug targets are there? *Nat Rev Drug Discov* **5**:993-996.

- Palczewski K (2006) G protein-coupled receptor rhodopsin, in *Annual Review of Biochemistry* pp 743-767, Annual Reviews, Palo Alto.
- Palczewski K (2010) Oligomeric forms of G protein-coupled receptors (GPCRs). *Trends BiochemSci* **35**:595-600.
- Palczewski K, Kumasaka T, Hori T, Behnke CA, Motoshima H, Fox BA, Le Trong I, Teller DC, Okada T, Stenkamp RE, Yamamoto M and Miyano M (2000) Crystal structure of rhodopsin: A G protein-coupled receptor. *Science* **289**:739-745.
- Patny A, Desai PV and Avery MA (2006) Homology modeling of G-protein-coupled receptors and implications in drug design. *Curr Med Chem* **13**:1667-1691.
- Percherancier Y, Planchenault T, Valenzuela-Fernandez A, Virelizier JL, Arenzana-Seisdedos F and Bachelier F (2001) Palmitoylation-dependent control of degradation, life span, and membrane expression of the CCR5 receptor. *J Biol Chem* **276**:31936-31944.
- Periole X, Knepp AM, Sakmar TP, Marrink SJ and Huber T (2012) Structural Determinants of the Supramolecular Organization of G Protein-Coupled Receptors in Bilayers. *J Am Chem Soc* **134**:10959-10965.
- Petrasek Z and Schwille P (2008) Precise measurement of diffusion coefficients using scanning fluorescence correlation spectroscopy. *Biophys J* **94**:1437-1448.
- Pober JS (1982) Proteolysis of rhodopsin. *Methods in Enzymology* **81**:236-239.
- Popot JL (2010) Amphipols, Nanodiscs, and Fluorinated Surfactants: Three Nonconventional Approaches to Studying Membrane Proteins in Aqueous Solutions, in *Annual Review of Biochemistry, Vol 79* (Kornberg RD, Raetz CRH, Rothman JE and Thorner JW eds) pp 737-775, Annual Reviews, Palo Alto.

- Pramanik A, Olsson M, Langel U, Bartfai T and Rigler R (2001) Fluorescence correlation spectroscopy detects galanin receptor diversity on insulinoma cells. *Biochemistry* **40**:10839-10845.
- Pugach P, Ketas TJ, Michael E and Moore JP (2008) Neutralizing antibody and anti-retroviral drug sensitivities of HIV-1 isolates resistant to small molecule CCR5 inhibitors. *Virology* **377**:401-407.
- Rasmussen SGF, Choi HJ, Fung JJ, Pardon E, Casarosa P, Chae PS, DeVree BT, Rosenbaum DM, Thian FS, Kobilka TS, Schnapp A, Konetzki I, Sunahara RK, Gellman SH, Pautsch A, Steyaert J, Weis WI and Kobilka BK (2011a) Structure of a nanobody-stabilized active state of the beta(2) adrenoceptor. *Nature* **469**:175-180.
- Rasmussen SGF, Choi HJ, Rosenbaum DM, Kobilka TS, Thian FS, Edwards PC, Burghammer M, Ratnala VRP, Sanishvili R, Fischetti RF, Schertler GFX, Weis WI and Kobilka BK (2007) Crystal structure of the human beta(2) adrenergic G-protein-coupled receptor. *Nature* **450**:383-U384.
- Rasmussen SGF, DeVree BT, Zou YZ, Kruse AC, Chung KY, Kobilka TS, Thian FS, Chae PS, Pardon E, Calinski D, Mathiesen JM, Shah STA, Lyons JA, Caffrey M, Gellman SH, Steyaert J, Skiniotis G, Weis WI, Sunahara RK and Kobilka BK (2011b) Crystal structure of the beta(2) adrenergic receptor-Gs protein complex. *Nature* **477**:549-U311.
- Reeves PJ, Callewaert N, Contreras R and Khorana HG (2002) Structure and function in rhodopsin: High-level expression of rhodopsin with restricted and homogeneous N-glycosylation by a tetracycline-inducible N-acetylglucosaminyltransferase I-

- negative HEK293S stable mammalian cell line. *Proc Natl Acad Sci U S A* **99**:13419-13424.
- Rich RL, Miles AR, Gale BK and Myszka DG (2009) Detergent screening of a G-protein-coupled receptor using serial and array biosensor technologies. *Anal Biochem* **386**:98-104.
- Robertson N, Jazayeri A, Errey J, Baig A, Hurrell E, Zhukov A, Langmead CJ, Weir M and Marshall FH (2011) The properties of thermostabilised G protein-coupled receptors (StaRs) and their use in drug discovery. *Neuropharmacology* **60**:36-44.
- Rosenbaum DM, Rasmussen SGF and Kobilka BK (2009) The structure and function of G-protein-coupled receptors. *Nature* **459**:356-363.
- Ruprecht JJ, Mielke T, Vogel R, Villa C and Schertler GFX (2004) Electron crystallography reveals the structure of metarhodopsin I. *Embo J* **23**:3609-3620.
- Salom D, Lodowski DT, Stenkamp RE, Le Trong I, Golczak M, Jastrzebska B, Harris T, Ballesteros JA and Palczewski K (2006) Crystal structure of a photoactivated deprotonated intermediate of rhodopsin. *Proc Natl Acad Sci U S A* **103**:16123-16128.
- Salon JA, Lodowski DT and Palczewski K (2011) The Significance of G Protein-Coupled Receptor Crystallography for Drug Discovery. *Pharmacol Rev* **63**:901-937.
- Samson M, Libert F, Doranz BJ, Rucker J, Liesnard C, Farber CM, Saragosti S, Lapoumeroulie C, Cognaux J, Forceille C, Muyldermans G, Verhofstede C, Burtonboy G, Georges M, Imai T, Rana S, Yi YJ, Smyth RJ, Collman RG, Doms RW, Vassart G and Parmentier M (1996) Resistance to HIV-1 infection in

- Caucasian individuals bearing mutant alleles of the CCR-5 chemokine receptor gene. *Nature* **382**:722-725.
- Scheerer P, Park JH, Hildebrand PW, Kim YJ, Krauss N, Choe HW, Hofmann KP and Ernst OP (2008) Crystal structure of opsin in its G-protein-interacting conformation. *Nature* **455**:497-U430.
- Schertler GFX and Hargrave PA (1995) Projection structure of frog rhodopsin in 2 crystal forms. *Proc Natl Acad Sci U S A* **92**:11578-11582.
- Schott M, Scherbaum WA and Morgenthaler NG (2005) Thyrotropin receptor autoantibodies in Graves' disease. *Trends Endocrinol Metab* **16**:243-248.
- Schwartz TW and Sakmar TP (2011) Structural biology: Snapshot of a signalling complex. *Nature* **477**:540-541.
- Schwille P, MeyerAlmes FJ and Rigler R (1997) Dual-color fluorescence cross-correlation spectroscopy for multicomponent diffusional analysis in solution. *Biophys J* **72**:1878-1886.
- Scita G and Di Fiore PP (2010) The endocytic matrix. *Nature* **463**:464-473.
- Seibert C, Ying W, Gavrilov S, Tsamis F, Kuhmann SE, Palani A, Tagat JR, Clader JW, McCombie SW, Baroudy BM, Smith SO, Dragic T, Moore JP and Sakmar TP (2006) Interaction of small molecule inhibitors of HIV-1 entry with CCR5. *Virology* **349**:41-54.
- Serrano-Vega MJ, Magnani F, Shibata Y and Tate CG (2008) Conformational thermostabilization of the beta 1-adrenergic receptor in a detergent-resistant form. *Proc Natl Acad Sci U S A* **105**:877-882.

- Sheikh SP, Zvyaga TA, Lichtarge O, Sakmar TP and Bourne HR (1996) Rhodopsin activation blocked by metal-ion-binding sites linking transmembrane helices C and F. *Nature* **383**:347-350.
- Shenoy SK and Lefkowitz RJ (2011) beta-arrestin-mediated receptor trafficking and signal transduction. *Trends Pharmacol Sci* **32**:521-533.
- Shimamura T, Shiroishi M, Weyand S, Tsujimoto H, Winter G, Katritch V, Abagyan R, Cherezov V, Liu W, Han GW, Kobayashi T, Stevens RC and Iwata S (2011) Structure of the human histamine H-1 receptor complex with doxepin. *Nature* **475**:65-U82.
- Slaughter BD, Schwartz JW and Li R (2007) Mapping dynamic protein interactions in MAP kinase signaling using live-cell fluorescence fluctuation spectroscopy and imaging. *Proc Natl Acad Sci U S A* **104**:20320-20325.
- Sprang SR, Chen Z and Du XL (2007) Structural basis of effector regulation and signal termination in heterotrimeric G alpha proteins. *Adv Protein Chem* **74**:1-65.
- Springer TA (1994) Traffic signals for lymphocyte recirculation and leukocyte emigration: the multistep paradigm. *Cell* **76**:301-314.
- Strizki JM, Tremblay C, Xu S, Wojcik L, Wagner N, Gonsiorek W, Hipkin RW, Chou CC, Pugliese-Sivo C, Xiao YS, Tagat JR, Cox K, Priestley T, Sorota S, Huang W, Hirsch M, Reyes GR and Baroudy BM (2005) Discovery and characterization of vicriviroc (SCH 417690), a CCR5 antagonist with potent activity against human immunodeficiency virus type 1. *Antimicrob Agents Chemother* **49**:4911-4919.

- Suda K, Filipek S, Palczewski K, Engel A and Fotiadis D (2004) The supramolecular structure of the GPCR rhodopsin in solution and native disc membranes. *Mol Membr Biol* **21**:435-446.
- Trkola A, Kuhmann SE, Strizki JM, Maxwell E, Ketas T, Morgan T, Pugach P, Xu S, Wojcik L, Tagat J, Palani A, Shapiro S, Clader JW, McCombie S, Reyes GR, Baroudy BM and Moore JP (2002) HIV-1 escape from a small molecule, CCR5-specific entry inhibitor does not involve CXCR4 use. *Proc Natl Acad Sci U S A* **99**:395-400.
- Tsamis F, Gavrilov S, Kajumo F, Seibert C, Kuhmann S, Ketas T, Trkola A, Palani A, Clader JW, Tagat JR, McCombie S, Baroudy B, Moore JP, Sakmar TP and Dragic T (2003) Analysis of the mechanism by which the small-molecule CCR5 antagonists SCH-351125 and SCH-350581 inhibit human immunodeficiency virus type 1 entry. *J Virol* **77**:5201-5208.
- Veazey RS, Klasse PJ, Ketas TJ, Reeves JD, Piatak M, Kunstman K, Kuhmann SE, Marx PA, Lifson JD, Dufour J, Mefford M, Pandrea I, Wolinsky SM, Doms RW, DeMartino JA, Siciliano SJ, Lyons K, Springer MS and Moore JP (2003) Use of a small molecule CCR5 inhibitor in macaques to treat simian immunodeficiency virus infection or prevent simian-human immunodeficiency virus infection. *J Exp Med* **198**:1551-1562.
- Vedadi M, Niesen FH, Allali-Hassani A, Fedorov OY, Finerty PJ, Wasney GA, Yeung R, Arrowsmith C, Ball LJ, Berglund H, Hui R, Marsden BD, Nordlund P, Sundstrom M, Weigelt J and Edwards AM (2006) Chemical screening methods to identify

- ligands that promote protein stability, protein crystallization, and structure determination. *Proc Natl Acad Sci U S A* **103**:15835-15840.
- Warne T, Moukhametzianov R, Baker JG, Nehme R, Edwards PC, Leslie AGW, Schertler GFX and Tate CG (2011) The structural basis for agonist and partial agonist action on a beta(1)-adrenergic receptor. *Nature* **469**:241-244.
- Warne T, Serrano-Vega MJ, Baker JG, Moukhametzianov R, Edwards PC, Henderson R, Leslie AGW, Tate CG and Schertler GFX (2008) Structure of a beta(1)-adrenergic G-protein-coupled receptor. *Nature* **454**:486-U482.
- Watson C, Jenkinson S, Kazmierski W and Kenakin T (2005) The CCR5 receptor-based mechanism of action of 873140, a potent allosteric noncompetitive HIV entry inhibitor. *Mol Pharmacol* **67**:1268-1282.
- White JF, Noinaj N, Shibata Y, Love J, Kloss B, Xu F, Gvozdenovic-Jeremic J, Shah P, Shiloach J, Tate CG and Grishammer R (2012) Structure of the agonist-bound neurotensin receptor. *Nature* **490**:508-+.
- White JH, Wise A, Main MJ, Green A, Fraser NJ, Disney GH, Barnes AA, Emson P, Foord SM and Marshall FH (1998) Heterodimerization is required for the formation of a functional GABA(B) receptor. *Nature* **396**:679-682.
- Whorton MR, Bokoch MP, Rasmussen SGF, Huang B, Zare RN, Kobilka B and Sunahara RK (2007) A monomeric G protein-coupled receptor isolated in a high-density lipoprotein particle efficiently activates its G protein. *Proc Natl Acad Sci U S A* **104**:7682-7687.
- Wu BL, Chien EYT, Mol CD, Fenalti G, Liu W, Katritch V, Abagyan R, Brooun A, Wells P, Bi FC, Hamel DJ, Kuhn P, Handel TM, Cherezov V and Stevens RC

- (2010) Structures of the CXCR4 Chemokine GPCR with Small-Molecule and Cyclic Peptide Antagonists. *Science* **330**:1066-1071.
- Wu HX, Wacker D, Mileni M, Katritch V, Han GW, Vardy E, Liu W, Thompson AA, Huang XP, Carroll FI, Mascarella SW, Westkaemper RB, Mosier PD, Roth BL, Cherezov V and Stevens RC (2012) Structure of the human kappa-opioid receptor in complex with JDTic. *Nature* **485**:327-U369.
- Wu LJ, LaRosa G, Kassam N, Gordon CJ, Heath H, Ruffing N, Chen H, Humblias J, Samson M, Parmentier M, Moore JP and Mackay CR (1997) Interaction of chemokine receptor CCR5 with its ligands: Multiple domains for HIV-1 gp120 binding and a single domain for chemokine binding. *J Exp Med* **186**:1373-1381.
- Yan ECY, Kazmi MA, Ganim Z, Hou JM, Pan DH, Chang BSW, Sakmar TP and Mathies RA (2003) Retinal counterion switch in the photoactivation of the G protein-coupled receptor rhodopsin. *Proc Natl Acad Sci U S A* **100**:9262-9267.
- Ye SX, Zaitseva E, Caltabiano G, Schertler GFX, Sakmar TP, Deupi X and Vogel R (2010) Tracking G-protein-coupled receptor activation using genetically encoded infrared probes. *Nature* **464**:1386-U1314.
- Zaitseva M, Peden K and Golding H (2003) HIV coreceptors: role of structure, posttranslational modifications, and internalization in viral-cell fusion and as targets for entry inhibitors. *Biochim Biophys Acta-Biomembr* **1614**:51-61.